CZECH TECHNICAL UNIVERSITY IN PRAGUE

Faculty of Electrical Engineering

Department of Telecommunication Engineering

Simulation of Large-Scale Optical Transmission Systems

Bc. Kevin James Aguilar

Supervisor: Ing. Michal Lucki, Ph.D.

Prague, May 2019

Čestné prohlášení

Prohlašuji, že jsem zadanou diplomovou práci zpracoval sám s přispěním vedoucího práce a konzultanta a používal jsem pouze literaturu v práci uvedenou. Dále prohlašuji, že nemám námitek proti půjčování nebo zveřejňování mé diplomové práce nebo její části se souhlasem katedry.

V Praze dne 23. 5. 2019

..............…......................
Podpis studenta

Honesty Declaration

I hereby declare that I wrote the master's thesis by myself under the careful supervision of my thesis supervisor and I have used only the literature mentioned in the reference list. I also declare that I agree with lending or publishing my work with the consent of the department.

V Praze dne 23. 5. 2019

..............…......................
Podpis studenta

MASTER'S THESIS ASSIGNMENT

I. Personal and study details

Student's name: **Aguilar Kevin** Personal ID number: **453199**

Faculty / Institute: **Faculty of Electrical Engineering**

Department / Institute: **Department of Circuit Theory**

Study program: **Communications, Multimedia, Electronics**

Branch of study: **Systems of Communication**

II. Master's thesis details

Master's thesis title in English:

Simulation of Optical Transmission Systems in OptSim

Master's thesis title in Czech:

Simulace optických přenosových systémů v prostředí OptSim

Guidelines:

The goal of this thesis is to simulate large-scale transmission optical systems in OptSim environment using the TDSS method. Some selected phenomena having destructive impact on optical transmission (such as for example, FWM, dispersion, attenuation, among many others) should be taken into consideration, as well as transmission range and number of end users. The simulations should be based on the current recommendations of the ITU or IEEE in this area. Please, examine possible configurations of optical networks and investigate physical limits of these networks, as well as possibilities of extending the selected regimes of operation of these networks or their upgrade (without planning a completely new network), and last but not least, potential transition to bit rates higher than 100 Gbps. For these purposes, consider (for example) the use of wavelength division multiplex, advanced modulations, signal recovery, and other tools, if necessary. The main evaluation criterion is whether the created simulations correspond well to real optical systems and paths. Auxiliary tools are so-called eye diagram, BER, and Q-factor.

Bibliography / sources:

[1] Agraval, G. P.: Lightwave Technology: Telecommunication Systems, Wiley Interscience, USA, New Jersey, 2005.
[2] Freude, W., Scgmogrow, R.: Quality Metrics for Optical Signals: Eye Diagram, Q-factor, OSNR, EVM and BER. Proceedings of 14th International Conference on Transparent Optical Networks, England, Coventry, paper Mo.B1.5, 2012.
[3]ITU-T G series Supplement 39: Transmission Systems and Media, Digital Systems and Networks, ITU, 2012.

Name and workplace of master's thesis supervisor:

Ing. Michal Lucki, Ph.D., Department of Telecommunications Engineering, FEE

Name and workplace of second master's thesis supervisor or consultant:

Date of master's thesis assignment: **10.10.2018**   Deadline for master's thesis submission: _____

Assignment valid until: **28.02.2020**

_____ _____ _____
Ing. Michal Lucki, Ph.D. doc. Ing. Radoslav Bortel, Ph.D. prof. Ing. Pavel Ripka, CSc.
Supervisor's signature Head of department's signature Dean's signature

III. Assignment receipt

The student acknowledges that the master's thesis is an individual work. The student must produce his thesis without the assistance of others, with the exception of provided consultations. Within the master's thesis, the author must state the names of consultants and include a list of references.

_____ _____
Date of assignment receipt Student's signature

© ČVUT v Praze, Design: ČVUT v Praze, VIC

Abstrakt:

Hlavním cílem této práce je simulovat přenos v velkokapacitních optických systémech v prostředí OptSim. Modelované systémy jsou založeny na metodách používaných v současných komerčních systémech a ve výzkumných laboratorních systémech. Práce prezentuje teoretický náhled do těchto metod a výsledky jejich implementace. Bylo zjištěno, že pro další zvyšování kapacity systémů nad 100G, je potřeba vyhovět vysokým požadavkům na OSNR v důsledku projevujících se nevyhnutelných fyzikálních mezi komunikace po optických vláknech. Tato zjištění jsou detailně popsána a podložena podrobnými simulačními výsledky v programu OptSim.

Klíčová slova:

OptSim, Wavelength Division Multiplexing WDM, Coherent Systems, CWDM/DWDM, Polarization Division Multiplexing, Digital Signal Processing (DSP)

Abstract:

The main purpose of this thesis is to simulate large-scale transmission of optical systems using the OptSim environment. The systems modeled are based on the methods used in both currently widely deployed systems and those under research. Theoretical insight behind these methods is provided as well as the implications involved in their implementation. It is found that in order to continue to increase system capacity beyond 100G, methods of accommodating for high OSNR requirements must be utilized as a result of pushing the unavoidable physical constraints of optical fiber communications. These findings are described and supported by the detailed results of OptSim simulations.

Index Terms:

OptSim, Wavelength Division Multiplexing WDM, Coherent Systems, CWDM/DWDM, Polarization Division Multiplexing, Digital Signal Processing (DSP)

Table of Contents

List of Figures

List of Tables

List of Abbreviations

ADC	Analog-to-Digital Converter
ASE	Amplified Spontaneous Emission
BW	Bandwidth
BER	Bit Error Rate
BPSK	Binary Phase Shift Keying
CD	Chromatic Dispersion
CMA	Constant Modulus Algorithm
CP	Coherently Detected Polarization Multiplexed
CW	Continuous Wave
DAC	Digital-to-Analog Converter
DBP	Digital Backpropagation
DCF	Dispersion Compensating Fiber
DCU	Dispersion Compensating Unit
DDA	Decision-Directed Algorithm
DGD	Differential Group Delay
DPSK	Differential Phase-Shift Keying
DQPSK	Differential Quadrature Phase-Shift Keying
DSP	Digital Signal Processing
DP	Dual-Polarization
DWDM	Dense Wavelength-Division Multiplexing
EDC	Electronic Dispersion Compensation
EDFA	Erbium-Doped Fiber Amplifier
FBG	Fiber Bragg Grating
FEC	Forward Error Correction
FTTX	Fiber-to-the-x
FWM	Four-Wave Mixing
GVD	Group Velocity Dispersion
IF	Intermediate Frequency
ISI	Inter-Symbol Interference
ITU	International Telecommunication Union
ITU-T	ITU Telecommunication Standardization Sector
IFWM	Intra-channel four wave mixing
IQ	In-phase/Quadrature
IXPM	Intra-channel cross-phase modulation
LEAF	Large Effective Area Fiber
LMS	Least Mean Squared
LO	Local Oscillator
LPF	Low Pass Filter
MIMO	Multiple Input Multiple Output
MZM	Mach-Zehnder Modulator
M-QAM	M-ary Quadrature Amplitude Modulation
NRZ	Non-Return Zero
OIF	Optical Internetworking Forum
OOK	On-off Keying
OSNR	Optical Signal-to-Noise Ratio
OTDM	Optical Time Division Multiplexing
PBC	Polarization Beam Combiner
PBS	Polarization Beam Splitter

PD	Photo Detector
PDL	Polarization Dependent Loss
PDM	Polarization-Division Multiplexing
PLL	Phase-Locked-Loop
PMD	Polarization Mode Dispersion
PM	Polarization Multiplexing
POLMUX	Polarization Multiplexing
PSK	Phase Shift Keying
QAM	Quadrature Amplitude Modulation
QPSK	Quadrature Phase Shift Keying
SBS	Stimulated Brillouin Scattering
SDM	Space Division Multiplexing
SMF	Single-Mode Fiber
SSMF	Standard Single-Mode Fiber
SPM	Self-Phase Modulation
SRS	Stimulated Raman Scattering
TIA	Transimpedance Amplifier
TDSS	Time-Domain Split-Step
WDM	Wavelength-Division Multiplexing
XPM	Cross-Phase Modulation
ZNL	Zero-Order Nonlinear

1 Introduction

Coherent 100G polarization-division multiplexing quadrature phase-shift keying (PDM-QPSK) has been a success with the industrial deployment of 100G wavelength-division multiplexing (WDM) systems for long-haul applications beginning in 2010 [1]. The next step for higher bit rates in WDM transmission will include 200G and 400G systems. Formats such as polarization multiplexed 16-ary quadrature amplitude modulation (PM-16QAM) and polarization multiplexed 64-ary quadrature amplitude modulation (PM-64QAM) have denser constellations and achieve data rates required for next generation technologies. However, the denser the constellation, the higher the required optical signal-to-noise ratio (OSNR) for a given link reach. This tradeoff between spectral efficiency and reach is a major challenge in addressing the need of transmitting higher bit rates over long distances reliably. Therefore, a compromise must be made between the order of modulation, data rate and spectral occupancy. According to a 2015 White Paper by the Optical Internetworking Forum (OIF) [1] ultra-long-haul links usually have distances beyond 2000 km and will most likely to be based on lower order constellations such as QPSK or eventually 8QAM [1]. However, by use of electronic dispersion compensation (EDC), digital signal processing (DSP) in coherent reception, and optimized physical characteristics; these distances will certainly soon be achievable using PM-16QAM.

1.1   Problem Statement

The use of wavelength division multiplexing, advanced modulation formats and signal recovery by use of digital signal processing are implemented in order to achieve bit rates higher than 100 Gb/s. The methods of increasing capacity and spectral efficiency carry certain consequences. Selected phenomena having destructive impact on long-haul optical transmission; dispersion, nonlinear impairments, and transmission range are considered as well as methods of compensating their effects. The limitations exhibited by the methods of realizing high capacity optical systems are presented in this thesis. Also, the necessary compromises between parameters are discussed; the order of modulation, data rate, spectral occupancy, bit error rate (BER) and transmission distance are all accounted for. The main evaluation criterion is whether the created simulations correspond well to real optical systems. Auxiliary tools that implement BER counting and required OSNR are utilized to determine system feasibility of implementation. The physical limitations of these systems, potential categorization as well as the trade-offs between spectral efficiency and reach, are discussed in detail. Considering the above, the goal of this work is the investigate the complexities that arise when implementing next generation optical transmission systems and their significance in affecting the future requirements.

1.2   Thesis Structure

Chapter 2 provides a theoretical overview and State of the Art of the techniques used for increasing system capacity. Chapter 3 presents the Optical Network Hierarchy to introduce target bit rates and distances. Chapter 4 introduces the OptSim environment; the Time-Domain Split-Step (TDSS) method used for simulating system behavior, simulation parameters, performance monitors, features used for enabling high bit rates, and the transmitter and receiver structures used are described. Chapter 5 includes a description of simulations and presentation of results. The first section includes a comparison of advanced modulation formats, which sets the focus of the sections that follow. The next two sections demonstrate the high capacity potential of PM-16QAM and industry trends. The long-haul capabilities of PM-QPSK are then demonstrated. The sections that follow provide comparisons of PM-QPSK and PM-16QAM WDM system performance as well as the effects of adjusting channel spacing and transmission distance. The final sections focus on optimizing ultra-long-haul PM-QPSK and PM-16QAM systems by pinpointing optimal transmitted powers and fiber lengths. The final chapter concludes with final thoughts, possible limitations of the studied topics and potential areas for further study.

2 State of the Art

Deploying coherent 100G WDM PM-QPSK has allowed keeping the existing infrastructure consisting of erbium-doped fiber amplifier (EDFA), G.652 standard single-mode fiber (SSMF) and 50 GHz dense WDM (DWDM) fixed grid while maintaining global-scale transmission reaches [1]. In addition to EDFA, WDM, coherent detection, and DSP at the receiver; polarization multiplexing higher order modulation formats is required to achieve the next steps in the evolution large scale optical transmission.

2.1   Long Distance Transmission Using SMF & EDFA

Standard single-mode optical fiber (SSMF), G.652, in long-haul systems is the most commonly deployed single-mode fiber for WDM data transmission and supports distances up to several thousand kilometers, with appropriate amplification and dispersion compensation [2]. SSMF has a loss of around 0.2 dB/km at a wavelength of 1550 nm and for long-haul systems, typically spans of 50 – 120 km of are followed by EDFA amplification for signal regeneration [3] as in figure 2.1.
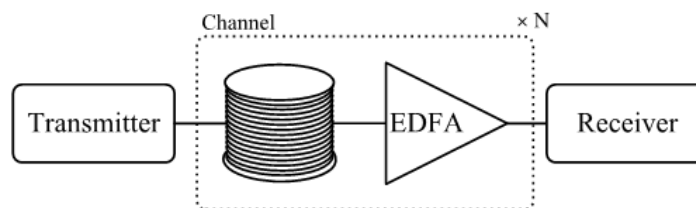
Fig. 2.1: *Transmission Link Consisting of N Fiber Spans and Amplifiers [4]*

Typically, EDFAs are used, however other amplification technologies exist, such as Raman amplifiers [5], semiconductor optical amplifiers [6] and phase-sensitive amplifiers [7]. The operating principle of an EDFA is that the fiber is doped with the rare-earth element Erbium which can be optically pumped to achieve population inversion and therefore optical gain [8]. As with any amplifier, the EDFA adds noise, hence regeneration distances should be optimal [4]. In this thesis, the EDFA is implemented in the 1530 – 1565 nm region, the C-band, where gain and noise figure can be approximated as flat values [2]. Noise originates from spontaneously emitted photons from the exited Erbium ions. These photons have random wavelength, phase and polarization and will experience gain as they propagate in the EDFA. Hence, the noise generated in the EDFA is called amplified spontaneous emission (ASE) [8]. As transmission systems extend to longer distances and higher bit rates, degenerative effects on transmission, attenuation and dispersion, become important limiting factors.

2.2   Linear & Nonlinear Transmission Impairments

Simulation of the signal and degeneration processes such as, chromatic dispersion (wavelengths travelling at different speeds), nonlinear self-phase modulation (Kerr effect) and fiber loss; is crucial for the correct interpretation of the received signal. Furthermore, signal and noise are nonlinearly mixed during propagation, and contributes to signal degeneration. These phenomena can be described by the one-dimensional, nonlinear Schrodinger equation, with stochastic input data [9]. Figure 2.2 provides a breakdown of the Schrodinger equation, where, $A(z,t)$ is the complex envelope of the optical field, hence the power is $|A(z,t)|^2$, α is fiber attenuation, β is the propagation constant and γ is the nonlinearity coefficient [10].

$$\frac{\partial A}{\partial z} + \boxed{\beta_1 \frac{\partial A}{\partial t} + \frac{i}{2}\beta_2 \frac{\partial^2 A}{\partial t^2}} + \boxed{\frac{\alpha}{2}A} = \boxed{i\gamma \,|A|^2\, A}$$

Chromatic Dispersion   Attenuation   Nonlinearity

Fig. 2.2: Breakdown of Nonlinear Schrodinger Equation [10]

Linear effects include group velocity dispersion (GVD) of SMF, fiber loss, adjacent channel cross-talk, polarization mode dispersion (PMD), ASE noise etc. [10]. Nonlinear effects include self-phase modulation (SPM), cross-phase modulation (XPM), stimulated Brillouin scattering (SBS), stimulated Raman scattering (SRS), and four-wave mixing (FWM) [10].

2.2.1 Fiber Losses

As the signal propagates along an optical fiber its power decreases exponentially with distance due to scattering and absorption processes, called fiber attenuation. If P_0 is the power launched at the input of a fiber of length L, the transmitted power P_T is given by:

$$P_T = P_0 \, exp(-\alpha L) \tag{2.1}$$

where the fiber attenuation coefficient α, is a measure of total losses, typically expressed in units of dB/km using the relation:

$$\alpha_{dB} = -\frac{10}{L} log\left(\frac{P_T}{P_0}\right) \approx 4.343\alpha \tag{2.2}$$
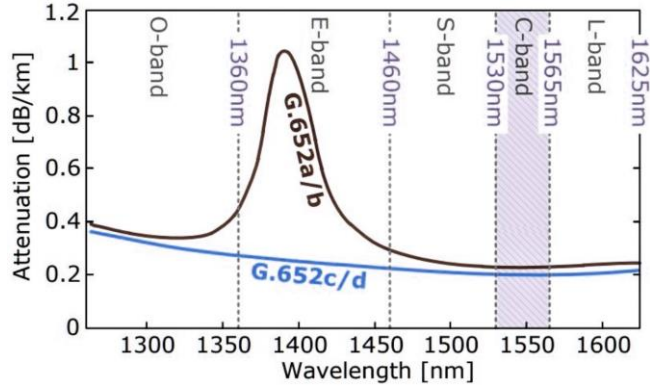
Fig. 2.3: *Attenuation Coefficient [dB/km] Vs. Wavelength [nm] of SMF on CWDM Grid, ITU-T G.694.2 [3]*

Single-mode fiber loss as a function of wavelength is depicted in figure 2.3 where, SMF exhibits a loss of about 0.2dB/km near 1550 nm [2]. This low loss allows for long-haul transmission links with 50 – 120 km fiber spans before amplification is needed [3]. The International Telecommunication Union Standardization (ITU-T) defined wavelength bands of interest for optical communication, as depicted in figure 2.3, and range from 1260 nm to 1625 nm. When combined, a total of approximately 200 wavelength channels on a 50-GHz wavelength-division multiplexing (WDM) grid are allowed. The range is lower-bounded by the fiber cut-off wavelength and upper-bounded by bending and SiO2-absorption losses [2]. The C-band (1530 nm-1565 nm) is generally used for long-haul optical communication [2] is used for the experiments in this thesis.

2.2.2 Chromatic Dispersion

Chromatic dispersion (CD) causes pulse broadening, therefore, distort pulses in a linear fashion. Optical fiber spectral components, composed of multiple spectral lines, propagate at different velocities due to two reasons; waveguide and material dispersion [11]. Waveguide dispersion is the wavelength dependence on the confinement of the electromagnetic wave to the core of the fiber. Material dispersion is

the wavelength dependence of the refractive index n. This implies that the group refractive index n_g which is the derivative of the refractive index n with respect to ω, also depends on wavelength ($f = \frac{c}{\lambda}$ and $\omega = 2\pi f$). The refractive index and group refractive index are related as $n_g = n + \omega\frac{dn}{d\beta}$ [3].

When a signal modulates within a fiber, multiple spectral components are created around the carrier frequency related to the wavelength of the signal travelling at different velocities, which leads to broadening of the modulated pulses, referred to as chromatic dispersion. When two neighboring pulses start to overlap, this crosstalk between pulses is referred to as inter-symbol interference (ISI) [11].

CD is defined as the amount of pulse spread per kilometer per nanometer in picoseconds. The pulse spread is related to the difference in group velocities of the spectral components in a pulse δt, over distance L, from [16]:

$$\delta t = -\frac{dt_g}{d\omega}\delta\omega = \frac{d}{d\omega}\left(\frac{L}{v_g}\right)\delta\omega = L\left(\frac{d^2\beta}{d\omega^2}\right)\delta\omega, \tag{2.3}$$

where t_g is the group delay of a single spectral component, ω is the angular frequency, v_g is the group velocity $\left(\frac{d\omega}{d\beta} = \beta^{-1} = \frac{c}{n_g}\right)$ and β is the propagation constant along the fiber axis. From Eq. 2.3, the term $\frac{d^2\beta}{d\omega^2} = \beta\left(\frac{ps^2}{km}\right)$, defined as group velocity dispersion (GVD), causes pulse broadening. Chromatic dispersion parameter D, is the group velocity dispersion related to wavelength:

$$D\left(\frac{ps}{nm\cdot km}\right) = \frac{1}{L}\frac{dt_g}{d\lambda} = \frac{d}{d\lambda}\left(\frac{1}{v_g}\right) = -\frac{2\pi c}{\lambda^2}\beta \tag{2.4}$$

Hence, CD depends on the fiber structure and wavelength of the signal [16]. The derivative of the GVD to angular frequency gives the slope of the GVD indicating the change in GVD with wavelength [2]. Typically, the GVD slope in SSMF is very small for broad channels, e.g. 50 GHz to 100 GHz, commonly used for transmission [3].
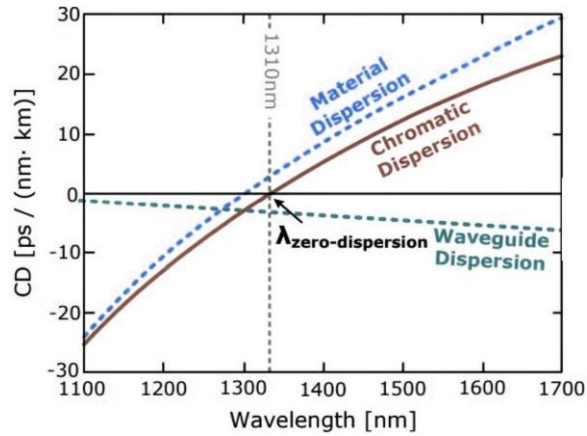
Fig. 2.4: CD vs. Wavelength for G.652 Fiber SSMF [3]

In figure 2.4, CD is the summation of the material dispersion with waveguide dispersion [3]. In SSMF the zero-dispersion wavelength, the wavelength at which the material and waveguide dispersion cancel out at around 1310 nm. In the C-band, CD is typically in the order of $17\frac{ps}{nm} \cdot km$ [3]. By adjusting the refractive index profile of the fiber, CD can be modified to obtain close to zero dispersion at the wavelength band of interest in dispersion-shifted fiber (G.653 [2]) and large effective area fiber (LEAF) [12]. The unitary and linear property of these effects allow for complete reconstruction of the transmitted signal by digital signal processing if the whole electrical field is detected, using coherent detection [13]. Coherent receivers, utilized in the simulations in this work, can completely compensate CD using digital signal processing (section 2.6.2), avoiding the need for optical CD mitigation [14].

2.2.3 Polarization Mode Dispersion

Whereas in CD distinct spectral components propagate at different speeds causing pulses to spread, with polarization mode dispersion (PMD), the non-ideal circular core of optical fibers causes the two orthogonal polarization components of the electromagnetic field to propagate with subtly dissimilar group velocities since they have slightly different (group) refractive indices, called birefringence [2]. As such, a pulse coupled to both polarizations at the fiber input will spread at the output due to differential group delay (DGD) [2], as shown in figure 2.6.
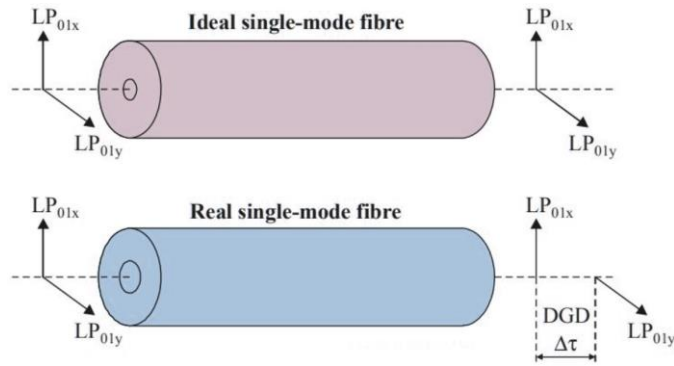
Fig. 2.5: *Illustration of DGD (Originating From PMD) in a Short Fiber Section [2]*

In figure 2.5 (bottom real single-mode model), light propagation is coupled into two birefringent axes, (LP_{01x}) and (LP_{01y}), results in a pulse broadening of $\Delta\tau$ due to the group velocity difference between the two axes [3]. Factors causing birefringence can be intrinsic and extrinsic. Internal factors are geometric irregularities arisen during fiber manufacturing or stress induced birefringence [2]. External causes for birefringence are perturbations from fiber spooling, cabling or embedding the fiber in the ground causing lateral stress, bending and twisting [2]. The axes of birefringence randomly change along the fiber length due to external factors, therefore, DGD in long fibers therefore does not simply add up and varies randomly with wavelength at a given time.
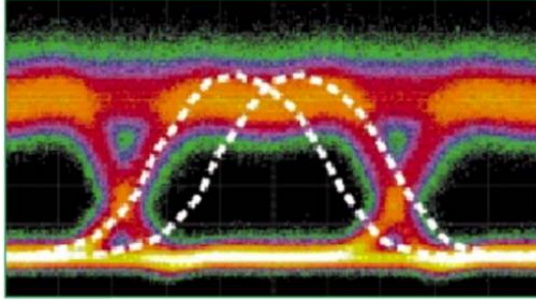
Fig. 2.6: *Eye diagram of a 10 Gbit/s signal transmitted on a Fiber with PMD [2]*

The PMD coefficient is the PMD value divided by the square root of the length, resulting in units $\frac{ps}{\sqrt{km}}$ and is the method of calculation for PMD used in OptSim [10]. Single-mode fibers can have a PMD value of less than $0.1 \frac{ps}{\sqrt{km}}$ [15]. However, deployed fiber systems might have PMD coefficients as large as $4.8 \frac{ps}{\sqrt{km}}$ [16]. Since the introduction of coherent receivers, PMD is not considered a problem in modern optical transmission systems.

2.3   Nonlinear Transmission Impairments

Nonlinear transmission impairments depend on the input power of the optical signal which interacts with the fiber core, known as the Kerr effect, which is the variation of the index of refraction with light intensity. Consequently, nonlinear phase and amplitude distortions of the propagating signal could be induced, making it difficult or impossible to compensate [9]. Optical communications systems operating at or above10 Gb/s, at higher transmitter powers, or in WDM systems, it is important to consider nonlinear effects. This makes nonlinearities a critical concern in long-haul transmission since high power lasers are used to transmit optical pulses over long spans to overcome attenuation. As such, there typically exists an optimal launch power into fiber spans where at lower launch powers, the system is limited by ASE noise generated in EDFAs and at higher launch power regions the system is limited by nonlinear distortions. The analysis of optimal launch powers is demonstrated in sections 5.5 and 5.6.

2.3.1   Intra-channel Nonlinear Transmission Impairments

For intra-channel interactions occurring within the same wavelength channel, either between neighboring pulses or between a pulse and noise produced by optical amplifiers, self-phase modulation (SPM) is the dominant nonlinear effect which can be further divided into isolated pulse SPM, intra-channel cross-phase modulation (IXPM) and intra-channel four-wave mixing (IFWM) [2, 17]. Isolated pulse SPM refers to the interaction of a pulse with itself, while IXPM and IFWM relate to the interactions between pulses within the same channel. IXPM is due to phase modulation across pulses due to GVD in adjacent pulses overlapping, causing non-linear phase-shifts, which after CD compensation, manifest as timing jitter at

the output of the fiber [2, 17]. IFWM is a process in which two waves create two other waves (energy exchange) due to the non-linear transmission medium. IFWM is revealed as amplitude fluctuations at the output of the fiber, or "ghost" pulses at positions where no energy was transmitted and depends largely on phase-matching between pulses [2, 17]. This effect can be suppressed by reducing the matched phase occurrence during transmission [2, 17]. When analyzing a system, it is common to refer to intra-channel nonlinear interactions as SPM, without considering the separate effects described here.

2.3.2   Inter-channel Nonlinear Transmission Impairments

Inter-channel signal-to-signal nonlinear distortions occur when two or more signals at different wavelengths propagate inside an optical fiber and is caused by the intensity dependence of the refractive index. The phase of optical signals is then affected by SPM as well as cross-phase modulation (XPM) and four-wave mixing (FWM). Inter-channel XPM represents a nonlinear optical effect where the wavelength of light can influence the phase of other wavelengths due to Kerr electro-optic effect [18]. In XPM, the phase of each optical channel is affected by the average power and the bit pattern of all other channels [9]. Modulation formats in which the amplitude of the electric field is changing (QAM) induce a larger phase change between the adjacent symbols of a channel than modulation formats with a quasi-constant amplitude like phase-modulated (PSK) formats [19]. Inter-channel FWM is very similar to intra-channel FWM, where the interaction of three wavelengths in a nonlinear medium can enable the rise of a fourth wavelength, which is created by dispersion of random photons [18]. Either three photons interact with each other to create a new photon at the sum of the three frequencies, or two photons mix to give life to two new photons at different frequencies [4]. One method of reducing the impact of FWM is to employ unequal channel spacing, which is not common for long-haul transmission systems since available spectrum is scarce [19]. FWM can also be reduced by avoiding phase-matching over long transmission periods by increasing GVD, thereby enlarging the difference in phase velocity [19]. Hence, FWM is mainly observed for low-dispersion fibers and if channel spacing is narrow as in DWDM systems [19].

The impact of intra-channel and inter-channel nonlinearities depends on many factors such as modulation format, fiber dispersion, channel spacing, launch power, among several others. As the focus of this work is on achieving high bit rates, nonlinear effects are not individually monitored, however, the effects of increasing nonlinearities due to the use of modulation formats of varying amplitude (QAM) and decreased channel spacing are revealed in OSNR vs. BER performance. Signal-noise nonlinear interactions grow with higher noise powers. Therefore, higher order modulation formats and high bit rate transmission is limited by nonlinear penalties and is therefore a major area of research on its own. In the past decade techniques such as, digital backpropagation (DBP) to compensate for deterministic intra-

channel nonlinearity through channel inversion [20], and Kalman filtering to mitigate the time-varying inter-symbol interference induced by inter-channel nonlinearity [21], have been proposed.

2.4   Dispersion Management

Several techniques exist to compensate CD in the optical domain among which is the use of dispersion compensating fibers (DCF), or Fiber Bragg Grating (FBG) [22]. A DCF is a type of fiber designed to have a large negative dispersion at a wavelength band of interest [23]. Compensation of dispersion at a wavelength around 1550 nm in a 1330 nm optimized single mode fiber can be achieved by specially designed fibers whose dispersion coefficient is negative and large at 1550 nm [23]. An FBG is a reflective device composed of an optical fiber that contains a modulation of its core refractive index over a certain length [21]. The Grating reflects light propagation through the fiber when its wavelength corresponds to the modulation periodicity. The reflected wavelength (λ_B) is called the Bragg wavelength, and defined by the relationship:

$$\lambda_B = 2\eta\Lambda, \tag{2.5}$$

where η is the effective refractive index of the grating in the fiber core and Λ is the grating period [22].

The dispersion compensating unit (DCU), which can be based on the above technologies, is typically located between fiber spans and amplifiers [10]. However, in this thesis, dispersion is managed by Electronic dispersion compensation (EDC) implemented prior to coherent reception. EDC is becoming a popular solution for its ability to correct for signal distortion after photo-detection, thereby promoting cost savings and network configurations with fewer regeneration sites [14].

2.5   Capacity Scaling Methods

There are several physical dimensions that can be used for the capacity scaling of optical signals that include the modulation of and multiplexing of optical fibers (Fig. 2.7) [24].
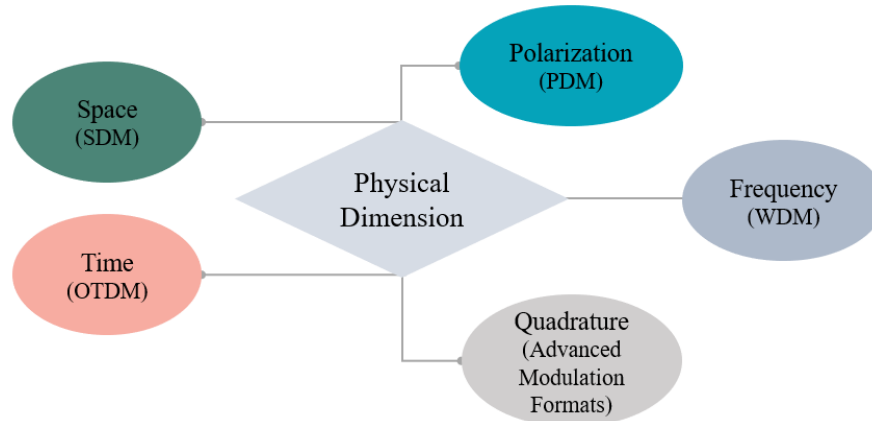
Fig. 2.7: Physical Dimensions Available for Capacity Scaling

Optical time division multiplexing (OTDM) was used in the 1990s in order to increase capacity by allocating different time slots to different channels [24]. The space dimension has been used by using parallel optical transmission links, such as multi-mode ribbon cable used in data centers [25, 26]. True space division multiplexing (SDM) has gained significant research as a promising solution to further increase system capacity by use of multimode SDM technology, but integration issues must be solved to enable commercially available SDM technology [27].

The quadrature dimension refers to the real and the imaginary parts of an optical signal and enables the generation of advanced modulation formats by modulating both amplitude and phase of the optical signal [28]. The polarization dimension refers to independent modulation of the two polarization states exhibited by an optical signal [28], referred to as polarization division multiplexing (PDM) and provides a two-fold increase in system capacity. The frequency dimension enables wavelength division multiplexing (WDM), which uses multiple channels to transmit data where each wavelength represents an individual channel [9]. Further to the frequency dimension of capacity scaling, reducing channel spacing enables an increase in the number of channels in WDM systems, thus improving spectral efficiency. Spectral efficiency is a measure of efficient utilization of the available bandwidth to achieve a target data rate. Highly spectrally efficient channels multiplexed together, refers to the concept of Super-channels [31]. The methods used to scale capacity in this thesis focus on wavelength division multiplexing (WDM) of coherent optical systems, implemented by polarization multiplexing of quadrature phase shift keying (QPSK) and/or quadrature amplitude modulation schemes (QAM).

2.5.1   Wavelength Division Multiplexing

WDM uses multiple wavelengths to transmit data, where each wavelength represents a channel, with a certain frequency separation between channels [4]. In figure 2.8, each optical carrier is transmitted by multiple transceivers (labeled TX_1), each operating at a different frequency. The signals are multiplexed and propagate through a shared optical fiber. At the receiver side, the signal is demultiplexed into individual channels and detected by its respective receiver (labeled RX_1).
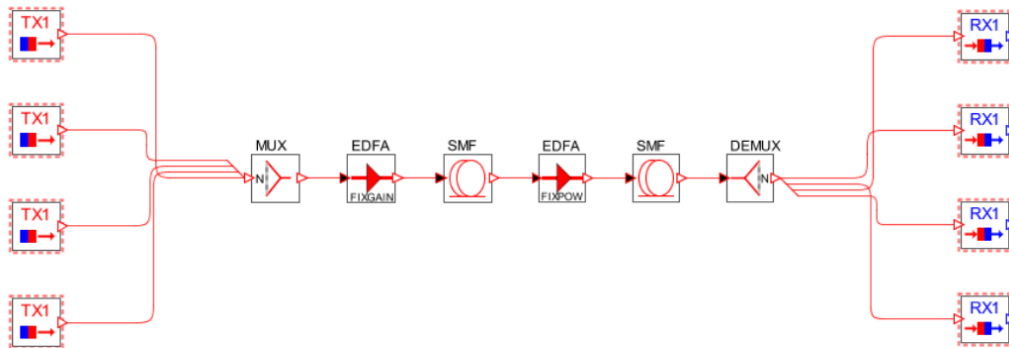
Fig. 2.8: Generic WDM Architecture

The value of the frequency separation between channels, or channel spacing, is determined by several factors such as data rate per channel, modulation format used for encoding data, pulse shaping and inherent characteristics of the optoelectronic components employed, e.g. bandwidth and roll-off of optical filters. In Course Wavelength Division Multiplexing (CWDM) systems, channel spacing is typically around 20 nm [29]. Current core and metropolitan networks employ WDM systems which operate at 50 and 100 GHz grid spacing, as standardized by the International Telecommunication Union (ITU) [29]. Dense Wavelength Division Multiplexing (DWDM) systems use 50 GHz channel spacing and operate in the C- and L-bands [29]. Demands for increased spectral efficiency motivated the research and development of technologies that enable 12.5 GHz channel spacing, such as optical vestigial sideband (VSB) filtering, demonstrated in [30]. The flexible DWDM grid, as defined by ITU G.694.1, allows for the accommodation of such highly spectrally efficient systems in addition to existing systems. While sometimes referred to as "gridless" channel spacing, the flexible channel plan is based on a 12.5-GHz grid pattern [29]. The standard supports mixed channel sizes in increments of $(n \cdot 12.5 \text{ GHz})$ and accommodates for both existing services and future requirements, for example; 100G $(4 \cdot 12.5 \text{ GHz} = 50 \text{ GHz})$ and future 400G $(12 \cdot 12.5 \text{ GHz})$ and 1 Tb optical rates [29].

2.5.1.1 Multi-carrier & Super-channels

Interfaces operating at 400 Gb/s are foreseen as the next standard after 100 Gb/s Ethernet [31] and super-channels are a promising method of fulfilling this requirement. A super-channel is a collection of optical signals that are multiplexed together with high spectral efficiency [32]. Typically, super-channels use spectrally efficient advanced modulation formats such as 16-QAM in combination with advanced multiplexing schemes, such as Nyquist-WDM, as shown in figure 2.9.
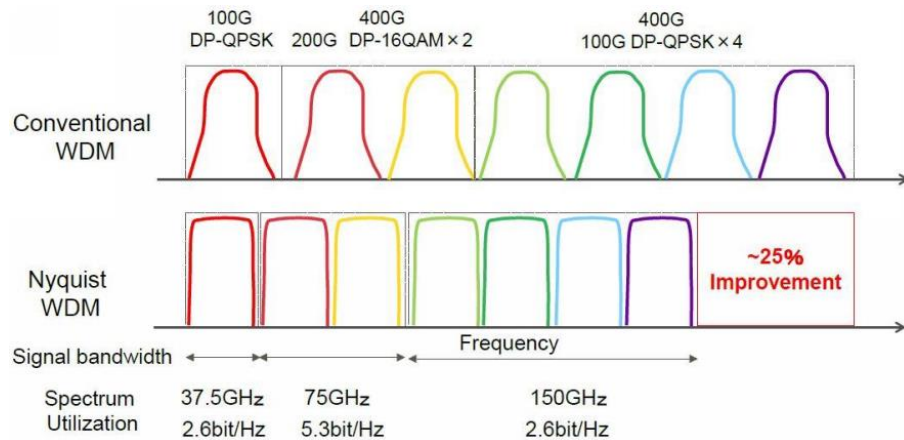
Fig. 2.9: Super-channel & Nyquist Filtering [33]

Spectral efficiency is defined as a ratio of symbol rate of the channel R_b and channel spacing Δf. The first step towards highly spectrally efficient systems is by implementing coherent systems, which

enable the use of higher-order modulation formats [34]. The digital coherent receiver allows linear mapping of optical field and enables the detection of amplitude and phase components of both polarizations and quadruples spectral efficiency [13]. Nyquist WDM enables a reduction of guard bands between channels creating spectrally efficient super-channels [35], in comparison to conventional WDM (Fig. 2.9). WDM systems are classified based on the channel bandwidth allocation relative to the modulation symbol rate of the channel to quantify efficient utilization of the available spectrum, as suggested in table 2-1 [36].

Table 2-1: Definitions of Various Classes of WDM [35]

Condition $\Delta f / R_b$	Definition	Example
> 50	Coarse WDM	10 Gb/s on 20 nm
> 5	WDM	10 Gb/s on 100 GHz
$1.2 \leq \Delta f / R_b \leq 5$	DWDM	28 GBaud PM-QPSK, 50 GHz
$1 \leq \Delta f / R_b \leq 1.2$	Quasi-Nyquist WDM	28 GBaud PM-QPSK, 33 GHz
$\Delta f / R_b = 1$	Nyquist WDM	28 GBaud PM-QPSK, 28 GHz
$\Delta f / R_b < 1$	Super-Nyquist WDM	28 GBaud PM-QPSK, 25 GHz

As shown in the table 2-1, in addition to CWDM, WDM and DWDM systems, recent advances in high spectrally efficient systems has created new regimes, identified as "Quasi-Nyquist" WDM, "Nyquist" WDM and "Super-Nyquist" WDM, respectively.

2.5.2 Modulation Formats

Modulation formats are often represented on a constellation diagram where the real and imaginary axes are termed the in-phase and quadrature axes respectively due to their 90° separation [28]. The amplitude of the in-phase signal is at the x-axis, and the amplitude of the quadrature signal is at the y-axis, for each symbol. The amplitude of each point along the in-phase axis is used to modulate a cosine (or sine) wave and the amplitude along the quadrature axis to modulate a sine (or cosine) wave [28]. Figure 2.10 shows five possible modulation formats: Binary Phase Shift Keying (BPSK), Quadrature Phase Shift Keying (QPSK), 8-ary quadrature amplitude modulation (8QAM), 16QAM, and 64QAM; containing 2, 4, 8, 16 and 64 possible states, respectively.

For Phase-Shift Keying (PSK), a finite number of phases are used. For QAM, the number in front of QAM indicates the number of constellation points, log2 of that number provides the number of bits encoded into one symbol. In both methods each of the phases, or amplitudes are assigned a unique pattern of bits, where the number of bits comprises the symbol that is represented by the phase or amplitude. For $M = 2^N$ alternative symbols, each symbol represents a message consisting of N bits [37]. If the symbol rate (baud rate) is f_s symbols/second (baud), the data rate is $N f_s$ bit/second [37].
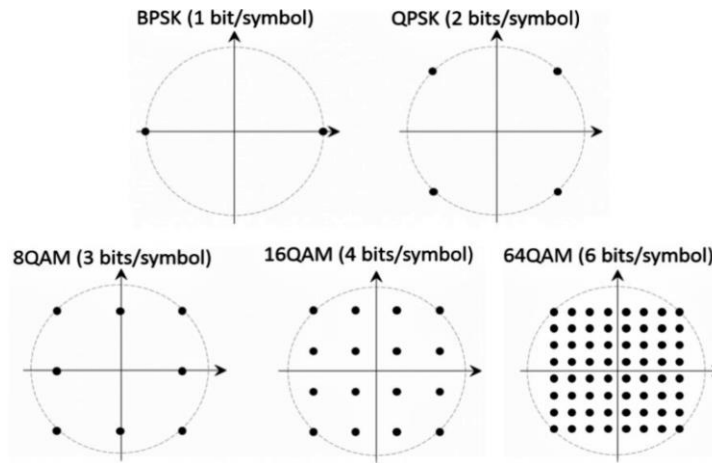
Fig. 2.10: Constellation Diagrams of Modulation Formats and Bits/Symbol in One Polarization State [28]

In the case of PSK, the phase is changed to represent the data signal [28]. There are two fundamental ways of utilizing the phase of a signal in this way: by viewing the phase itself as conveying the information, in which case the demodulator must have a reference signal to compare the received signal's phase against; or by viewing the change in the phase as conveying information — differential schemes, some of which do not need a reference carrier [28]. Quadrature amplitude modulation (QAM), as the name indicates, refers to the modulation of both the phase and amplitude of the optical signal to encode (more than two) bit streams into symbols to achieve higher spectral efficiencies [28].

2.5.2.1 Phase-Shift Keying (PSK)

BPSK is the simplest form of phase shift keying (PSK). It uses two phases which are separated by 180° [28]. BPSK is only able to modulate at 1 bit/symbol so it is unsuitable for high data-rate applications when bandwidth is limited [37]. However, Quadrature Phase-Shift Keying (QPSK), can encode two bits per symbol [28]. QPSK can be used either to double the data rate compared to a BPSK system while maintaining the same bandwidth of the signal, or to maintain the data-rate of BPSK but halving the bandwidth needed [28].

2.5.2.2 8QAM

8QAM encodes three bits per symbol, so it does not double the data rate with respect to QPSK [37]. To achieve a doubling in data rate, the symbol rate should be increased, which also implies spectral broadening and as such possible detrimental filtering penalties. Therefore, 8QAM up to now, is not often considered for long-haul transmission systems. However, with new digital to analog converter (DAC) technology, it may eventually be an interesting alternative compared to 16QAM [38]. Also, 8QAM might offer improvement over QPSK when the same net bit rate is concerned by using the additional bit for forward-error correction code (FEC) [39].

13

2.5.2.3   16QAM

16-level quadrature amplitude modulation (16QAM) is one of the most attractive modulation formats for transmission of 200 Gbit/s and beyond, since it achieves a good trade-off between spectral efficiency and reach. The encoding of 4 bits per symbol allows for an equal spectrum occupation as QPSK at 100 Gbit/s. Although high OSNR requirements and limited tolerance towards nonlinear transmission impairments hinders maximum reach, advances in FEC, pulse shaping, and back-propagation have proven to enable transoceanic distances using 16QAM [40].

2.5.2.4   64QAM

64QAM encodes six bits per symbol, however, transmission of QAM modulation beyond 16QAM over single-mode fiber seems to be of limited interest because of high OSNR requirements, implying a short reach application. Despite suffering from these penalties and low tolerance towards nonlinear transmission impairments, 64-level quadrature amplitude modulation (64QAM) transmission has been shown recently over very short reach and error-floors in the order of $5 \cdot 10^{-3}$ [41].

2.5.3   Polarization Multiplexing

Polarization multiplexing in research is abbreviated with many different terms: polarization-multiplexing (POLMUX), dual-polarization (DP) and coherently detected polarization multiplexed (CP), are seen in literature. The optical field propagating in a single-mode fiber can be described by an electric field and magnetic field with two orthogonal components x and y, called polarizations [42]. To achieve polarization-multiplexing two orthogonal fields, E_x and E_y, are modulated by two separate in-phase/quadrature (IQ-modulators) and combined using a polarization-beam combiner (PBC) [42], as shown in figure 2.11. Polarization-multiplexed transmission in combination with coherent detection enables greater robustness when combined with the modulation formats mentioned previously; PM-QPSK, PM-8QAM, PM-16QAM and PM-64QAM [42].
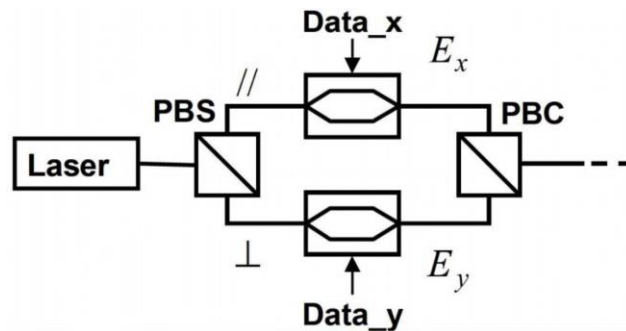
Fig. 2.11: *POLMUX Model with Polarization Beam Splitter (PBS) & Polarization Beam Combiner (PBC) [42]*

2.6 Coherent Optical Systems

Coherent systems are typically based on advanced amplitude/phase modulation, polarization multiplexing and coherent detection for the translation of the whole optical field information (amplitude, phase, polarizations) into the electrical domain and DSP after detection [42]. Ultimately, coherent systems enable a larger density of transmitted channels and use of highly spectrally efficient modulation formats.

After a transmitted signal passes through an optical link it may then be detected directly, differentially, or coherently (as in the simulations sections). A direct detection receiver is simply a photodiode and electrical amplitude and is capable of discerning amplitude modulation as shown in figure 2.12. The phase of the carrier is not considered. Current generation optical networks operating at 10 Gb/s and 40 Gb/s generally utilize direct detection schemes to receive on-off keying (OOK) signals [43].
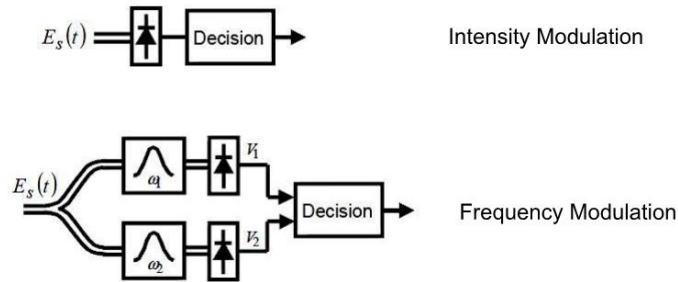
Fig. 2.12: Non-coherent Modulation Based on Intensity and Frequency Modulation [43]

Differential receivers (Fig. 2.13) enable direct detection schemes to receive phase-based formats e.g. differential phase-shift keying (DPSK) and differential quadrature phase-shift keying (DQPSK) but cannot recover phase information, preventing the use of advanced modulation formats [42].
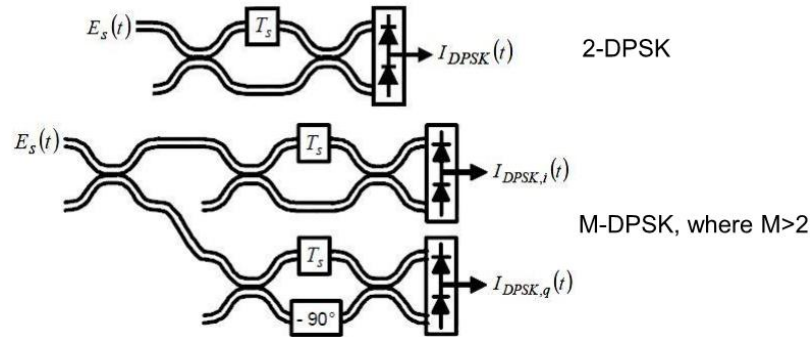
Fig. 2.13: Differentially Coherent Receiver [43]

Direct detection offers the advantage of simplicity; however, differential direct detection schemes limit post DSP because the receiver optical signal has already undergone an irreversible nonlinear transformation and photodiode pair. All signal processing (EDC, polarization demultiplexing, equalization) for direct-detection systems must consequently be performed before detection. Furthermore, direct detection does not benefit from local oscillator (LO) gain, limiting receiver sensitivity [43].

2.6.1   Coherent Detection

There are multiple ways of implementing coherent detection; homodyne, heterodyne and intradyne detection (phase diversity). The difference between these three methods depends on the frequency at which the LO is running (ω_{LO}) relative to the frequency of the transmitter laser (ω_S). For heterodyne detection $\omega_{LO} - \omega_S = \omega_{IF}$, the inter-mediate frequency (IF) ω_{IF} is larger than the electrical bandwidth (BW) of the signal.
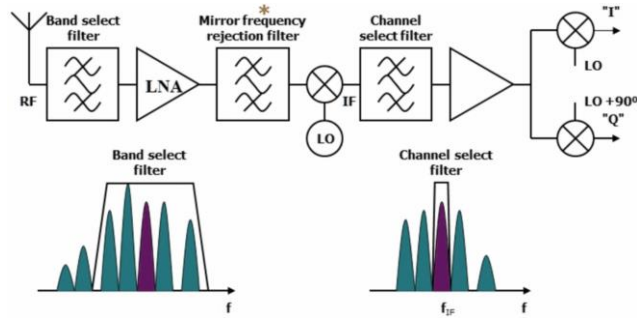
Fig. 2.14: *Heterodyne Receiver [42]*

In the heterodyne receiver (Fig. 2.14), the signal goes through a band select filter for channel selection, and the mirror frequency rejection filter removes undesired frequency. At the output of the rejection filter, at the local oscillator, the in-phase and quadrature components are obtained by (electrically) down-mixing the sine wave with a cosine (in-phase) and sine (quadrature) running at the ω_{IF} [43]. Then the channel is selected and amplified [42]. The main drawback of heterodyne detection is the photodiode needs a bandwidth of at least twice the signal bandwidth, due to the IF restriction, to avoid signal distortions [43]. A heterodyne receiver therefore needs broadband photodiodes, amplifiers and analog-to-digital converters (ADCs), which makes high symbol rate transmission cumbersome [43].

For homodyne detection $\omega_{LO} - \omega_S = 0$, i.e. both frequencies are the same and do not need intermediate frequency conversion; the received signal is directly down-converted to baseband at the receiver. Figure 2.15 is a block diagram of a homodyne receiver.
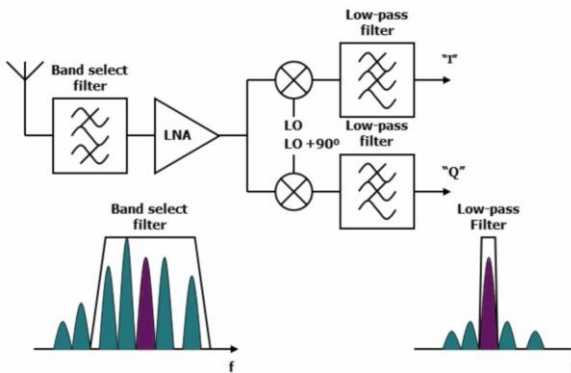
Fig. 2.15: *Homodyne Receiver [42]*

16

With the local oscillator frequency, the same as the received frequency, this structure becomes a phase detector. However, to fulfill the homodyne requirement, active control of the LO is needed, e.g. by using a phase-locked-loop (PLL), which puts stringent requirements on the laser linewidth [44].

Intradyne detection (phase-diversity detection) is similar to homodyne detection, with the exception that the frequency difference between the LO and transmitter laser is approximately zero; $\omega_{LO} - \omega_S \approx 0$, where the frequency difference tolerated depends upon digital signal processing [44]. Intradyne detection relies on detection of both the in-phase and quadrature component to compensate for frequency and phase offset between the LO and transmitter laser and is therefore also known as a phase-diversity receiver. The typical physical structure of a polarization-diversity receiver, as proposed by the Optical Internetworking Forum implementation agreement [45], is shown in figure 2.16. The schematic is similar to the homodyne receiver, except that there is no need to lock the local oscillator frequency to the received signal's frequency. The structure employs a component called an optical hybrid, where the received signal is heterodyned to get four intermediate frequency components, each 90-degrees apart, so the outputs are at the phase of 0, 90, 180, and 270 [45].
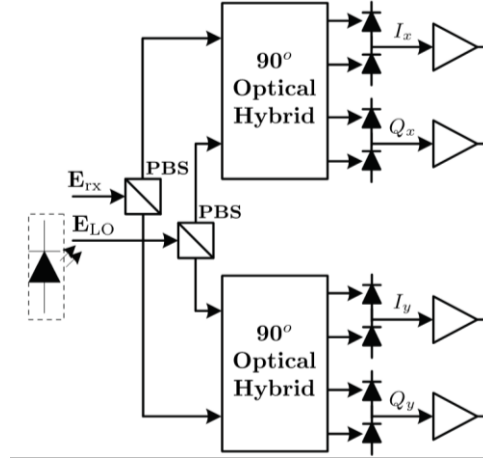
Fig. 2.16: Phase Diversity Receiver [42]

Considering figure 2.16, the dual-polarization received optical field, $E_{rx}(t) = \left[E_{x,rx}(t) E_{y,rx}(t)\right]^T$, where $E_{x,rx}(t)$ and $E_{y,rx}(t)$ are the signal components corresponding to the x and y polarizations. The local oscillator (LO) laser runs without any hardware feedback for frequency and/or phase synchronization. A polarization beam splitter (PBS) is used to decompose the E_{rx} and E_{LO} optical fields into their orthogonal polarization components. Since polarization demultiplexing can be performed in the digital domain [42], no optical dynamic control is required for polarization state alignment. A pair of 90° optical hybrids is used to mix the received signal with the LO reference carrier, producing four outputs shifted by from each other by 180° [46], containing both direct detection ($|E_{x/y,rx}|^2$and

$|E_{x/y,LO}|^2$) and coherent detection ($Re\{E_{x/y,rx}E_{x/y,LO}\}$ and $Im\{E_{x/y,rx}E_{x/y,LO}\}$) terms. The in-phase (I) information is contained in the $Re\{E_{x/y,rx}E_{x/y,LO}\}$ terms, whereas the quadrature (Q) information is conveyed in the $Im\{E_{x/y,rx}E_{x/y,LO}\}$ terms. Grouping the 90° optical hybrid outputs into 180° shifted optical fields, the optical-to-electrical down-conversion is performed by two pairs of photodiodes in balanced configuration, yielding the in-phase and quadrature electrical currents, $I_{x,y}$ and $Q_{x,y}$. The electrical outputs of the balanced photodiodes are then fed to linear amplifiers to adjust the signal to be sent to the DSP subsystem for post-processing [42].

The phase-diversity receiver offers flexibility over the other two methods, i.e. LO frequency and phase offset tolerance as well as relaxed bandwidth requirements compared to heterodyne detection. For this reason, the polarization-diversity intradyne receiver the common choice for commercial use [42] and is utilized in the receiver models in this thesis.

2.6.2   Coherent System Implementation with DSP

This section provides a theoretical overview of the coherent transmitter and receiver structures, with a focus on the DSP implementation at the receiver; which are utilized in the OptSim simulations of this work. As an example, the PM-QPSK transmitter and receiver layouts (Fig. 2.17 and Fig. 2.18), with DSP at the receiver, enable coherent system implementation by providing a polarization multiplexed signal at the transmitter and by utilizing DSP algorithms within the dynamic receiver structures. The CMA (constant modulus algorithms), DDA (decision directed algorithms) and Viterbi-Viterbi phase estimation, enable coherent reception within the receiver structures in the OptSim simulations of this work.
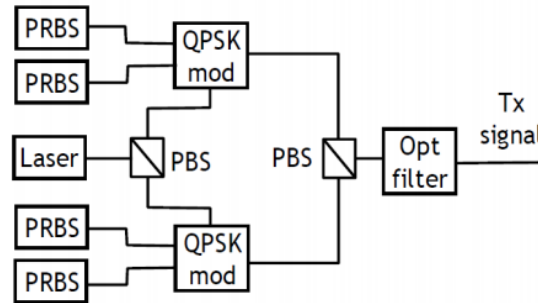
Fig. 2.17: Block Diagram of Single-Channel PM-QPSK Transmitter [47]

The transmitter schematic, figure 2.17, uses two QPSK modulators, each with two data inputs from two data sources for PM-QPSK (for MQAM, the number of data sources would adjust based on N for $M = 2^N$); one is in-phase and the other is in-quadrature. The laser beam is split into x' and y' polarizations, and each polarization is modulated by an individual QPSK modulator.
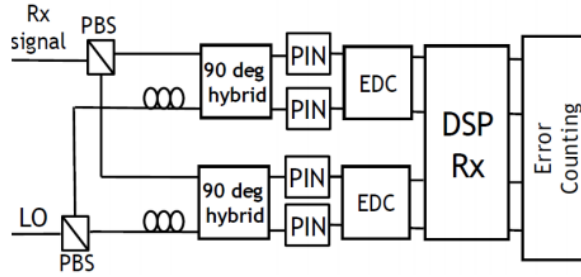
Fig. 2.18: Block Diagram of Single-Channel PM-QPSK Receiver [47]

At the receiver (Fig. 2.18), the components of the phase diversity receiver are included (Fig. 2.16). At the inputs, the received signal and the local oscillator signal are mixed, then two 90-degree hybrid components shift the optical fields and after the four photodiodes yield the in-phase and quadrature components of the electrical signal, EDC is applied and the DSP algorithm recovers polarization and phase of the constellation. Finally, in the last block, the receiver then provides error counting. Figure 2.19 provides a detailed look at the DSP block at the receiver and related algorithms.
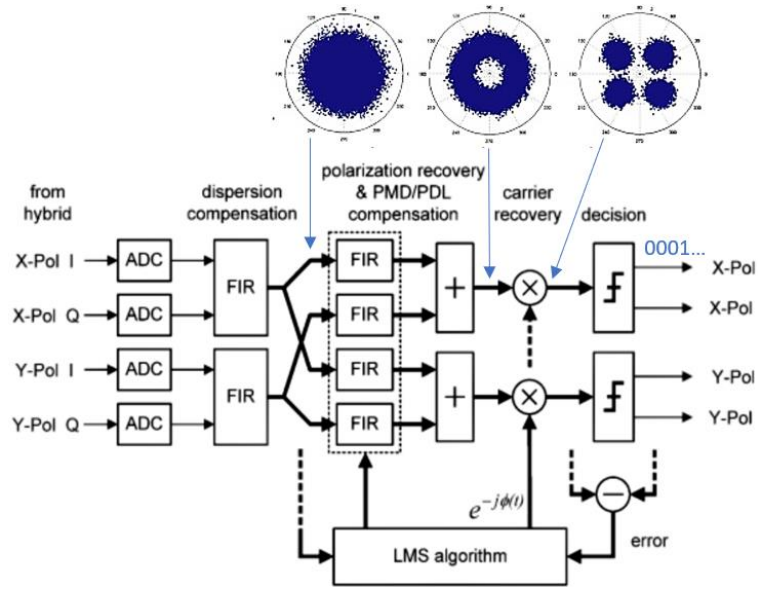
Fig. 2.19: DSP Implementation at the Receiver [48]

The received samples pass through four distinct stages. After sampling of data takes place at the outputs of the 90-degree hybrids and photodiodes, the four outputs are filtered and fed into the inputs of an electronic dispersion compensator (EDC). Then, equalization using finite impulse response filters (FIR) for polarization recovery in addition to PMD compensation and compensation from polarization dependent loss (PDL) due to cross-talk between polarizations takes place, carrier recovery is realized, and finally, the decision threshold is applied for data recovery. These processes are explained in this section.

Polarization demultiplexing in a single mode fiber application is a 2x2 multiple input/multiple output (MIMO) process governed by the Jones matrix that describes the fiber and the alignments of the transmitter and receiver E-fields. For dual-polarization fiber transmission, the MIMO equalizer is arranged in a "butterfly" structure, figure 2.20. The equalizer adapts four sets of complex coefficients, bridging possible path from x and y inputs to x' and y' outputs, to jointly minimize the resulting error at the output [49].

Schematic representation	Constant modulus algorithm[9]	Decision directed algorithm
	$\mathbf{h}_{xx} = \mathbf{h}_{xx} + \mu\varepsilon_x x' \cdot \overline{\mathbf{x}}$ $\mathbf{h}_{xy} = \mathbf{h}_{xy} + \mu\varepsilon_x x' \cdot \overline{\mathbf{y}}$ $\mathbf{h}_{yx} = \mathbf{h}_{yx} + \mu\varepsilon_x y' \cdot \overline{\mathbf{x}}$ $\mathbf{h}_{yy} = \mathbf{h}_{yy} + \mu\varepsilon_x y' \cdot \overline{\mathbf{y}}$ $\varepsilon_x = \left(1 - \left|x'\right|^2\right) \ \varepsilon_y = \left(1 - \left|y'\right|^2\right)$	$\mathbf{h}_{xx} = \mathbf{h}_{xx} + \mu\varepsilon_x \overline{\mathbf{x}}$ $\mathbf{h}_{xy} = \mathbf{h}_{xy} + \mu\varepsilon_x \overline{\mathbf{y}}$ $\mathbf{h}_{yx} = \mathbf{h}_{yx} + \mu\varepsilon_x \overline{\mathbf{x}}$ $\mathbf{h}_{yy} = \mathbf{h}_{yy} + \mu\varepsilon_x \overline{\mathbf{y}}$ $\varepsilon_x = \exp(j\phi_x)d_x - x'$ $\varepsilon_y = \exp(j\phi_y)d_y - y'$ $d_x, d_y = decoded\ QPSK\ symbols$ $\phi_x, \phi_y = phase\ between\ x'\ and\ d_x$

Table 1. Algorithms used in the adaptive equalizer (where $\overline{\mathbf{x}}$ and $\overline{\mathbf{y}}$ denote the complex conjugate of $\mathbf{x}$ and $\mathbf{y}$ respectively)

Fig. 2.20: Implementation of Constant Modulus and Decision Directed Algorithms [49]

The schematic representation is on the left side of figure 2.20 where the incoming electrical signals that correspond to x' and y' polarizations are filtered through FIR filters. There are four FIR filters with different impulse responses; $h_{xx}, h_{xy}, h_{yx}, and\ h_{yy}$. The output signals are denoted in the second column; $x' = h_{xx}x + h_{xy}y$ and $y' = h_{yx}x + h_{yy}y$ in the case of CMA [42]. The constant modulus algorithm (CMA) will adapt a bank of equalizers to minimize inter-symbol interference (ISI) in a dispersive environment given that that there are as many polarization modes at both the transmitter and receiver, and that there exists a matrix with non-zero determinant that describes the channel [50]. The first requirement is met by proper choice of modulation format (PM-QPSK or PM-16QAM) and use of a dual-polarization receiver. The latter is met by the fact that fiber transmission can be modeled by the Jones matrix [42], and the process of polarization demultiplexing may be expressed as the receiver's estimate of the inverse Jones matrix based on observation of the input signal. The symmetry of the CMA is guaranteed for all complex-valued transmissions that have 90° phase ambiguity (i.e. the constellation is identical when rotated by 90°). CMA is an algorithm that minimizes the dispersion of the equalizer output around a circular contour (Fig. 2.19). The CMA algorithm adapts filter coefficients at each time k in order to minimize the '2-2 modulus error', ε, $\varepsilon_k = |y_k|^2 - A^2$, where y is the output symbol and A is a real, positive radial constant to which the equalizer attempts to constrain the output; as shown in the block diagram figure 2.21.

$$\varepsilon_k{}^2 = |y_k|^2 - A^2$$
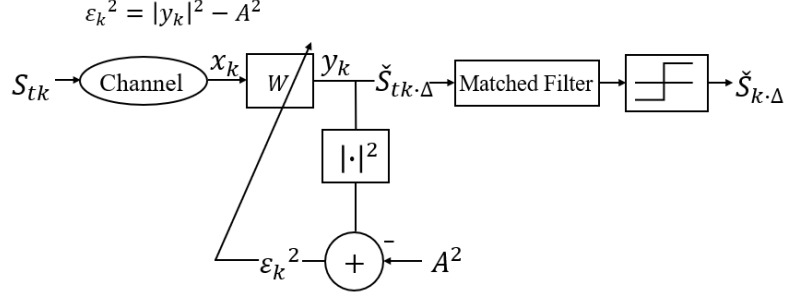
Fig. 2.21: Block Diagram of Constant Modulus Algorithm [51]

The error calculation vector assists the equalizer in finding and maintaining coefficients to achieve stable operation at an ISI minimum [50]. Specifically, the update rule for each, $h_{xx}, h_{xy}, h_{yx}, and\ h_{yy}$ for CMA is shown in figure 2.20, where h_k are the filter taps, ε is the error given, x' and y' are the input symbols, and μ is the step size. The resulting CMA error signal is generated to reduce the modulated constellation to a unit circle on the I-Q plane. Therefore, the CMA algorithm can equalize any rotationally symmetric modulation format, e.g. QPSK and QAM [52].

The next phase, as shown in the block diagram of figure 2.22, is called Carrier Phase Estimation where the Viterbi-Viterbi algorithm is used. Carrier phase recovery is the process of estimating the phase distortion of the received signal induced by the time-varying, random frequency offset between the carrier and LO lasers or by the fiber nonlinearities.
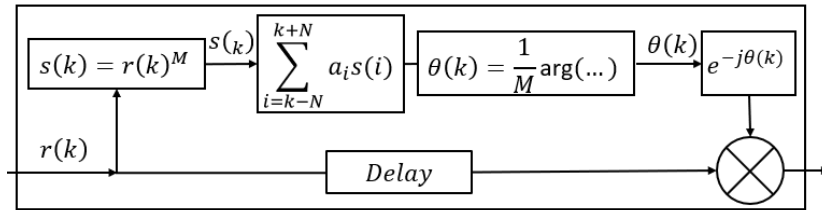
Fig. 2.22: Carrier Phase Estimation (Viterbi-Viterbi) [53]

In the first block of figure 2.22, the Viterbi-Viterbi algorithm takes the Mth power of the symbols in order to remove phase modulation from the phase modulated signal, with M as the number of phase states. As an example, in the case of QPSK, fourth power of symbols $r(k)$ are taken to remove phase modulation effect from the QPSK signal. In the second block, a running average is taken over the complex vector N pre-cursor and N post-cursor symbols [42]. Since OptSim takes averaging over the entire simulation window, this gives the argument at the third block, where the $1/M^{th}(1/4^{th}$ e.g. for QPSK) argument gives the phase correction factor $\theta(k)$. The phase correction factor $\theta(k)$ is then used to apply a correction to the original symbols [42].

Typically, if ASE is dominant, a larger number of symbols for carrier phase estimation is more optimal as this will average out the Gaussian noise and therefore obtain a better phase estimation [42]. On

the other hand, if cross phase modulation (XPM) is the main nonlinear impairment, then a smaller number of symbols is preferred as this allows better tracking of the fast change in phase offset [42].

Finally, the decision process is implemented for error counting and to provide aggregate flow of data. In figure 2.23, the output from the channel is fed to the Wiener filter, who's coefficients are optimized using Least Mean Squared Error (LMS) criterion. The LMS equalizer is a classical adaptive filter that can also be considered a stochastic gradient algorithm; its derivation is covered in [54]. The purpose of this filter is to remove any residual CD and ISI in the channel, and to output a single sample per symbol for detection. The LMS equalizer is used as part of the Directed Decision Algorithm (DDA).
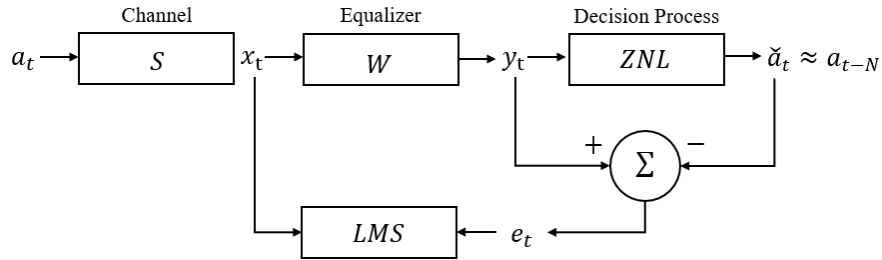
Fig. 2.23: *Decision Directed Algorithm (DDA) Block Diagram [54]*

In the Decision Directed Algorithm, there is a zero-order non-linear (ZNL) decision process after the equalizer that examines the equalizer output and replaces it with the closest channel input (a_t) values [42]. If the input sequence (a_t) is known, which is the case when a training sequence is transmitted, the classical approach is to use LMS ($[E(y_t - a_{t-N})^2]^2$) criterion to minimize error. In practice the input of the channel (a_t) is not known, so this two-step approach is used where the transmitter sends a known initialization sequence (training sequence) and the receiver performs the LMS criterion on the equalizer to find the tap weights for the filters [42]. The receiver then uses the output of the zeroth non-linear (ZNL) process as an estimate of the input (a_t) and performs the LMS criterion on the equalizer [42] – this comprises as the Decision Process as depicted in figure 2.23.

In Summary, the coherent system model recovers Jones matrix of the channel and applies its inverse to separate data on orthogonal polarizations. It then estimates local oscillator-to-signal phase to allow separation between in-phase (I) and quadrature (Q) signals for each polarization. Finally, error counting is applied to all four signals as well as averages related to aggregate flow. The drawbacks are that coherent optical systems are more complex to model compared to legacy intensity modulation/direct detection systems. The transmitter and receiver structures are more complex and there is more complex interplay of signal and noise. Additionally, the analytical or semi-analytical methods for BER estimation are often inaccurate, therefore, the only option is for direct error counting, which is time and resource consuming [42]. BER counting is explained in section 4.31, where the coherent receiver models used in OptSim simulations are described.

3   Optical Network Hierarchy

The optical network regions of focus in this study for high capacity transmission are those that accommodate for regional, long-haul and ultra-long-haul networks.
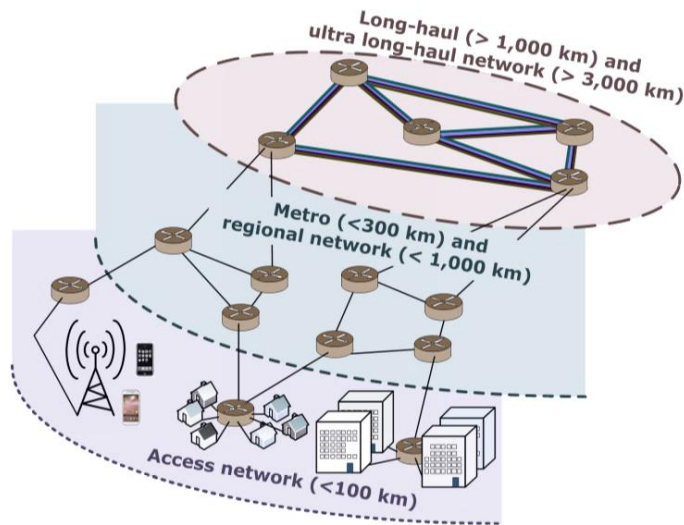
Fig. 3.24: Optical Network Hierarchy [3]

The lowest section in figure 3.24, the access network (< 100 km) represents connections for actual subscribers and is well-known as a fiber-to-the-x (FTTX) (where the "x" represents the home, office, curb or building) network. Previously these networks consisted of copper wire [55]. The optical fiber, depending on transmission distance is either single-mode or multi-mode fiber. Typical connections offer several Mb/s and up to 1 Gb/s, therefore, current limitations of FTTX originate from transmitter and receiver equipment, rather than optical fiber.

The next section above the access network, consisting of metro networks (<300 km) and regional networks (< 1000), connects cities to other cities or even smaller countries to other countries using single-mode fiber. Current communication systems in metropolitan and regional networks are evolving to operate up to 100 Gb/s and are projected to grow to 400 Gb/s and 1 Tb/s [56].

The highest tier consists of long-haul networks (>1,000 km) and ultra-long-haul optical transmission networks (>3,000 km). Transmission distances can reach over 10,000 km for transoceanic connections between United States of America and Asia, for example [57]. Therefore, the technology supporting the high data rates between these connections is pushing the limits of physical constraints of the links and limits of single-mode fiber as a medium.

4 OptSim Environment

The simulation of high capacity optical systems based on the methods described previously are completed using OptSim and utilize OptSim's features enabling coherent optical transmission systems, such as; PM-QPSK and PM-QAM transmitter/receiver components, DWDM/CWDM systems with optical amplification using EDFA, Electronic Dispersion Compensation (EDC) and coherent reception with Digital Signal Processing (DSP).

4.1 Time Domain Split Step Method

The Time Domain Split Step engine in OptSim is known as sample-mode in OptSim. In this method, in order to get the output, a linear convolution is done instead of circular convolution. The advantage is that there is no aliasing error and there is no assumption on the periodicity of signal and noise [58]. With regards to speed and efficiency, the TDSS method has a very small memory footprint because only one signal sample is propagated from one model to the next at a time, making TDSS very suitable for the simulation of long bit sequences. Simulation time linearly proportional to the number of simulated bits [58]. Furthermore, for coherent systems this is helpful in bit error rate (BER) counting down to $10^{-4} - 10^{-5}$ [10]. The TDSS method is based on the following formula:

$$\frac{\partial A(t,z)}{\partial z} = (L + N) \cdot A(t,z), \tag{4.1}$$

where $A(t, z)$ is the complex envelop, L is the operator which describes linear effects and N describes the impact of non-linear phenomena on signal propagation. The Split-Step algorithm applies L and N operators to calculate $A(t, z)$ over small fiber spans, ∂z separately [58]. The TDSS algorithm calculates L in the time domain by applying convolution in sampled time [58]:

$$A_L[n] = A[n] * h[n] = \sum_{k=-\infty}^{\infty} A[k] \cdot h[n-k], \tag{4.2}$$

Where h is the impulse response of a linear operator L.

4.2 Used Monitors

BER and OSNR are important metrics in measuring the performance of optical communications networks. In this thesis, most simulations include parametric scans of BER vs. OSNR using the pre-forward error correction Bit Error Rate (pre-FEC BER) of 10^{-3} (based on OptSim documentation [59]) as a threshold to determine the minimum OSNR requirements for a system.

4.2.1 Bit Error Rate

The Bit Error Rate (BER) is one of the most important measures of performance in high capacity optical transmission systems and the major basis of performance evaluation in the simulation sections. BER in

the simulations sections is accomplished by use of the coherent receiver models available in OptSim (section 4.3.1). In telecommunication transmission, the bit error rate (BER) is the percentage of bits that have errors (N_{error}) relative to the total number of bits (N_{total}) received in a transmission, as shown in equation 4.3 [60].

$$BER = \frac{N_{error}}{N_{total}} \qquad (4.3)$$

For example, a transmission might have a BER of 10^{-6}, meaning that, out of 1,000,000 bits transmitted, one bit was an error [60], indicating how often data must be retransmitted because of an error. The BER may be improved by choosing a strong signal strength (unless this causes cross-talk and more bit errors), by choosing a robust modulation or line coding scheme, and applying channel coding schemes such as redundant forward error correction codes [60].
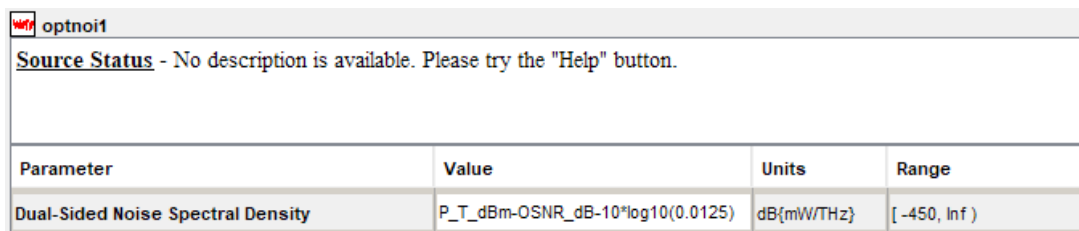
The transmission BER is the number of detected bits that are incorrect before error correction, divided by the total number of transferred bits (including redundant error codes) [60]. This is referred to as the pre-forward error correction BER (pre-FEC BER), and as per OptSim documentation [59], the threshold used for satisfactory transmission is 10^{-3} pre-FEC BER.

4.2.2 Bit Error Rate vs. Optical Signal-to-Noise Ratio

The receiver sensitivity (BER vs. OSNR) functions are obtained from parameter scans to produce correlation diagrams used in the presented results. OSNR represents the ratio of optical power of the signal to noise in dB. The OSNR for simulations is measured over a bandwidth of 12.5 GHz, typical for spectrum analyzers [10]. The noise spectral density is calculated as:

$$noise\_spectral\_density[dB\left(\frac{mW}{THz}\right)] = P\_T\_dBm - OSNR\_dB - 10 * log10(0.0125), \qquad (4.4)$$

Where P_T_dBm is the transmitted (signal) power measured in dBm, $OSNR\_dB$ is a parameter representing the target signal to noise ratio in dB, and $0.0125\ THz$ equal to 12.5 GHz, is the bandwidth over which the noise is measured [10]. Optical noise is injected by the white noise generator module, called, *optnoi1* (Fig. 4.25), which generates a spectrally flat (over the entire simulation bandwidth) Gaussian random process [10]. The noise density is double sided, which adds the same amount of noise power whether single or double polarization.

optnoi1			
Source Status - No description is available. Please try the "Help" button.			
Parameter	**Value**	**Units**	**Range**
Dual-Sided Noise Spectral Density	P_T_dBm-OSNR_dB-10*log10(0.0125)	dB{mW/THz}	[-450, Inf)

Fig. 4.25: OptSim White Noise Generator & Parameters

4.3 OptSim Features

The coherent receivers used in this thesis enable the use of multi-level modulation formats and provide DSP functionality and bit error counting. The fixed power amplifier model accounts for amplified spontaneous emission throughout cascading EDFAs and the Ideal Dispersion Compensator compensates for dispersion in the electronic domain.

4.3.1 Coherent Reception

The dynamic receiver models, shown in figure 4.26, are all utilized at the receiver in section 5.1 for the comparisons of advanced modulation formats. The QPSK and 16QAM dynamic receiver models are then used in most other simulations.
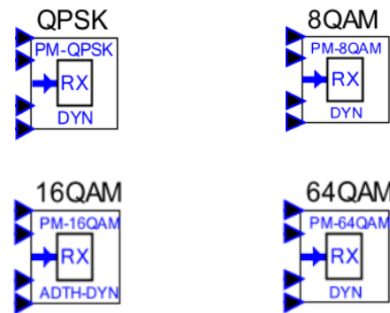
Fig. 4.26: Coherent Receiver Models with BER Counting [61]

The LMS Dynamic Training Sequence and Tracking Based Receivers, are dynamic receivers for coherent polarization multiplexed modulation formats. The receivers decompose a signal into data frames of length $N_{sym,frame}$ (Fig. 4.27) [61]. At the beginning of each frame a $N_{sym,ts}$ number of symbols is used as training sequence to calculate the initial equalization coefficients [61]. During the decision driven phase, the received symbols are considered error free and used to adjust the equalization coefficients and as a result, can follow the dynamic variations of the channel [61].

Fig. 4.27: Received Data Frame [61]

Then the LMS algorithm is used to calculate the initial equalization coefficients during the training sequence and update their values during the decision driven phase (Fig. 4.28) [61]. Equalization is calculated recovering the Jones matrix of the entire channel, including the phase mismatch with respect to the receiver local oscillator, and applying its inverse in order to separate data flows transmitted on orthogonal polarizations [61]. This component, besides recovering polarization and phase rotations, compensates for pattern dependent phenomena such as residual chromatic dispersion and PMD [61]. After the application of equalization, the threshold decision is performed on the four resulting signals and error counting is applied [61].
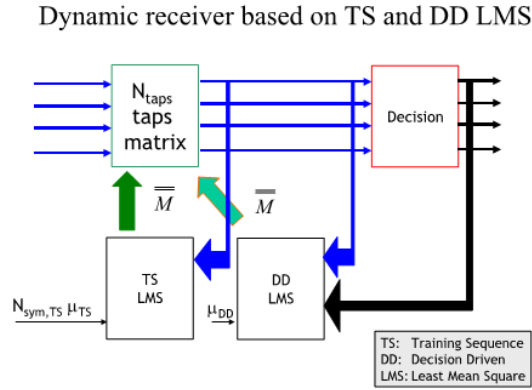
Fig. 4.28: Dynamic Receiver Based on Training Sequence and Decision Driven [61]

In order to properly estimate a certain BER level OptSim suggests simulating a proper number of bits to allow counting tens of error [42]. For example, if it is expected to operate around a pre-FEC BER $= 10^{-3}$, OptSim suggests simulating 2^{15} or 2^{16} symbols in addition to the training sequence [61]. Therefore, some of the simulations in this thesis take hours or up to an entire day to simulate, depending on the total distance of fiber spans, the number of channels as well as the number of steps included in parameter scans.

4.3.2   EDFA Models

The two amplifier models used in this work are the Fixed Gain Amplifier model and the Fixed Power Amplifier model. The fixed gain amplifier model is used to compensate for signal loss in optical fibers, as such, this model is utilized within the loop iteration components consisting of SMF spans and EDFAs. In the fixed power model, which is used on the transmitting and receiving ends of the system layouts, the amplifier gain is set in order to keep the total output power constant. In both cases, the evaluation of output optical power accounts for internally generated ASE noise that appears at the output of EDFAs [62]. Properties of ASE can be modified by nonlinear interactions during fiber propagation [62]. This has interesting implications in long-haul transmission systems where multiple stages of fixed-gain amplifiers are used to fully compensate for SMF span loss, thereby maintaining the channel power value. However,

since each amplifier adds its own internally generated ASE to the optical signal, total power (signal plus noise) along the link will increase with accumulating noise (Fig 4.29). This noise build-up reflects in optical signal to noise ratio (OSNR), which degrades with every amplifier along the propagation path [62].
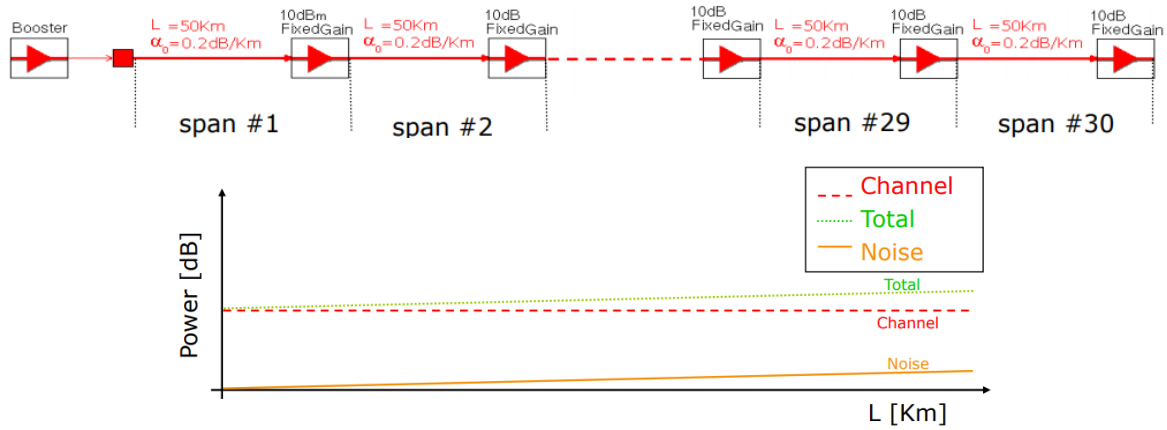
Fig. 4.29: Fixed Power Amplifier Model [62]

4.3.3   Ideal Dispersion Compensator

The ideal electronic dispersion compensator (EDC) component is used in most simulations that incorporate PM-QPSK and PM-16QAM modulation formats in this thesis. The EDC requires four electrical input signals and four electrical output signals [61]. The input signals must derive from a coherent homodyne receiver and are the in-phase and quadrature components on the two polarizations of the incoming received optical field [61]; as is the case with the PM-QPSK and PM-16QAM systems used in the majority of simulations performed in this work. The implemented EDC applies the same amount of compensation on signals deriving from both polarization components [61]. The compensated value applies a negative dispersion in $\frac{ps}{nm}$ and can be based on the number of fiber spans and their distance in km, as shown in figure 4.30.
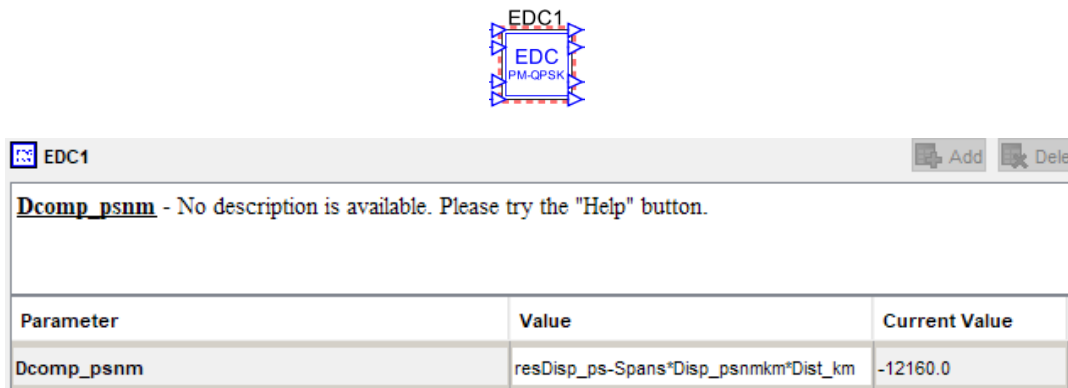
Fig. 4.30: Electronic Dispersion Compensator & Parameters

28

4.4 Transmitter & Receiver Structures

This section provides descriptions of the transmitter and receiver components used in the simulations.

4.4.1 PM-QPSK Transmitter & Receiver Structures

Fig. 4.31 provides details regarding the internals of the PM-QPSK transmitter components, *TX1*.
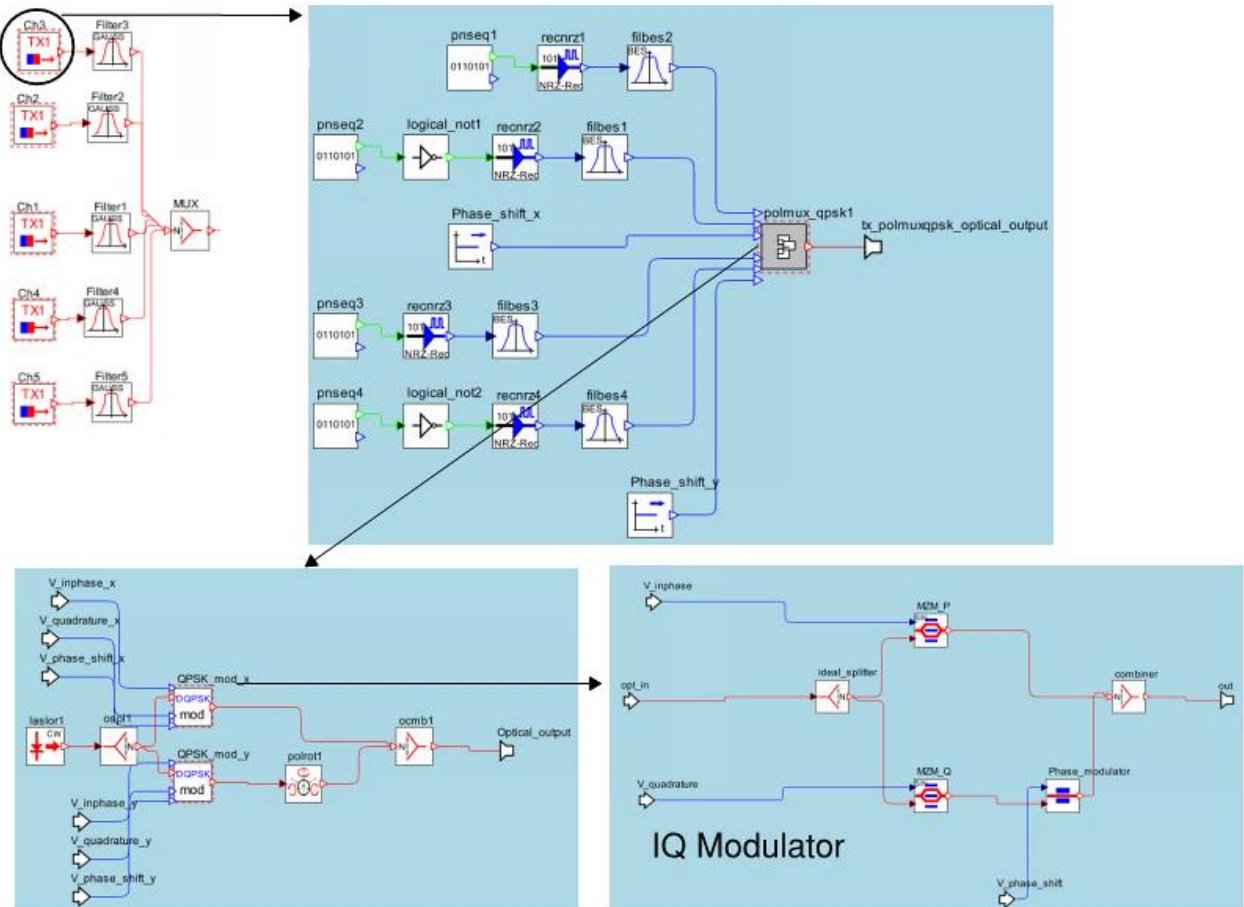
***Fig. 4.31:** PM-QPSK Transmitter Structure with 2 Data Sources for Each Polarization*

The transmitter implements the data source (labeled *pnseqx*) simulates the pseudorandom bit sequence at the specified bit rate in Gbit/s (typically 28-32 Gbit/s). The driver (labeled *recnrzx*) simulates the non-return-zero (NRZ) rectangular driver which has an electrical output signal which can assume one of the two electrical levels depending on the transmitted bit e.g. when a "1" is fed into the driver, the output signal is at the low level during the entire bit time [63]. When a "0" is fed into the driver, the output signal is at the high level during the entire bit time [63]. The laser source (laslor1) models the transmitter's continuous wave (CW) laser source configured based on central wavelength and power [63]. The CW Lorentzian laser also maintains the output state of polarization aligned so that it is compatible with the polarization rotator [63]. The Mach-Zehnder modulator (*MZMx*) is used to create the

29

transmitter's phase-modulated output signal and the Optical Phase Modulator (Phase-modulator) changes the phase of the input signal as a function of the electrical driving voltage [63]. The PM-QPSK receiver structure also follows the basic schematic mentioned in section 2.6.2 as depicted in figure 4.32.
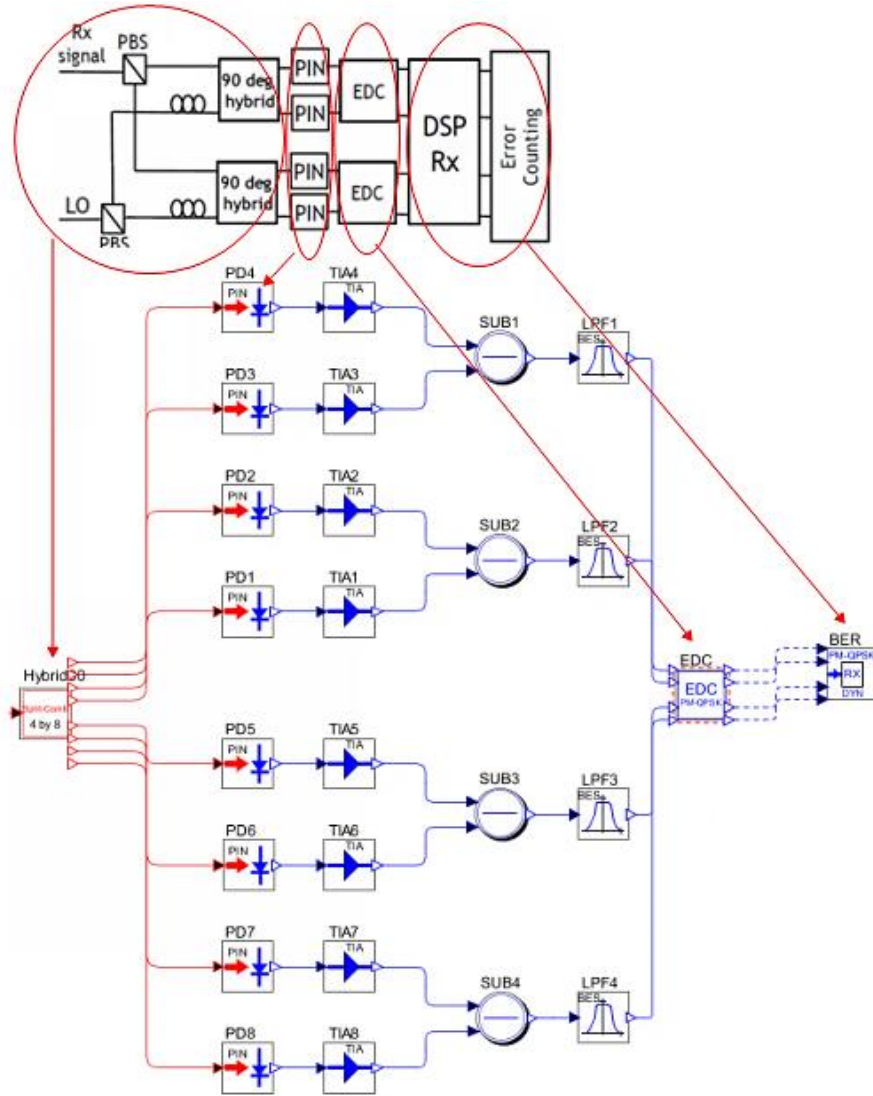
Fig. 4.32: PM-QPSK Receiver Structure with PM-QPSK Dynamic Receiver

In figure 4.32, the photodiode (labeled *PDx*) handles the opto-electrical conversion, the trans-impedance amplifier models the trans-impedance amplifier as white Gaussian noise added at the input signal, the electrical subtractor (labeled *SUBx*) subtracts the two incoming signals resulting in electrical output signal, and the low pass filter (labeled *LPFx*) implements the low pass Bessel filter for modeling the non-ideal characteristics of the binary-to-electrical conversion [63]. The electronic dispersion (EDC) component feeds into the dynamic receiver component (labeled as *BER)*. This dynamic receiver component (labeled as *BER*) is utilized most simulations, unless otherwise specified, as higher bit rates at longer distances can be obtained using dynamic reception.

Figure 4.33 describes the component labeled as "*Hybrid90*" in figure 4.32 and is a single-ended 90-degree hybrid and is chosen here as it includes a local oscillator with 4+4 outputs for balanced photodiode configuration, necessary for coherent reception [61]. The input optical signal is split into the two polarization x' and y' components by a polarization beam splitter (PBS) [61] as described in section 2.6.1. The two resulting signal components are sent to two 90-degree hybrid that mixes the received signals with the LO reference carrier, producing four outputs shifted by from each other by $180°$ for each polarization, as described in section 2.6.1. Inserting the photodetectors (labeled as *PDx* in the previous Fig.4.32) at the four output ports 1,3,5,7 or 2,4,6,8 are used to obtain four electric current signals proportional to the mentioned four components of received optical signal, allowing coherent detection.
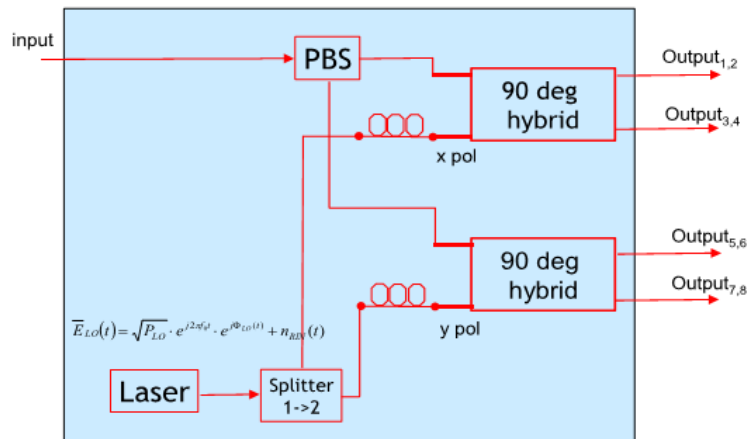
Fig. 4.33: *Diagram of 90 Degree Hybrid OptSim Component [61]*

4.4.2   PM-16QAM Transmitter & Receiver Structures

The next figure 4.34 provides details regarding the internals of the PM-16QAM transmitter compound components, *TX1*. The PM-16QAM transmitter structure comprises of a similar structure and components used in the PM-QPSK transmitter, except that four data sources are required to generate the symbol for each polarization for the 16QAM constellation. Also, for the PM-16QAM system, gray encoding using the XOR operators (Fig. 4.34), is used to ensure that input logical values that differ by a single bit are translated into adjacent electrical levels [63]. The result provides the 16QAM constellation. Finally, the x and y phase shifts labeled (*Phase_shift_x* and *Phase_shift_y*) provide the two polarization states.
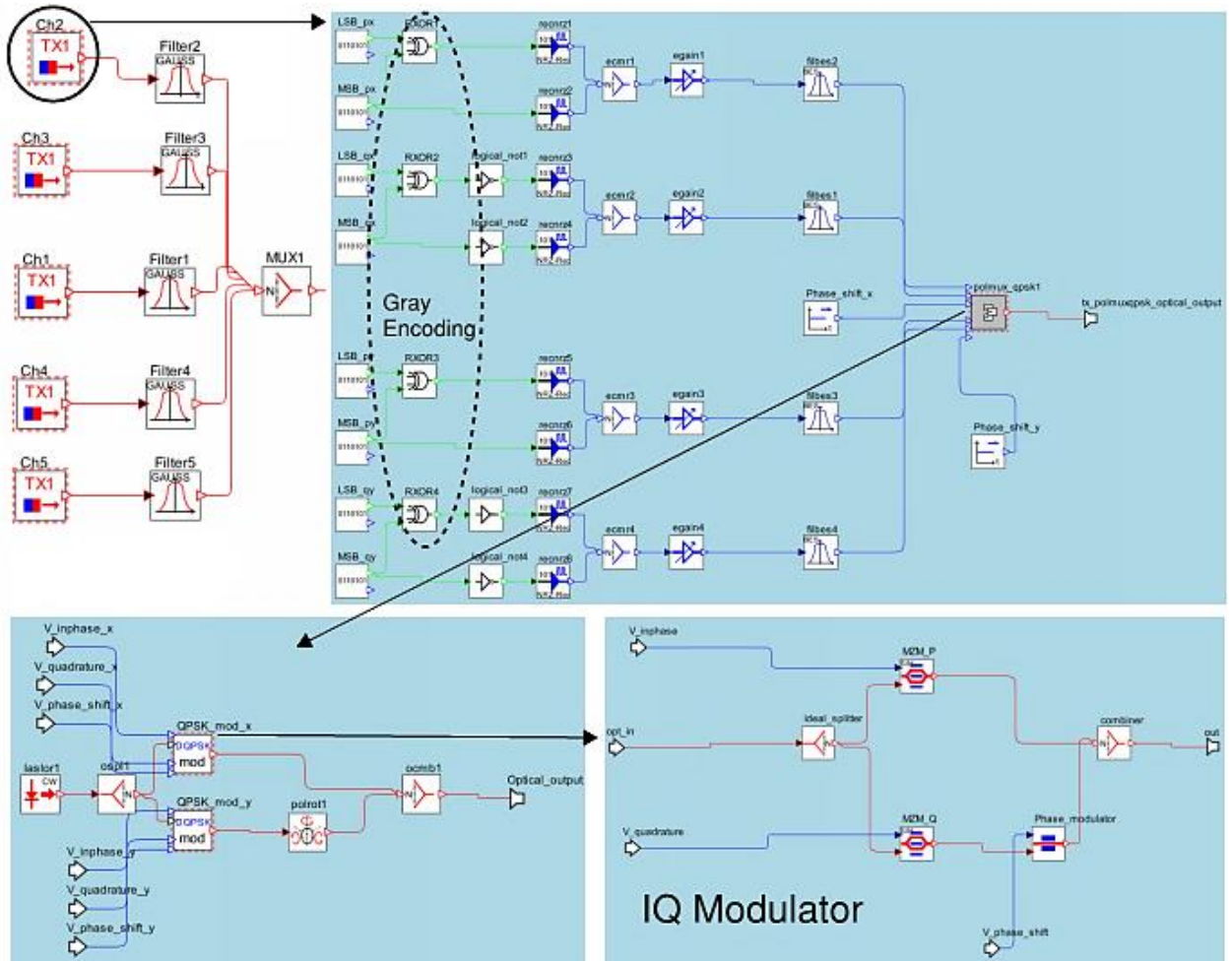
Fig. 4.34: *PM-16QAM Transmitter Structure with 4 Data Sources for Each Polarization*

In reference to the PM-16QAM receiver structure shown in figure 4.35, the receiver can be encapsulated in a compound component, and as such in some schematics shown in the simulations sections for the purpose of saving space. Here it is labeled as *LO_Hyb_PD1*. Most of the same components utilized in the PM-QPSK receiver can be used for the PM-16QAM receiver, as described in section 2.6.2. The major difference lies in the parameters of the PM-16QAM dynamic receiver component account (labeled as *Rx1*), which accounts for the four data sources for each polarization in comparison to two data sources for each polarization as in the PM-QPSK transmitter/receiver structures [61]. The electronic dispersion compensation module (*EDC1*) is used prior to the dynamic receiver (*Rx1*) for coherent PM-16QAM modulation based on training sequence and LMS algorithm, as described in section 4.3.1.
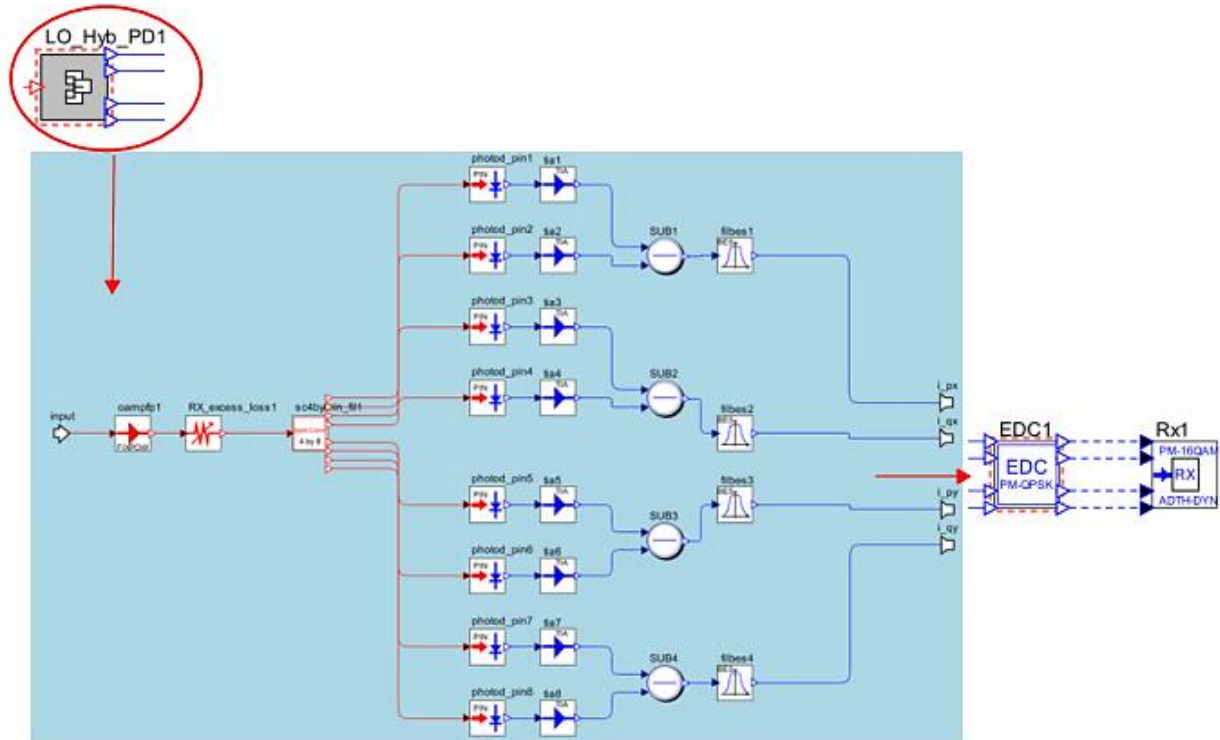
Fig. 4.35: *PM-16QAM Receiver Structure with PM-16QAM Dynamic Receiver*

4.4.3   PM-8QAM & PM-64QAM Transmitter & Receiver Structures

For the transmitter and receiver structures for PM-8QAM and PM-64QAM (figures 4.36 – 4.39), the obvious required adjustments lie in the required number of transmitted data sources to create the constellations.

One additional feature utilized in the PM-64QAM transmitter is the "*8QAM MOD*" component (Fig. 4.38) that is used as an NRZ electrical driver with Gray Encoding built-in. This component is used to implement the electrical NRZ driver for 8QAM performing gray encoding on the three incoming logical signals. The three input logical signals are mapped onto eight electrical output levels. As for PM-16QAM, gray encoding ensures that input logical values that differ by a single bit are translated into adjacent electrical levels [63]. Also, the parameters of each receiver structure (section 4.3.1) account for the required number of transmitted data sources multiplied by two polarization states (section 4.4.1). For PM-8QAM three data sources are multiplied by two polarization states, thus accounting for the six total data sources (labeled *PRBSx*) used in the transmitter structure shown in figure 4.36.
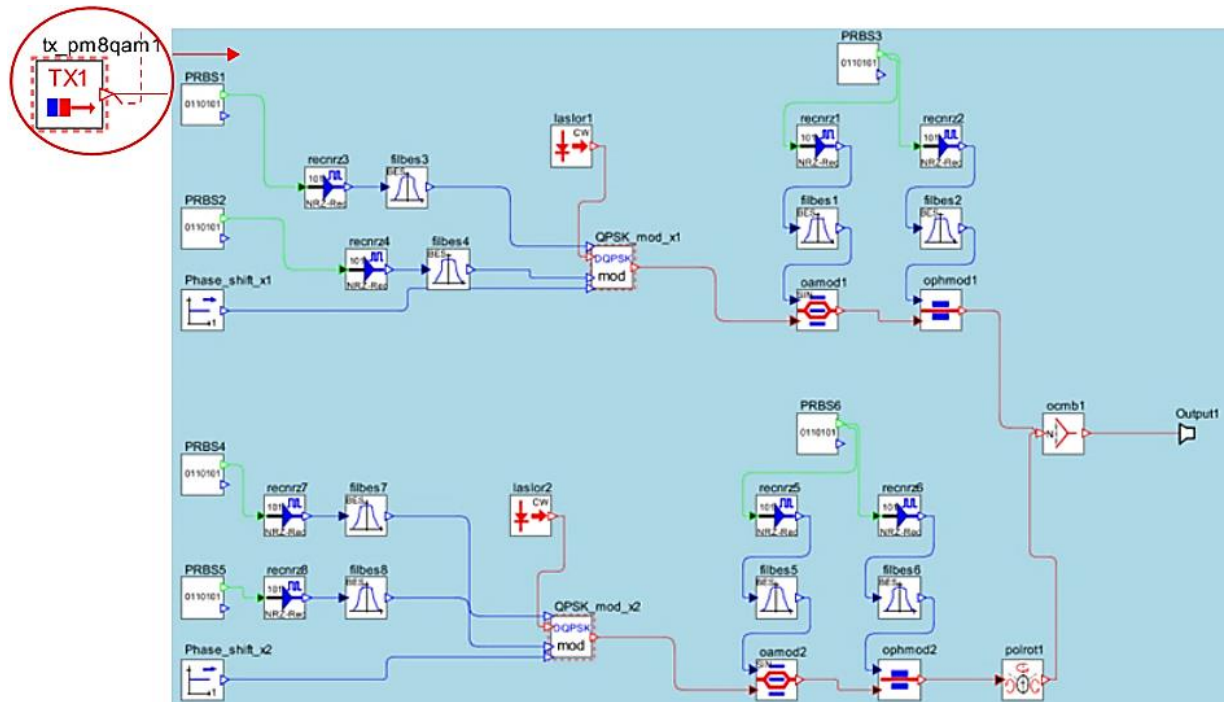
Fig. 4.36: *PM-8QAM Transmitter Structure with 3 Data Sources for Each Polarization*
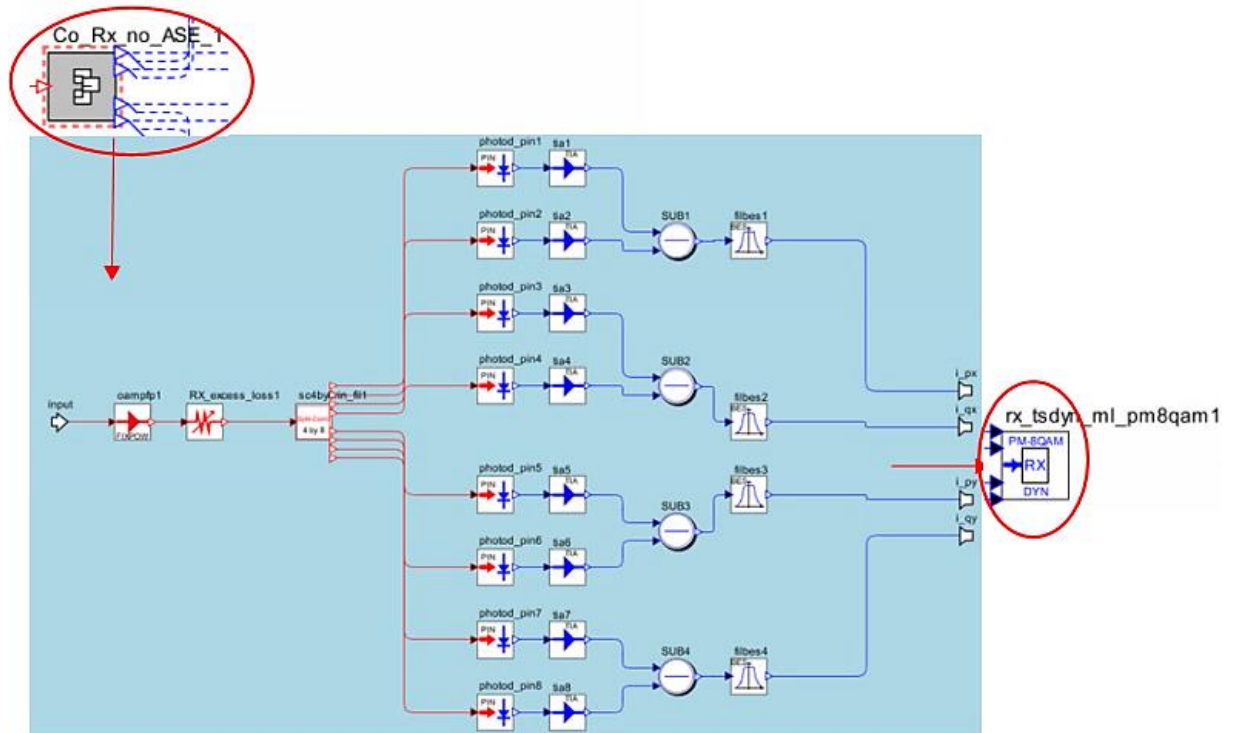
Fig. 4.37: *PM-8QAM Receiver Structure with PM-8QAM Dynamic Receiver*

34
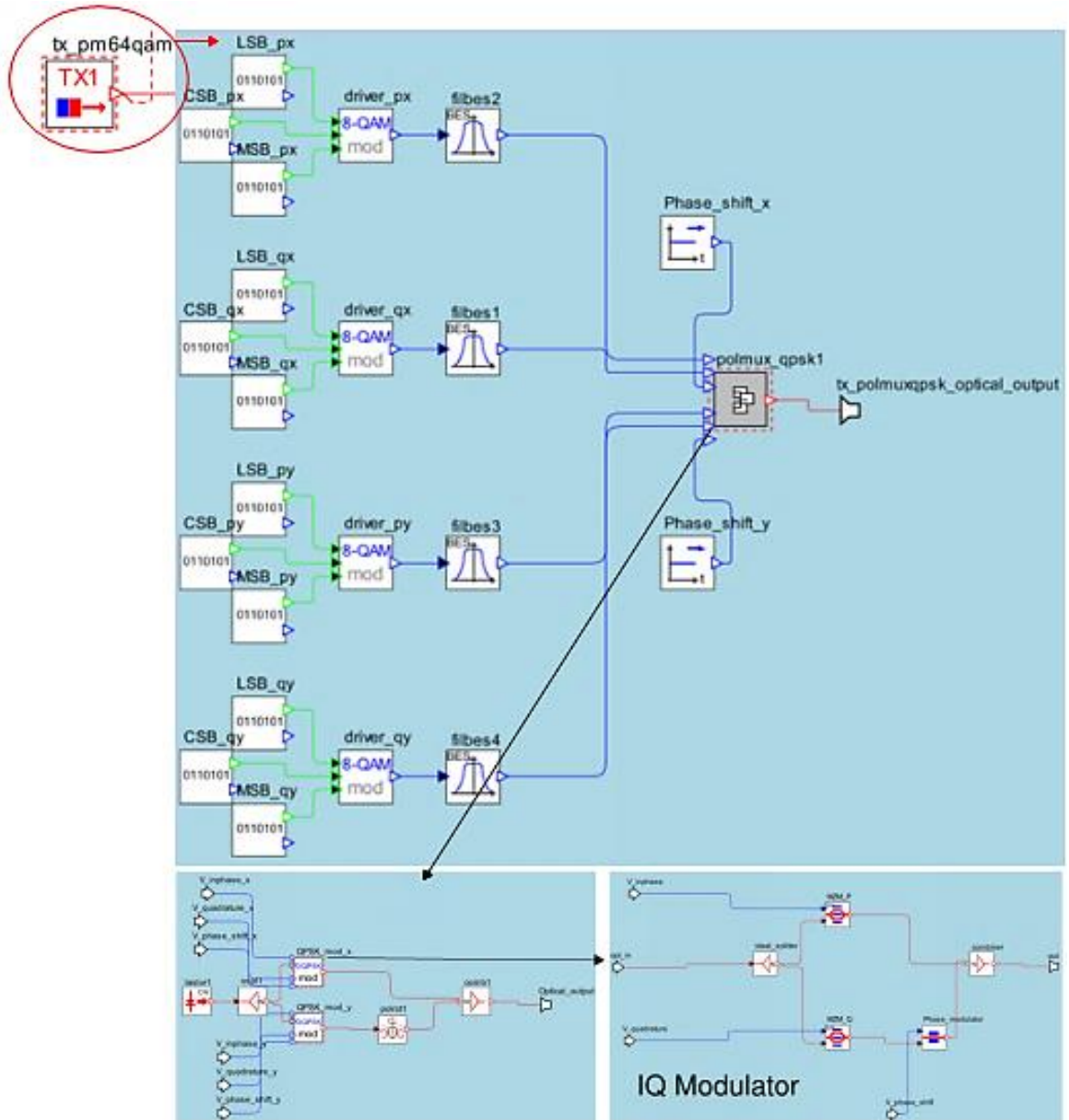
Fig. 4.38: *PM-64QAM Transmitter Structure with 6 Data Sources for Each Polarization with "8-QAM MOD" Components*
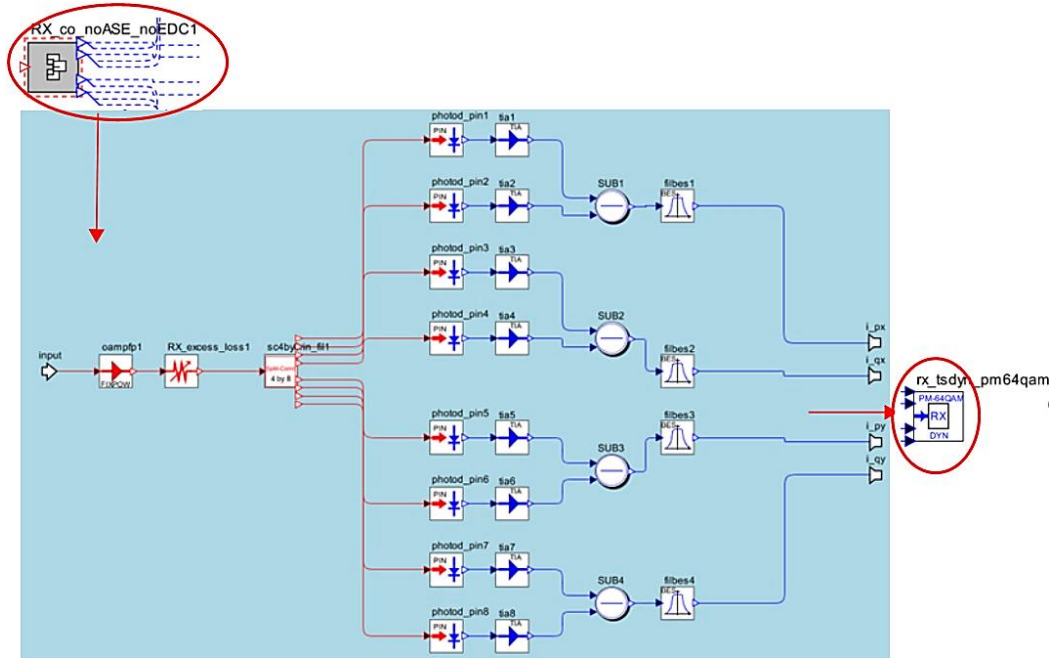
Fig. 4.39: PM-64QAM Receiver Structure with PM-64QAM Dynamic Receiver

It should be noted that the PM-8QAM and PM-64QAM transmitter and receiver structures described in this section do not incorporate the use of electronic dispersion compensation (EDC) components as this component is not utilized for their simulation. PM-8QAM and PM-64QAM systems are simulated in this work for the sole purpose of receiver sensitivity comparisons (section 5.1), therefore, the EDC component is not needed.

5   Simulations of High Capacity Optical Systems

Polarization multiplexing of QPSK and QAM modulation formats, wavelength division multiplexing (WDM), coherent receivers with digital signal processing (DSP) and electronic dispersion compensation; all methods previously described, are employed in the following sections in order to analyze the physical limitations and trade-offs between spectral efficiency and reach. For each simulation, the purpose is described along with the top-level schematic to provide a visual aid to the description along with featured parameters; baud rate, number of channels, and channel spacing, etc. The results often include parameter scans with BER vs. OSNR (receiver sensitivity) correlation diagrams as the performance monitor for most simulations. Tables are provided which represent the results of the parameter scans and the comments that follow outline the results and often lead into the purpose of the next simulations.

5.1   Receiver Sensitivity Comparisons

In order to isolate modulation formats most suitable for high-capacity (potential for 400G), long-haul transmission and for comparison against the proven performance capabilities of PM-QPSK; this set of

simulations focuses on the noise resiliency/sensitivity (BER vs. OSNR) of PM-8QAM, PM-16QAM and PM-64QAM receiver models against a PM-QPSK model. This analysis provides an example of the consequence of higher OSNR requirements required to achieve a certain bit rate.

The figures 5.40 and 5.41 are layouts of the PM-QPSK system, and the same layout shown is used for the PM-8QAM, PM-16QAM and PM-64QAM systems, where these QAM systems differ only in the transmitter and receiver components used that were described in section 4.4.2 and 4.4.3. Each system uses the same components without fiber spans to focus on receiver sensitivity. The transmitted power for each fixed power amplifier in each system is set at 0 dBm and the receiving power at the fixed power amplifier is set at 5 dBm for each. The transmitters for the PM-QPSK, PM-8QAM, PM-16QAM and PM-64QAM systems include 2, 3, 4 and 6 data sources, respectively. The Dynamic Receivers (section 4.3.1) account for the respective number of data sources for coherent detection and bit error rate counting. The "SCATD_IX" components included are used to obtain scattering diagrams of the in-phase and quadrature signals at the output of the transmitter and another at the receiver to see noise effects at the receiver.
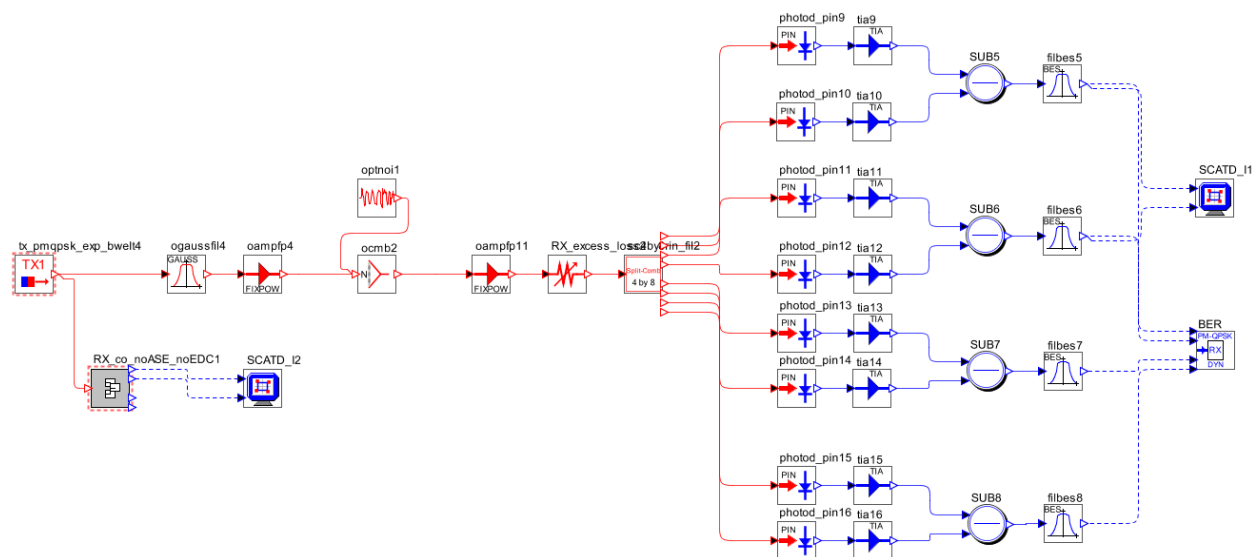
Fig. 5.40: PM-QPSK System Layout
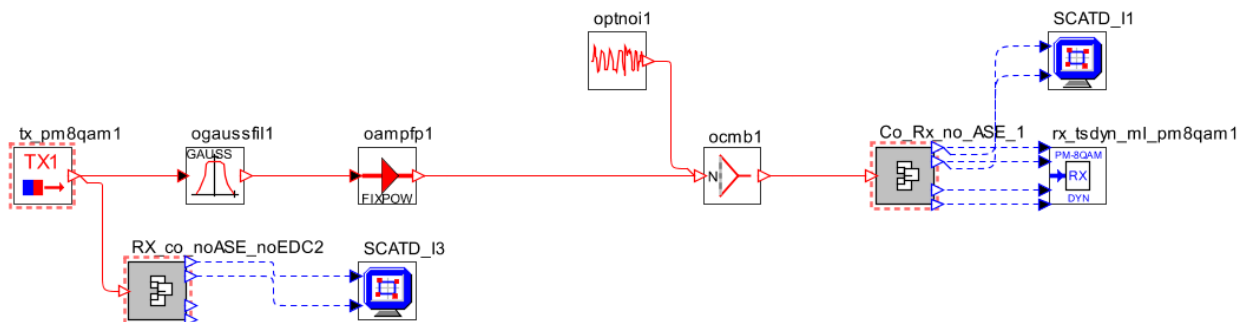
Fig. 5.41: PM-8QAM, PM-16QAM & PM-64QAM System Layouts (The Top-Level Layout is the Same for Each)

37

The number of points shown in the scattering diagrams, obtained from the *SCATD* components at the transmitter outputs, figure 5.42 (a – d), correspond to constellation points of the modulation format. Figure 5.42 (e – h), represent scattering diagrams obtained from the *SCATD* components at the receivers describe visually how noise affects each system. The higher number of constellation points (4 points for QPSK, 8 for 8QAM, 16 for 16QAM and 64 for 64QAM), the lesser the spacing between the symbols, hence the higher the OSNR required to recover the signal.
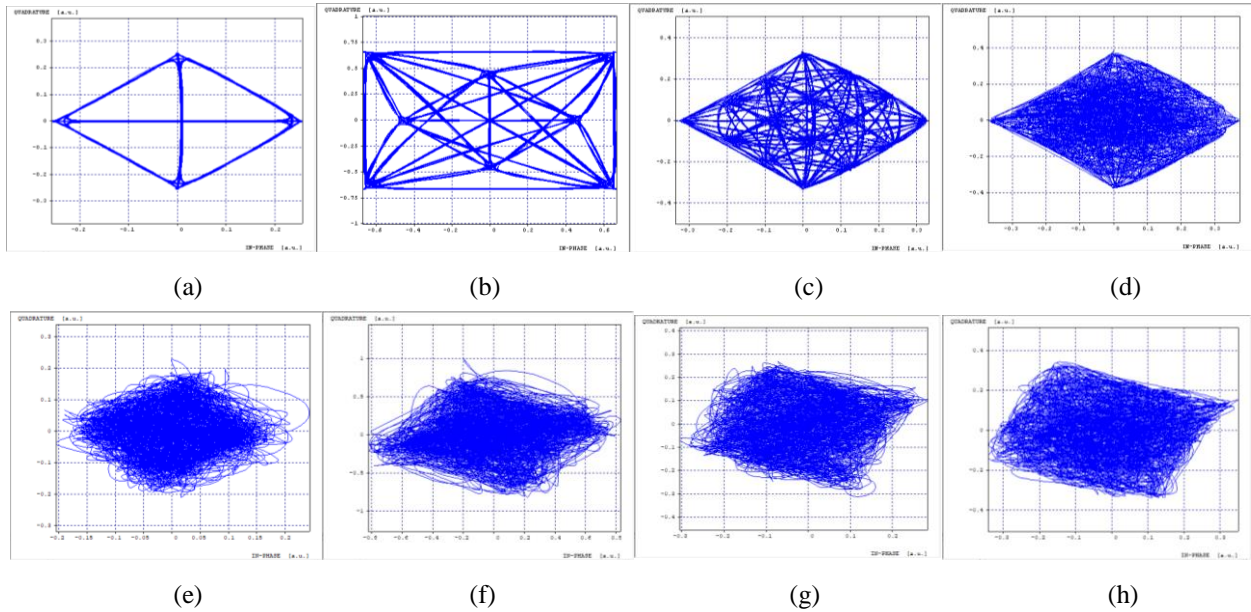
Fig. 5.42: *Scattering Diagrams at the Transmitter (a – d): a) PM-QPSK b) PM-8QAM c) PM-16QAM d) PM-64QAM & Receiver with Noise (e – h): e) PM-QPSK f) PM-8QAM g) PM-16QAM h) PM-64QAM*

The differences in the scattering diagrams can be seen at the edges of the scattering where the density of the scattering increases and is more contained on the edges as the density of each constellation increases for each system, from PM-QPSK, to PM-8QAM, PM-16QAM and finally PM-64QAM in the last diagram. The resiliency to this noise for each is shown in the BER vs. OSNR performance (Fig. 5.43).

The system symbol rate for PM-QPSK is 28 Gbaud and for each QAM system is 32 Gbaud, with 20 number of samples per symbol. The total data rate for each system is listed in table 5-2 and increases based on the number of data sources.

Table 5-2: *Total Bit Rate for Each Modulation Format*

Modulation Format	Symbol Rate (Gbaud)	Data Sources	Polarizations	Total Data Rate (Gb/s) = Symbol Rate*Data Sources*Polarizations
PM-QPSK	28	2	2	**112**
PM-8QAM	32	3	2	**192**
PM-16QAM	32	4	2	**256**
PM-64QAM	32	6	2	**384**

The receiver sensitivity (BER vs. OSNR) curves are obtained from parameter scans and are shown in figure 5.43. The results of the four modulation formats are overlaid into one graph, which helps to describe the capacity verses noise resiliency exhibited in each modulation format.
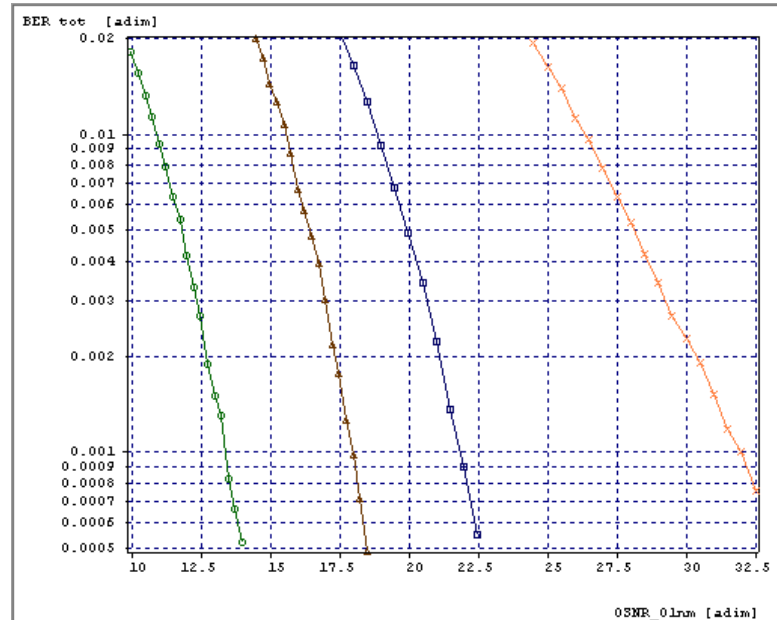
Fig. 5.43: *Receiver Sensitivities: PM-QPSK (Green), PM-8QAM (Brown), PM-16QAM (Blue), & PM-64QAM (Orange)*

These four curves confirm that the denser the constellation, the higher the OSNR required to achieve a desired bit error rate (BER). Trade-offs are outlined in terms of their potential for long-haul transmission, which is better suited with resiliency to noise at the receiver (lower required OSNR), and scalability, which requires high capacity transmission in terms of bit rate.

The PM-QPSK system is the most resilient to noise, confirming its suitability for long-haul distances. For this receiver model, in order to achieve the target pre-FEC BER of 10^{-3}, the required OSNR is only 13 dB. However, the total bit rate is the lowest out of all systems at 112 Gb/s and is the reason for exploring QAM modulation formats and their potential applications. Of course, while considering the use of PM-QAM modulation formats, the scalability and noise resiliency of PM-QPSK systems should be considered as well, especially when looking at specific applications, such as ultra-long-haul transmission links.

Although PM-8QAM is the most resilient to noise out of the three QAM modulation formats, but its total bit rate is the lowest of the three QAM systems at 192 Gb/s and for a target pre-FEC BER of 10^{-3}, the required OSNR is almost 18 dB. PM-8QAM could be implemented for long-haul transmission with high-bit rates. But, when comparing this to the performance of PM-QPSK, which achieves the same target BER at only 13 dB, PM-8QAM may not be the most compelling option in terms of scalability given the

proven stability of PM-QPSK at larger distances. Also, the required OSNR trade-off for obtaining higher bit rates using PM-16QAM may be worth considering for current industry topics, such as Nyquist WDM Super-channels.

For PM-16QAM, in order to reach the target pre-FEC BER of 10^{-3}, the required OSNR is about 21 dB. However, the capacity is 256 Gb/s, which is double in comparison to PM-QPSK. Comparing this with the OSNR requirement sacrificed, 21 dB for PM-16QAM and 13 dB for PM-QPSK, we gain 256 – 112 = 144 Gb/s in capacity as a trade-off for a higher OSNR requirement. The main point from this comparison is that in terms of achieving greater capacity at the consequence of less noise resiliency, there is more to gain in using PM-16QAM in comparison to PM-8QAM in terms of future requirements. Therefore, I have omitted considering PM-8QAM for further analysis in consideration for long-haul high-capacity transmission.

The PM-64QAM system demonstrates high bit rate capability at 384 Gb/s, but very little scalability due to its very high sensitivity to noise requiring an OSNR over 30 dB in order to achieve the target pre-FEC BER of 10^{-3}. The high capacity potential of PM-64QAM is very compelling, so in order to better understand these capabilities and consequences of its low noise resiliency, the next simulation includes an 80 km fiber span with BER vs. OSNR analysis.

5.1.1   PM-64QAM Simulation with Fiber Span

One fiber span of 80 km with EDFA amplification is included in order to better understand the limitations of implementing PM-64QAM in terms of distance and noise penalties. As shown in figure 5.44, the fiber span and EDFA is included within the SMF_EDFA1 component.
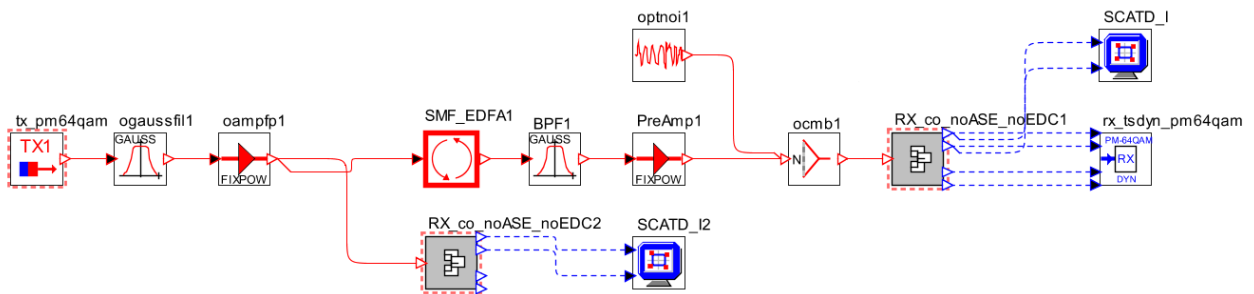
Fig. 5.44: *PM-64QAM System with 80km Fiber Span*
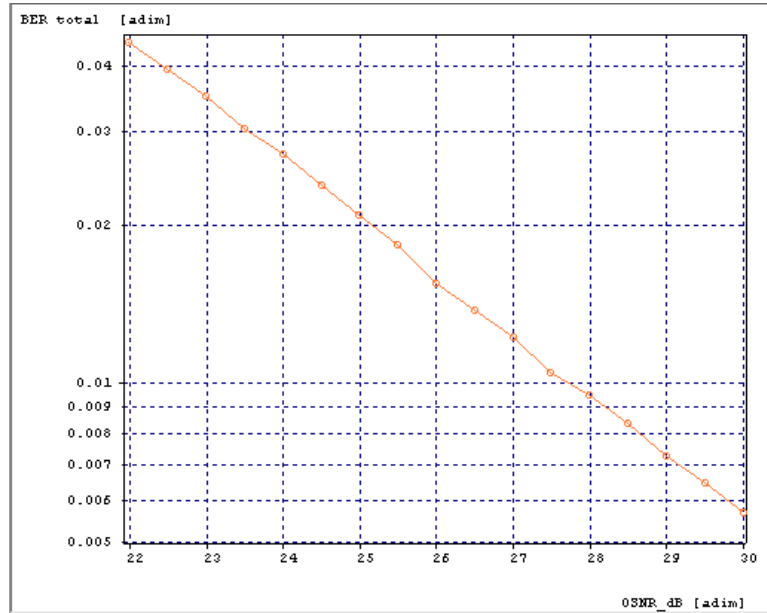
Fig. 5.45: PM-64QAM Receiver Sensitivity (BER Vs. OSNR) with 80km Fiber Span

The scattering diagrams in figure 5.46 illustrate the amount of noise induced at the receiving end in comparison to the scattering diagram at the output of the fixed power optical amplifier without noise (prior to the fiber span). The scattering diagram on the left is without noise and the diagram on the right is with noise after the 80 km fiber span and EDFA amplification.
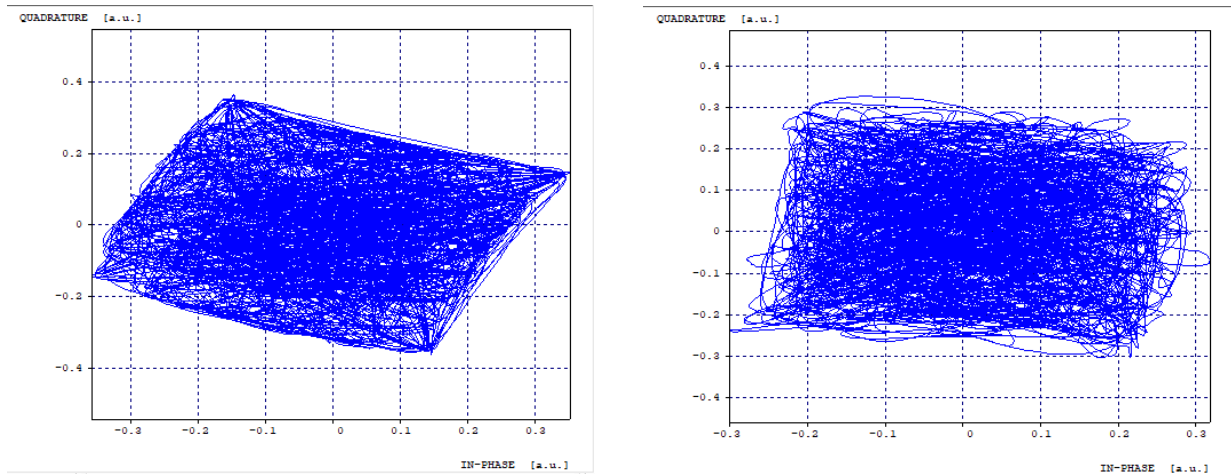
Figure 5.46: PM-64QAM Signal Scattering Diagram Without Noise (Left) and With Noise After the 80km Fiber Span with EDFA (Right)

This simulation demonstrates that PM-64QAM systems can achieve high data rates, however, given its even higher sensitivity to noise, after only an 80 km fiber length, this system will not be ideal for long haul transmission as the target BER is not achieved (Fig. 5.45). For this reason, the following subsections 5.2.1 and 5.2.2 demonstrate the potential of PM-16QAM for high capacity long-haul transmission.

41

5.2   PM-16QAM for Next Generation Optical Transport

In order to meet increasing spectral efficiency demands and data rates up to 400G, 16-QAM is often considered as the next most logical step from QPSK with 16-QAM coherent transceivers already commercially available [32]. With high spectral efficiency, it is shown that reduced transmission reach is unavoidable, due to the high OSNR requirements.

5.2.1   Two Channel 400G PM-16QAM System

The following system demonstrates the performance capabilities of PM-16QAM at metro and/or long-haul distances utilizing 2-channels totaling to 400 Gb/s (512 Gb/s including FEC overhead) spaced 45 GHz apart. According to the OIF, the minimum required reach for 400G must be above 1000 km [1]. Additionally, according to the OIF, coherent 2x200G PM-16QAM systems may achieve a reach as low as 400 km, which is clearly insufficient for long-haul application requirements, with a total spectral occupancy of 75 GHz over DCF-free G.652 fiber transmission using purely EDFA amplification [1]. A similar setup is used here, however, a larger total spectral occupancy of 90 GHz (45 GHz per channel) is used to achieve longer reaches, in comparison to 75 GHz spacing as mentioned by the OIF, with EDFA only amplification. The purpose is to explore longer distances than the 2x200G system referenced above.

The following simulations include BER vs. OSNR sensitivity scans at different transmitted powers of systems for 640 km, 1040 km and 2000 km fiber lengths in order to investigate the physical limitations of this 400G PM-16QAM system. The results include individual parametric scans for each system with transmitted power levels of; -5 dBm, 0 dBm and 5 dBm. These results are included within a table and are then discussed in further detail. Another parametric scan at -3 dBm for each transmission distance is included with the plots overlaid on each other for a better visual aid. The schematic of the system is included in figure 5.47.
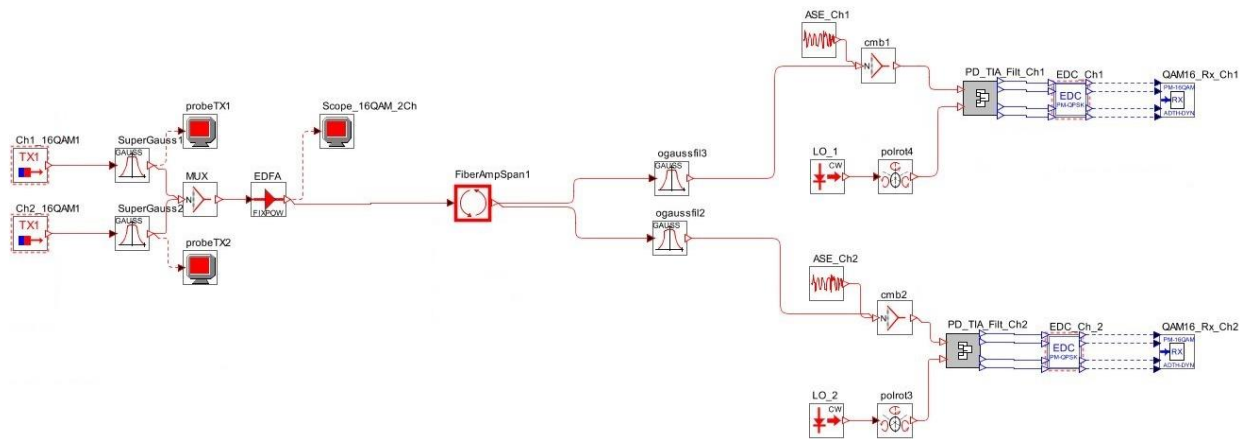
Fig. 5.47: 400G, Two Channel, PM-16QAM system

This system consists of two 16QAM channels, 80-km spans and EDFAs (8 spans for the 640 km system, 13 spans for the 1,040 km system, and 25 spans for the 2,000 km system), demultiplexer, and receivers comprised of 90-degree hybrids with local oscillators, balanced pairs of photo-diodes (PD), trans-impedance amplifiers (TIA), electronic dispersion compensation (EDC), and PM-16QAM dynamic receiver structure (section 4.4.2). The dual-sided noise spectral density parameter in the optical noise generator model is defined as an expression in terms of OSNR to facilitate parameter scan over OSNR. A total of 300,000 bits are transmitted per channel for reliable counting of the bit error rate. Transmitters, "Ch1/2_16QAM" consist of the components from section 4.4.2. The transmitted two-channel spectrum spaced at 45 GHz prior to EDFA amplification, is shown in figure 5.48.
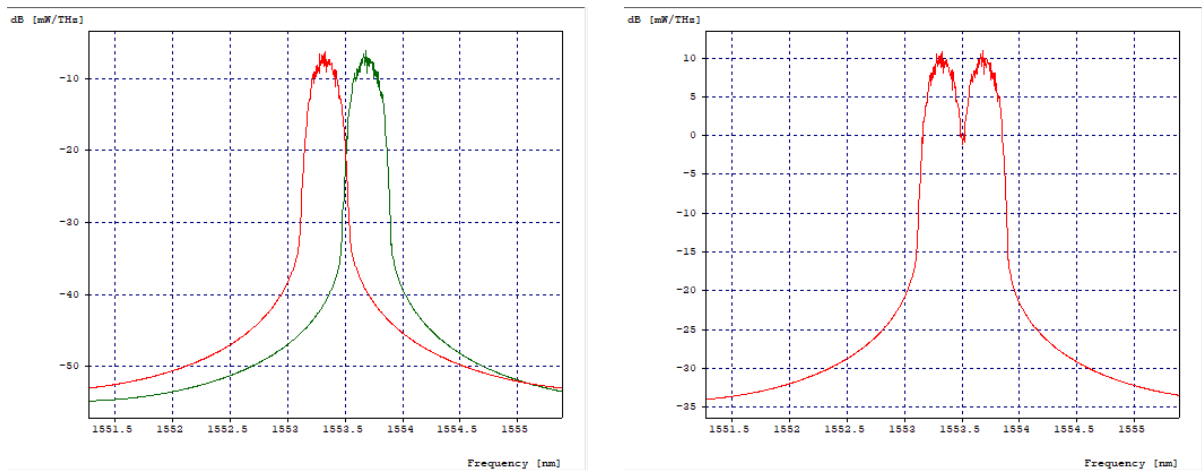
Fig. 5.48: *Transmitted spectrum at the output: Two Channels 45 GHz apart (Left) & Filtered, 2-Channel, 400G, PM-16QAM Spectrum at the 2-Channel Transmitter (Right)*

In order to describe the two-channel 400G receiver sensitivity (BER vs. OSNR) after 640 km, 1040 km, 1520 km and 2000 km of fiber and EDFA amplification, I've completed parametric scans in figure 5.49 with transmitted powers of -5 dBm (black), 0 dBm (blue) and 5 dBm (red) from OSNRs ranging from 22 to 30 dB. Larger transmitted power produces stronger nonlinearities requiring a higher OSNR to achieve the required BER (horizontal red line). These effects are more pronounced with increased transmission distance, as shown in the figures.

(a)

(b)

(c)

(d)
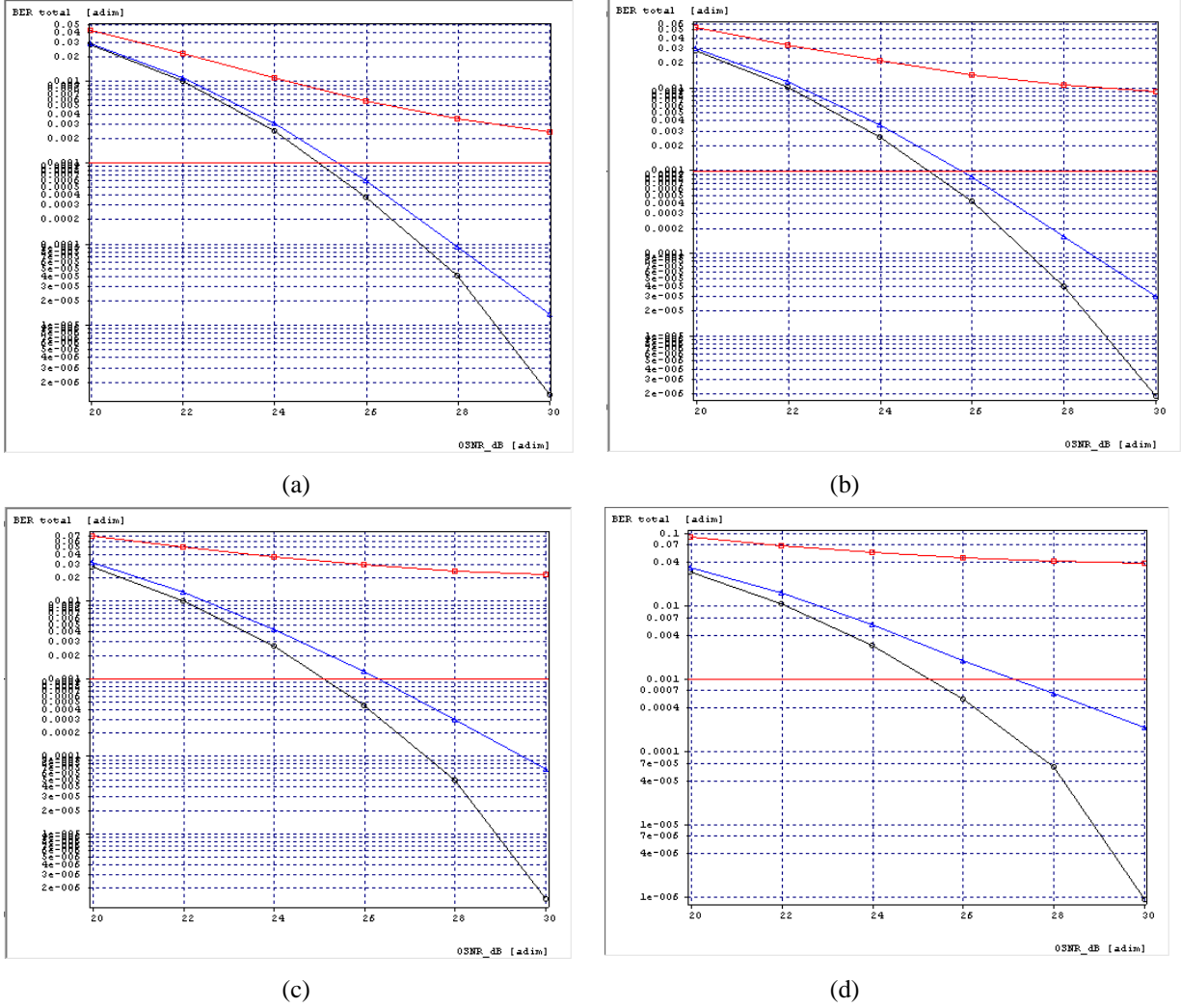
Fig. 5.49: *BER vs. OSNR: a) 640 km b) 1040 km c) 1520 km d) 2000 km with Output Power Levels: 5 dBm (red), 0dBm (blue), -5dBm (black)*

Table 5-3: *Results for Two Channel 400G PM16QAM, BER vs. OSNR*

Modulation Format	Net Bit Rate Per Channel (Gb/s)	Symbol Rate (Gbaud)	Number of Channels	Total Data Rate (Gb/s)	Grid (GHz)	Transmitted Power (dBm)	Distance (km)	Spectral Efficiency (bit/s/Hz)	OSNR pre-FEC BER = 10^{-3}
PM-16QAM	256	32	2	512	45	-5	640	5.69	24.98
PM-16QAM	256	32	2	512	45	0	640	5.69	25.40
PM-16QAM	256	32	2	512	45	5	640	5.69	N/A
PM-16QAM	256	32	2	512	45	-5	1040	5.69	25.07
PM-16QAM	256	32	2	512	45	0	1040	5.69	25.77
PM-16QAM	256	32	2	512	45	5	1040	5.69	N/A
PM-16QAM	256	32	2	512	45	-5	1520	5.69	25.12
PM-16QAM	256	32	2	512	45	0	1520	5.69	26.32
PM-16QAM	256	32	2	512	45	5	1520	5.69	N/A
PM-16QAM	256	32	2	512	45	-5	2000	5.69	25.27
PM-16QAM	256	32	2	512	45	0	2000	5.69	27.15
PM-16QAM	256	32	2	512	45	5	2000	5.69	N/A

44

As shown in the 640 km system, to maintain a 10^{-3} pre-FEC BER, an OSNR of nearly 25 dB is required at a transmitted power of -5 dBm and over 25 dB with a launch power of 0 dBm. A 5 dBm launch power produces strong nonlinearities and an OSNR over 30 dB is required in order to achieve the target pre-FEC BER. Despite the high OSNR requirement needed to achieve a satisfactory BER, this two-channel PM-16QAM system shows potential for 400G transmission deployment in metro and regional networks.

For the 1040 km system at a launch power of -5 dBm, the BER remains stable in comparison to the 640 km link and at 0 dBm, the BER rate has shifted very close to an OSNR of 26 dB in comparison to the 640km link (in order to maintain a 10^{-3} pre-FEC BER). Stronger nonlinearities are exhibited with a transmitted power of 5 dBm.

For the 1520 km system at a launch power of -5 dBm, the BER still remains stable in comparison to the 640 km link and at 0 dBm, the required OSNR has shifted to over 26 dB in comparison to the 640km link. Nonlinearities are increasing with a transmitted power of 5 dBm.

The same trend is followed in the 2,000 km system where the launch power at -5 dBm produces slightly stronger non-linearities as the required OSNR is shifted closer to 26 dB and even stronger non-linearities are produced with launch powers of 0 dBm and 5 dBm. At 0 dBm the required OSNR has shifted to 27 dB and at 5 dBm, the red line has shifted to an even higher point on the graph as well.

As a result of these simulations, it can be noted that 2x200G PM-16QAM 400G systems within a 90 GHz spectral occupancy are capable of reliable metro and possibly long-haul transmission at launch powers of -5 dBm and 0 dBm in this example, with the requirement of maintaining a significantly high OSNR.

In order to summarize the results of the transitioning OSNR requirements from increasing transmission distance towards this system's physical limit, another parameter scan is performed at one transmitted power level so that the curves can be processed in one correlation diagram, figure 5.50. A conservative transmitted power of -3 dBm is chosen (intentionally between -5 and 0 dBm) so that the BER vs. OSNR scan falls within the results obtained from the -5 dBm and 0 dBm launch powers.
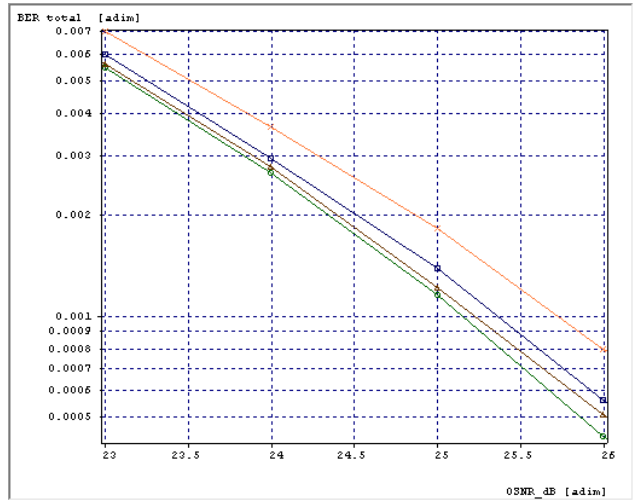
Fig. 5.50: *400G, Two Channel, PM-16QAM System, Increasing Transmission Distance, BER vs. OSNR for Constant Power Level of -3 dBm 640 km (Green), 1040 km (Brown), 1520 km (Blue) & 2000 km (Orange)*

The results describe the increasing non-linear effects with increase in transmission distance. With each increase in distance, the greater the increase in the required OSNR required to achieve the target BER. The largest increase is shown between the 1520 km and the 2000 km curves, where the buildup in nonlinear effects causes even greater disparity.

5.2.1.1 Effects of Decreased Channel Spacing, 400G PM-16QAM System

The purpose of the following simulations is to demonstrate the tradeoff between spectral efficiency and required OSNR using the 2X200G PM-16QAM system transmitted over 640 km of fiber with a launch power of -3 dBm as an example. Channel spacing is reduced to 37.5 GHz based on the referenced 2X200G system (first paragraph 5.2.1) mentioned by the OIF with a total spectral occupancy of 75 GHz [1]. Both transmitted two-channel spectrums spaced 37.5 GHz and 45 GHz are shown in figure 5.51.
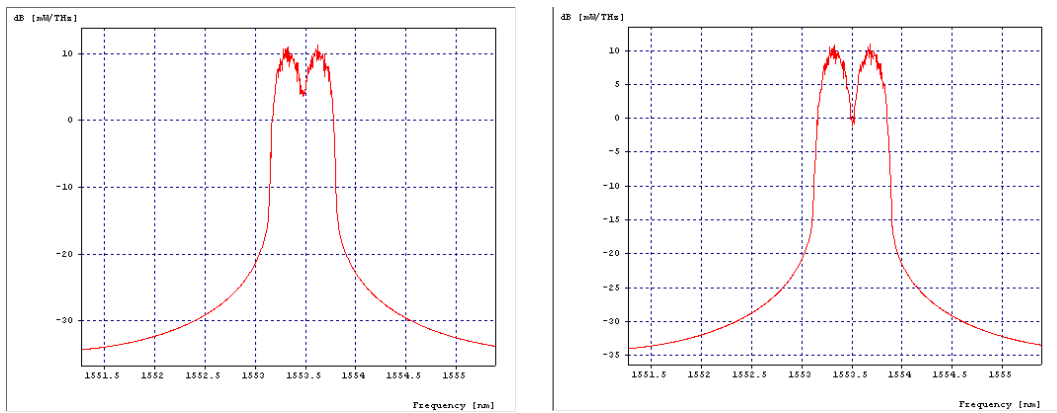
Fig. 5.51: *Transmitted spectrum at the Output Filtered, 2-Channel, 400G, PM-16QAM Spectrum 37.5 GHz (Left) & 45 GHz (Right)*

46

Referring to figure 5.51, the spectral efficiency for the 37.5 GHz spaced 2x200G PM-16QAM system on the left is 6.83 bit/s/Hz. The spectral efficiency for the 45 GHz spaced 2x200G PM-16QAM system on the right is 5.69 bit/s/Hz.
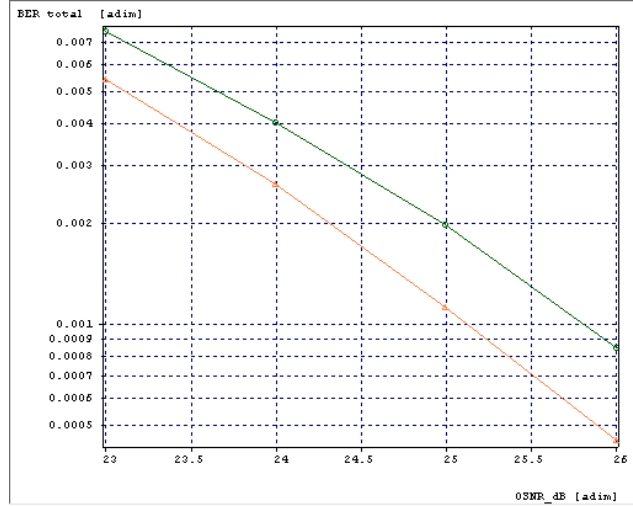
Fig. 5.52: BER vs. OSNR Transmitted Power -3 dBm, 640 km, 37.5 GHz (Green) & 45 GHz (Orange)

Table 5-4: Results for Decreased Channel Spacing, BER vs. OSNR for Output Power Level of -3 dBm 640 km, 37.5 GHz (Green) & 45 GHz (Orange)

Modulation Format	Net Bit Rate Per Channel (Gb/s)	Symbol Rate (Gbaud)	Number of Channels	Total Data Rate (Gb/s)	Grid (GHz)	Transmitted Power (dBm)	Distance (km)	Spectral Efficiency (bit/s/Hz)	OSNR pre-FEC BER = 10^{-3}
PM-16QAM	256	32	2	512	45	-3	640	5.69	25.13
PM-16QAM	256	32	2	512	37.5	-3	640	6.83	25.82

For the PM-16QAM system with 37.5 GHz channel spacing, there is an increase in spectral efficiency to 6.83 bit/s/Hz, but consequently, the required OSNR to meet the target pre-FEC BER of 10^{-3} has increased to nearly 26 dB (Fig. 5.52, Table 5-4). Despite the high OSNR requirements, PM-16QAM systems are capable of high bit rate transmission while achieving a high spectral efficiency.

5.2.2   Nyquist WDM PM-16QAM Super-Channel

A promising solution for next-generation 400G and 1T optical transmission systems is the concept of the "Super-Channel". A super-channel is a collection of optical signals that are modulated and multiplexed together with high spectral efficiency at a common originating site, transmitted and routed over common optical link as a single entity and received at a common destination site [32]. To achieve ultimate spectral efficiency, WDM channel spacing is reduced until the spectra of neighboring channels start to noticeably overlap, where linear crosstalk between becomes a main source of degradation [32]. An efficient

countermeasure to limit the crosstalk is relies on accurate spectral shaping of each channel. Finisar Waveshaper filters are used in practice for Nyquist filtering, and are modeled as super-Gaussian filters (labeled as *ogaussfilx*) of orders 2 to 4 [64]. The super-Gaussian filters are set to 4 here, which provides a steeper transfer function, in order to mitigate crosstalk degradation arising from tight channel spacing. The layout (Fig. 5.53), based on reference [64], demonstrates back-to-back Nyquist-WDM PM-16QAM system with nine channels at 240 Gb/s.
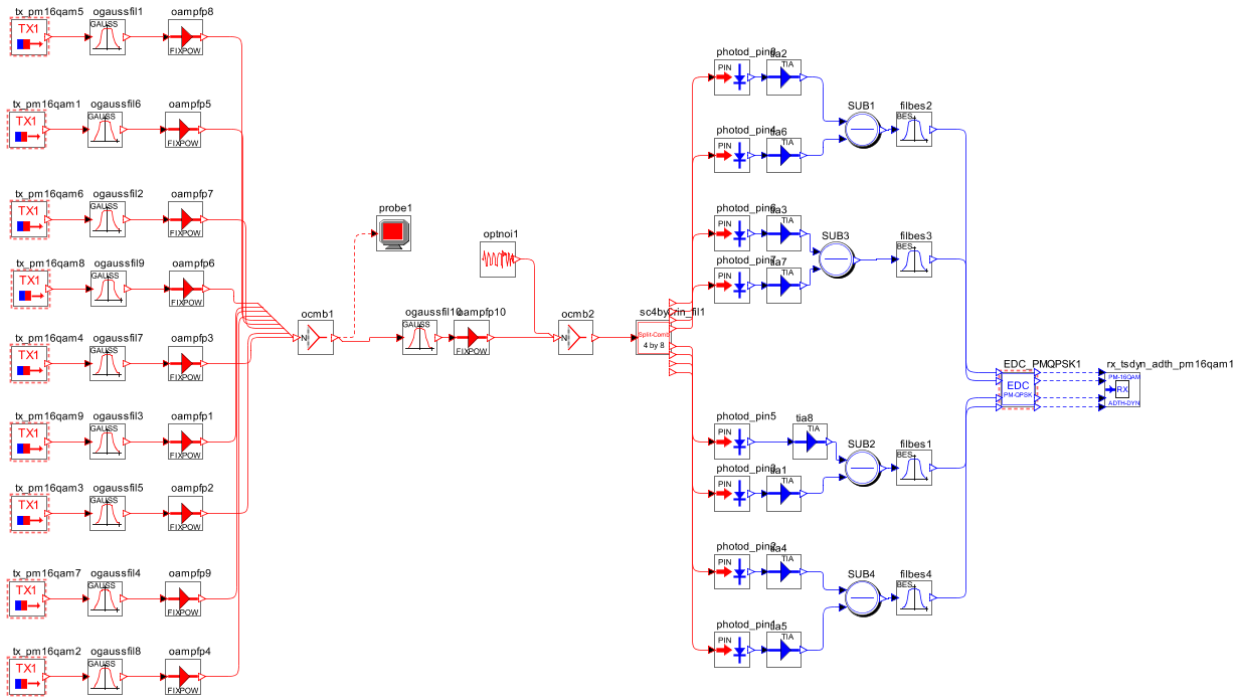
Fig. 5.53: *Layout of Nyquist WDM Super-channel System*

The system consists of nine PM-16QAM transmitters as subcarriers of the Super-Channel. Each of the transmitters operates at a symbol rate of 30 GBaud. The optical noise adder has noise spectral density defined in terms of OSNR to facilitate a parameter scan over the OSNR. The receiver model follows the layout of 4.5.2. Roughly 76000 bits are transmitted with the parameter scan obtaining the BER vs. OSNR curve. Finally, channel spacing follows Nyquist guidelines (section 2.5.1.1) and is 1.1 times the symbol rate (30 Gbaud x 1.1 = 33.33 GHz channel spacing). The spectrum of the Super-Channel is shown in figure 5.54, where neighboring pulses start to overlap, creating a Nyquist WDM "comb".
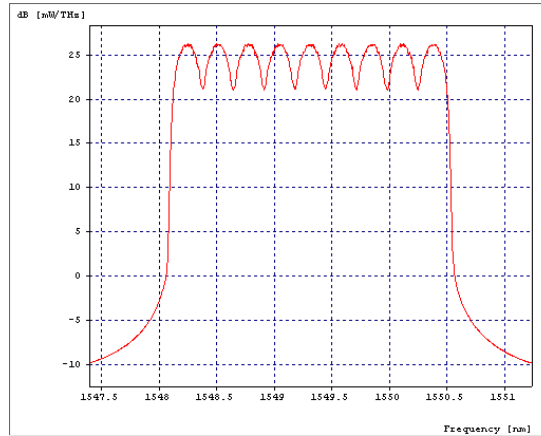
Fig. 5.54: *Super-channel System Super-channel Spectrum with Nine Subcarriers*

With a per channel bit rate of 240 Gb/s and channel spacing of 33.33 GHz, this PM-16QAM system achieves a spectral efficiency of 7.2 bit/s/Hz. After roughly 2 Tb transmission on this system, the below BER vs. OSNR curve shown in figure 5.55 indicates a receiver sensitivity of just over 23 dB at the 10^{-3} pre FEC BER.
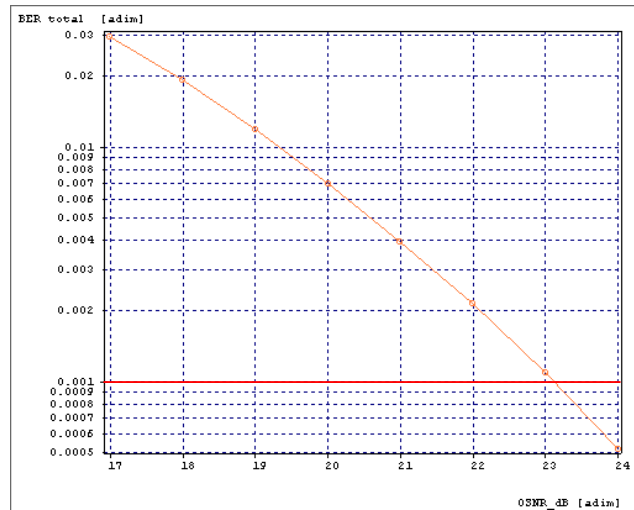
Fig. 5.55: *BER vs. OSNR for Nyquist WDM Super-channel*

Due to the high bit rate, and tight channel spacing along with the dense PM-16QAM modulation format, strong non-linearities occur when attempting to include SMF spans. In order to achieve adequate BER vs. OSNR results, more advanced DSP at the receiver as researched in [30] could be attempted. However, the results demonstrated the high capacity, highly spectral efficient, capabilities of PM-16QAM.

In this thesis, I am focused employing techniques that enable high capacity large scale transmission using single mode fiber and EDFA only amplification, therefore the next example demonstrates this using PM-QPSK.

49

5.3 Long-Haul Transmission Using PM-QPSK

The previous examples of advanced modulation formats; 8-QAM, 16-QAM, 64-QAM, enable higher spectral efficiency, but the propagation of dense signal constellations invariably requires enhanced SNR, thus reducing the transmission reach and system reliability. The purpose of the next simulation is to outline the long-distance capabilities of PM-QPSK.

5.3.1 Simulation of Long-Haul Transmission Using PM-QPSK

The following system in figure 5.56 demonstrates the implementation of a 9-channel WDM PM-QPSK system with a total line rate nearly 1TB. The results gain insight into the BER rate effects vs. transmission length of the system. Each channel generates a single PM-QPSK signal from four 28 Gb/s data sources with overhead included to account for forward error correction [33]. The optical signals are filtered and combined over 2,250 km of fiber, composed of 25 loops of 90 km SMF with EDFA amplification. After the fiber spans, optical noise is added to the signal and filtered again. At the receiver, a 90-degree hybrid single ended combiner divides the signal into two polarization components and returns the x' and y' components of each polarization (section 4.4.1). A DSP-based coherent receiver is used to convert the received PM-QPSK signal into electrical signals representing the in-phase and quadrature components of each optical polarization, and the parameter scan includes the pre-FEC BER as a function of span loss in order to demonstrate the suitability of this system for high-capacity long distance transmission.
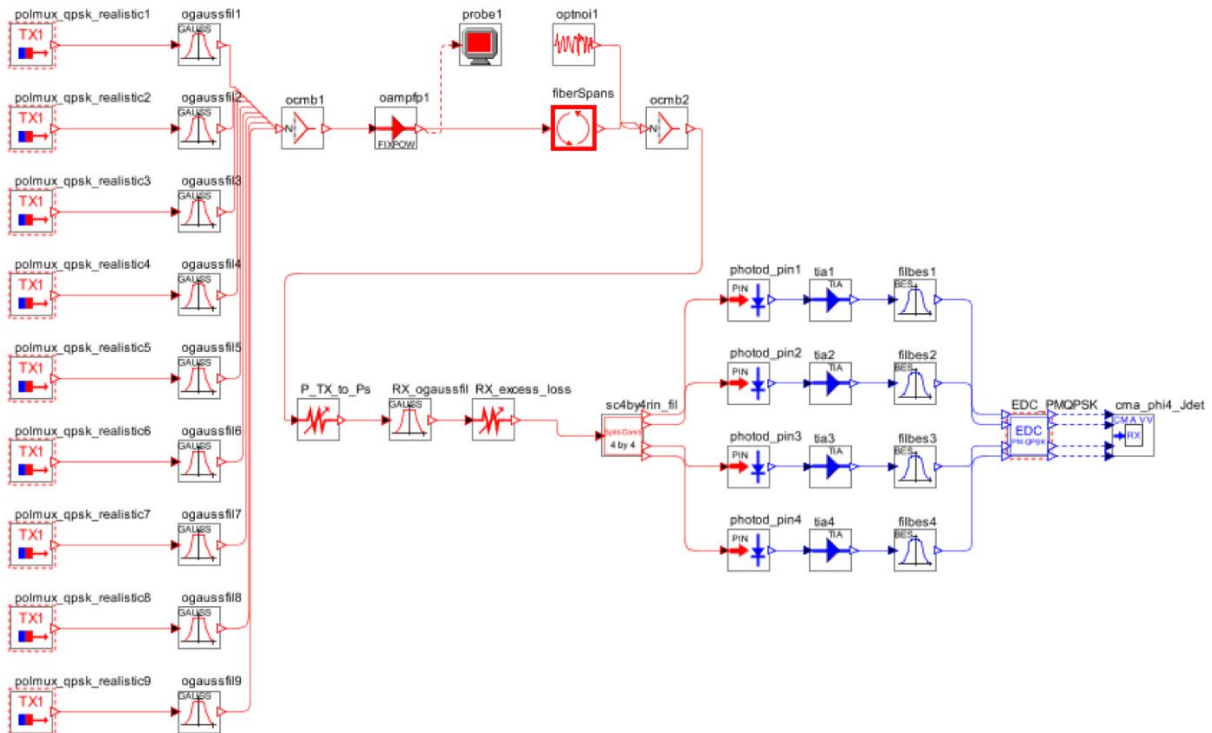
Fig. 5.56: PM-QPSK WDM 2000 km, 1 Tb Transmission Link

The nine transmitters, represented by the "*polmux_qpsk1*" component, with four data sources, comprise of the same PM-QPSK transmitter structure detailed in section 4.4.1. Figure 5.57 shows the 9-channel spectrum of the PM-QPSK system.
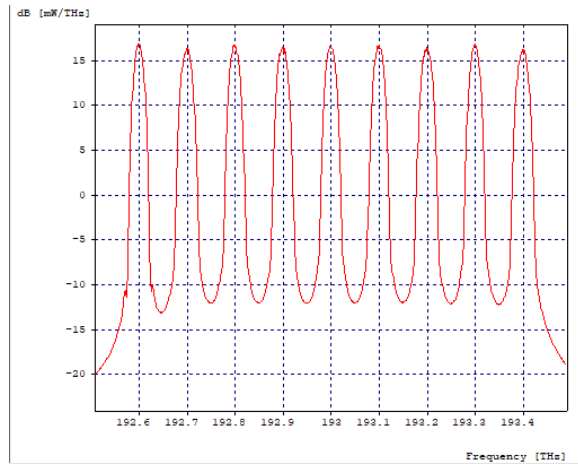
Fig. 5.57: PM-QPSK Spectrum with Nine Subcarriers

The parameter scan is set up to provide BER vs. Number of Spans (25 km fiber spans) in order to demonstrate the stability and long transmission capability of PM-QPSK system at nearly 1 Tb transmission rate.
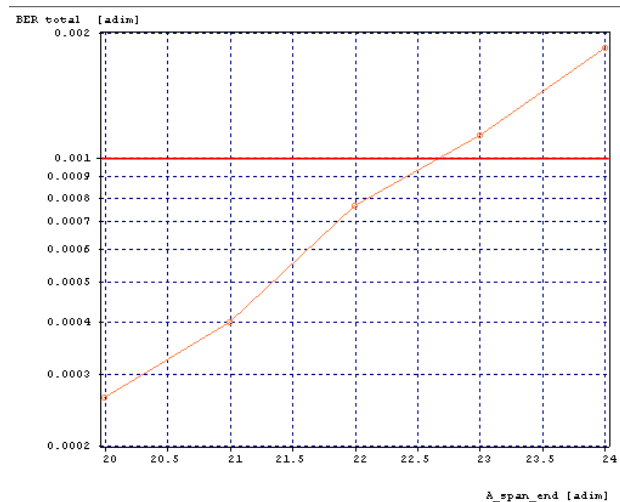
*Fig. 5.58: BER rate vs. Number of Spans (24 * 90km = 2160 km total length)*

At 23 fiber spans with a total length of 2070km (23 x 90km), the pre-FEC BER rate is still stable at 10^{-3}, confirming that this system is capable of long-haul 1 Tb transmission. Although the spectral efficiency of the 9-channel PM-QPSK link is quite low (112 Gb/s / 100 GHz = 1.12 Gb/s/Hz) in comparison to the 9-channel Nyquist WDM Super-channel PM-16QAM link (240 Gb/s / 33.33 GHz = 7.2 Gb/s/Hz), long-haul transmission of nearly 1 Tb is achievable using PM-QPSK with the use of single mode fibers and EDFA only amplification.

51

This example of long-haul PM-QPSK link can be improved by use of DSP at the receiver. The component used for coherent reception in this example is the Memoryless blind receiver for coherent polarization multiplexed QPSK modulation, figure 5.59.
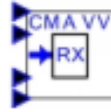
Fig. 5.59: *Blind Receiver for Coherent PM-QPSK Modulation [61]*

This component separates data flows transmitted on orthogonal polarizations and estimates the average local-oscillator-to-signal phase in order to the separation between in-phase and quadrature signals using the CMA [61]. The key point for improvement here, is that this component is a memoryless receiver, therefore it recovers only polarization and phase rotations using the Viterbi & Viterbi algorithm [61]. In the next simulations, dynamic receivers for coherent polarization multiplexed modulations are training sequence and tracking based using the LMS algorithm (section 4.3.1). The improved result from the use of the dynamic receiver component is that, besides recovering polarization and phase rotations; this component compensates also for pattern dependent phenomena such as residual chromatic dispersion and polarization mode dispersion [61]. Improvements in the next simulations include increased transmission distances achieved and a lower required OSNR to achieve the required BER.

5.4   Comparison of PM-16QAM & PM-QPSK WDM

The next set of simulations provide thorough comparisons of two very similar long-haul systems with one utilizing PM-QPSK and the other PM-16QAM. It is very important to consider these two modulation formats for long-haul transmission, now and in terms of future growth.

5.4.1   PM-16QAM & PM-QPSK WDM: 1040 km, 50 GHz & 37.5 GHz Channel Spacing

The following two high-speed coherent five channel WDM systems provides a comparison between PM-QPSK and PM-16QAM at a baud rate of 32 Gb/s. BER vs. OSNR plots obtained for 1040 km and 2000 km for both 50 GHz and 37.5 GHz channel spacings. The 37.5 GHz channels spacing chosen for narrowing the grid for each system fits into the 12.5 GHz incremented grid, or flexible grid, as specified by G.694.1. The channel spacing is adjusted for both transmission lengths in order to determine how the two systems compare in terms of how adversely they are affected by narrowing of the channel grid and increasing transmission distances.
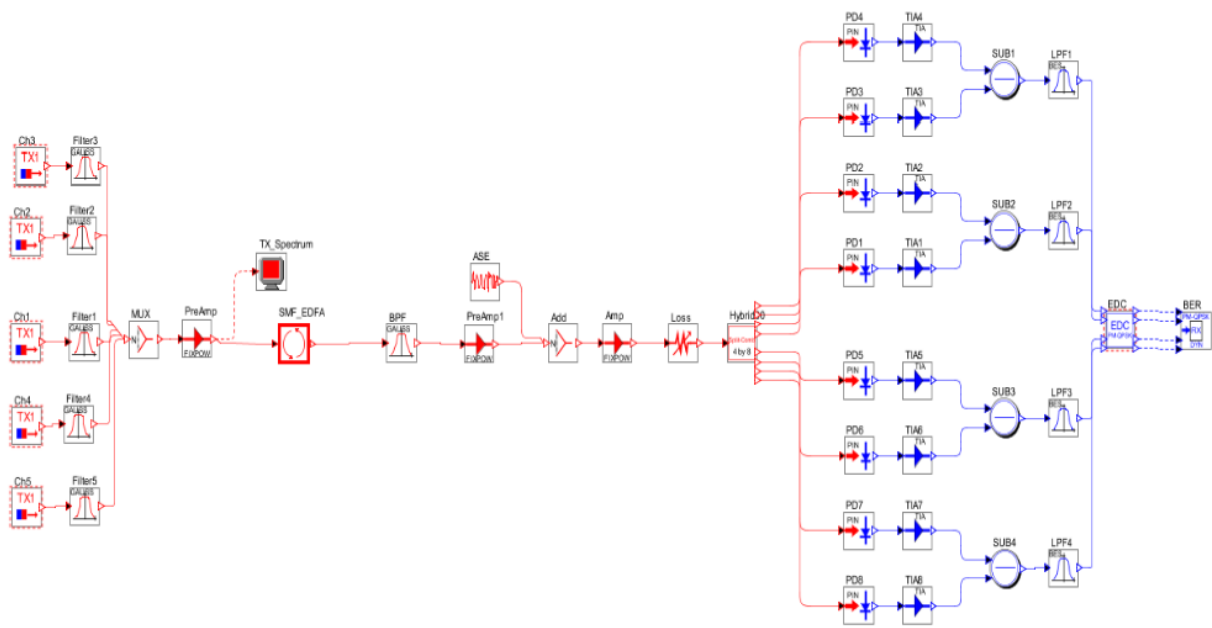
Fig. 5.60: *Five Channel PM-QPSK System*
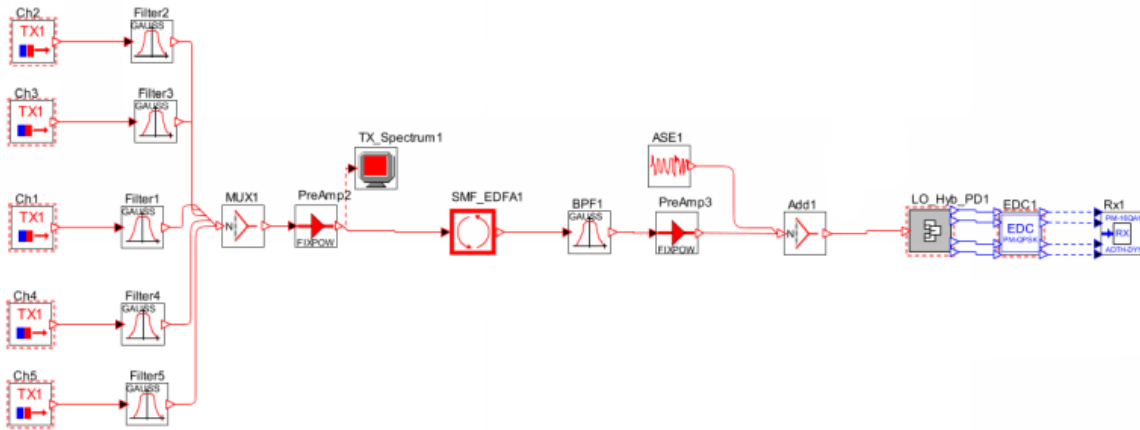
Fig. 5.61: *Five Channel PM-16QAM System*

The 1040 km long transmission links comprise of 13 spans of standard single mode fiber (80 km per span) with EDFA amplification. For the PM-QPSK system, the 32 GBd channel baud rate results in a per channel bitrate of 128 Gb/s for a total transmission rate of 640 Gb/s. For the PM-16QAM system the 32 GBd channel baud rate results in a per channel bitrate of 256 Gb/s for a total transmission rate of 1.28 Tb/s including FEC overheads. Both systems include coherent dynamic receivers as detailed in section 4.3.1. System performance is again observed in terms of BER vs. OSNR, in this case for a given transmission power (as demonstrated in the 2x200G PM-16QAM system). Error counting is performed based on 300,000 bits transmitted with 20 samples per bit for a total of 6 million samples per data-stream.

The transmitted spectrums in figure 5.62 and 5.63 at the outputs of the two systems illustrate the difference in the spectral efficiencies achieved by the two systems. PM-QPSK is shown first below with

50 GHz spacing with spectral efficiency 128 Gb/s/50 GHz = 2.56 bit/s/Hz on the left and the 37.5 GHz spaced channel plan with spectral efficiency 128 Gb/s/37.5 GHz = 3.41 bit/s/Hz is shown on the right. The PM-16QAM channel plans are shown in the second pair of spectrums in figure 5.63 in the same order. The spectral efficiencies attained by the PM-16QAM systems (256 Gb/s/50Hz = 5.12 bit/s/Hz and 256 Gb/s/37.5 GHz = 6.83 bit/s/Hz) are double that of the PM-QPSK systems (128 Gb/s/37.5 GHz = 3.41 bit/s/Hz and 128 Gb/s/50Hz = 2.56 bit/s/Hz).
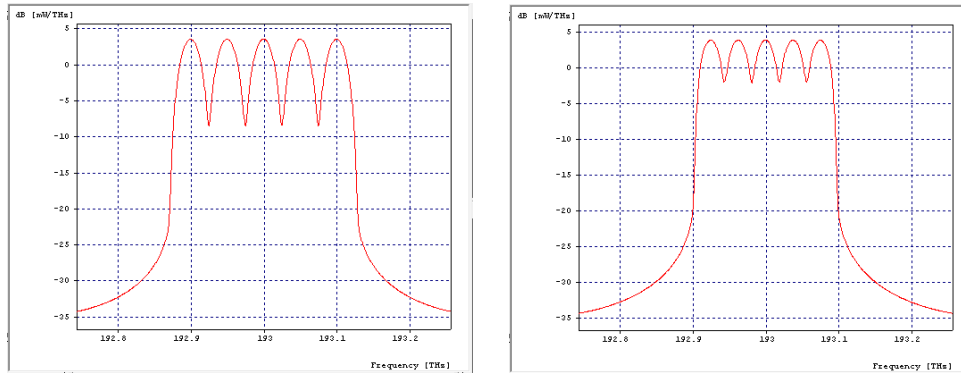
Fig. 5.62: *PM-QPSK 50 GHz (Left) & 37.5 GHz (Right)*
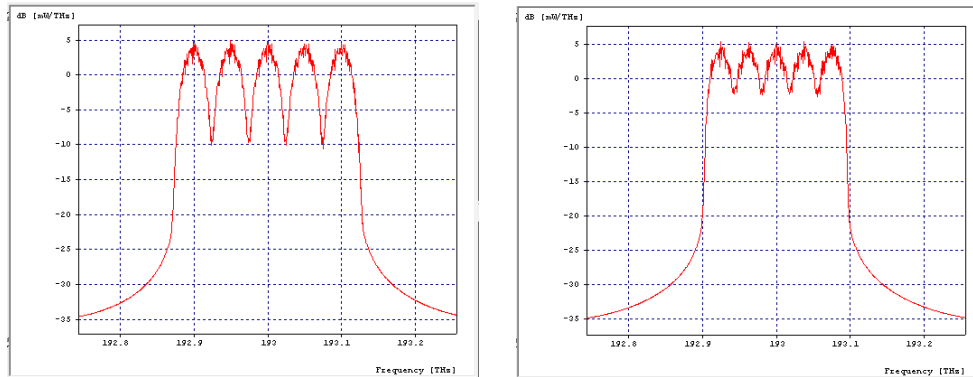
Fig. 5.63: *PM-16QAM 50 GHz (Left) & 37.5 GHz (Right)*

The BER vs. OSNR for different values of transmitted power (-5, 0 and 5 dBm) is obtained by performing a parameter scan simulating transmission over the 1040 km of single mode fiber. This provides more insight into the tradeoffs between spectral efficiency and the BER vs. OSNR results achieved for both modulation formats. The first figure 5.64 shows the BER vs. OSNR curves for the PM-QPSK system (50 GHz on the left and 37.5 GHz on the right) and the second set figure 5.65 shows the BER vs. OSNR for the PM-16QAM system in the same order. The table includes results from the four correlation diagrams in detail.

Figure 5.64: *PM-QPSK 1,040 km, BER vs. OSNR with Output Power Levels: 5 dBm (red), 0dBm (blue), -5dBm (black) for 50 GHz Spacing (Left) & 37.5 GHz Spacing (Right)*

Fig. 5.65: *PM-16QAM 1,040 km, BER vs. OSNR with Output Power Levels: 5 dBm (red), 0dBm (blue), -5dBm (black) for 50 GHz Spacing (Left) & 37.5 GHz Spacing (Right)*

Table 5-5: *Results for PM-QPSK & PM16QAM BER vs. OSNR for Both 50 GHz and 37.5 GHz Channel Spacing*

Modulation Format	Net Bit Rate Per Channel (Gb/s)	Symbol Rate (Gbaud)	Number of Channels	Total Data Rate (Gb/s)	Grid (GHz)	Transmitted Power (dBm)	Distance (km)	Spectral Efficiency (bit/s/Hz)	OSNR pre-FEC BER = 10^{-3}
PM-QPSK	128	32	5	640	50	-5	1040	2.56	14.02
PM-QPSK	128	32	5	640	50	0	1040	2.56	14.06
PM-QPSK	128	32	5	640	50	5	1040	2.56	14.19
PM-16QAM	256	32	5	1280	50	-5	1040	5.12	21.93
PM-16QAM	256	32	5	1280	50	0	1040	5.12	22.05
PM-16QAM	256	32	5	1280	50	5	1040	5.12	24.75
PM-QPSK	128	32	5	640	37.5	-5	1040	3.41	14.52
PM-QPSK	128	32	5	640	37.5	0	1040	3.41	14.53
PM-QPSK	128	32	5	640	37.5	5	1040	3.41	14.70
PM-16QAM	256	32	5	1280	37.5	-5	1040	6.83	23.37
PM-16QAM	256	32	5	1280	37.5	0	1040	6.83	23.68
PM-16QAM	256	32	5	1280	37.5	5	1040	6.83	N/A

For the PM-QPSK system with 50 GHz channel spacing, the required OSNR for a pre-FEC BER of 10^{-3} is around 14 dB for all three launch powers with little disparity between the 5 dBm launch power from the -5 dBm and 0 dBm launch powers. For the PM-QPSK system with 37.5 GHz channel spacing, the required OSNR for a pre-FEC BER of 10^{-3} is around 14.5 dB for all three launch powers with slightly greater disparity between the 5 dBm launch power from the -5 dBm and 0 dBm launch powers throughout the length of the curve, but even at a greater launch power, the PM-QPSK remains quite stable.

The results for the PM-16QAM system with 50 GHz channel spacing show that the required OSNR for a pre-FEC BER of 10^{-3} is just under 22 dB at -5 dBm transmitted power and 22 dB at 0 dBm transmitted power. This demonstrates the tradeoff between spectral efficiency and reach/required OSNR. PM-16QAM also shows more sensitivity for higher launch power, where there is much more deviation from the -5 dBm and 0 dBm to the launch power of 5 dBm, where its required OSNR is about 24.5 dB. Whereas, there was only a slight increase in OSNR to just over 14 dB for the PM-QPSK system when the launch power is at 5 dBm. The trade-offs between spectral efficiency and reach between PM-QPSK and PM-16QAM are obvious. The results for the PM-16QAM system with 37.5 GHz channel spacing show that the required OSNR for a pre-FEC BER of 10^{-3} is just over 23 dB at -5 dBm transmitted power and closer to 24 dB at 0 dBm transmitted power. This not only demonstrates the tradeoff between spectral efficiency and reach between PM-QPSK and PM-QAM, but it also the increased sensitivity of PM-16QAM when narrowing the grid. PM-16QAM also shows more sensitivity for the higher launch power when narrowing the channel spacing to 37.5 GHz, where there more deviation from the -5 dBm and 0 dBm to the launch power of 5 dBm, where the target pre-FEC BER of 10^{-3} is not reached. Whereas, there was only a 1.5 dB increase in the required OSNR for the PM-16QAM system with 50 GHz channel spacing.

In order to summarize these results in one diagram, a parameter scan is performed at one transmitted power of -3 dBm is chosen (intentionally between -5 and 0 dBm) so that the BER vs. OSNR scan falls within the results obtained from the -5 dBm and 0 dBm launch powers.
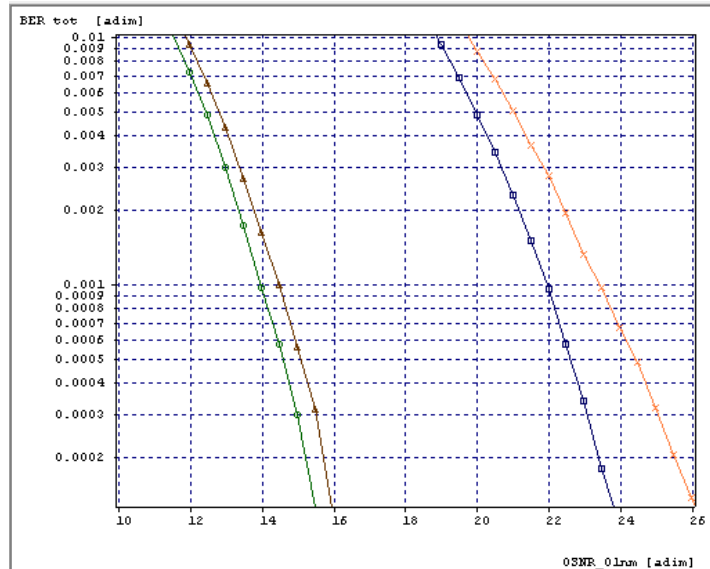
Fig. 5.66: BER Vs. OSNR for PM-QPSK & PM-16QAM 1040 km with -3 dBm Output Power Level for 50 GHz & 37.5 GHz Spacing

The differences in the effects of narrowing the grid for the five channel PM-QPSK and PM-16QAM systems are apparent as the PM-16QAM more adversely impacted to decreasing channel spacing. The next set of simulations provides insight into how increasing transmission distance as well as decreasing channel spacing may impact the performance of these two systems.

5.4.2 PM-16QAM & PM-QPSK WDM: Increased Transmission Distance

The following BER vs. OSNR results show that limitations of the PM-16QAM 256 Gb/s five channel system are pushed after 2,000 km of fiber spans, whereas the stability of the PM-QPSK 128 Gb/s system is highlighted.

5.4.2.1 PM-QPSK WDM, Effects of Increased Transmission Distance

In order to provide an initial understanding of the resulting OSNR requirements in the PM-QPSK system due to increasing the transmission distance from 1040 km to 2000 km for both channel plans, correlation diagrams in figure 5.67 are plotted overlaid on one another with the transmitted power held constant at -3 dBm. The change in BER vs. OSNR for the 50 GHz system is shown the left and 37.5 GHz system on the right in figure 5.67.

Figure 5.67: *PM-QPSK Transition to Longer Transmitted Distance, BER vs. OSNR with Output Power Level of -3 dBm for 1000 km (Orange) & 2000 km (Green), 50 GHz Spacing (Left) & 37.5 GHz Spacing (Right)*

Modulation Format	Net Bit Rate Per Channel (Gb/s)	Symbol Rate (Gbaud)	Number of Channels	Total Data Rate (Gb/s)	Grid (GHz)	Transmitted Power (dBm)	Distance (km)	Spectral Efficiency (bit/s/Hz)	OSNR pre-FEC BER = 10^{-3}
PM-QPSK	128	32	5	640	50	-3	1040	2.56	13.98
PM-QPSK	128	32	5	640	50	-3	2000	2.56	14.04
PM-QPSK	128	32	5	640	37.5	-3	1040	3.41	14.50
PM-QPSK	128	32	5	640	37.5	-3	2000	3.41	14.64

Table 5-6: *Results for Increasing Transmission Distance of PM-QPSK Systems from 1040 km to 2000 km for 50 GHz and 37.5 GHz Channel Spacing*

In table 5-6 the results for transitioning the PM-QPSK 50 GHz system from 1040 km to 2000 km setup show that there is very little effect on the overall required OSNR for achieving a pre-FEC BER of 10^{-3}. This shows that the 50 GHz PM-QPSK system is very stable when increasing the transmission distance from 1040 km to 2000 km. The results for the PM-QPSK 37.5 GHz system is only slightly more affected by increasing the fiber transmission distance from 1040 km to 2000 km, but still quite stable.

In order to evaluate the effects of decreasing channel spacing for the 2000 km PM-QPSK system, the BER vs. OSNR for the 2000 km systems with individual output power levels plotted at -5, 0 and 5 dBm are shown in figure 5.68 for the 50 GHz system on the left and 37.5 GHz on the right.
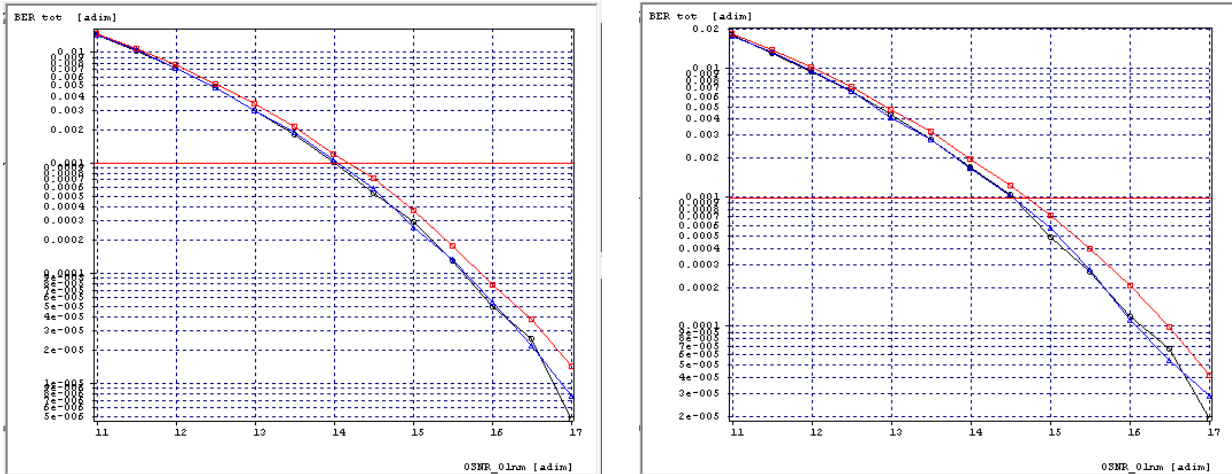
Figure 5.68: *PM-QPSK 2000 km, BER vs. with Output Power Levels: 5 dBm (red), 0dBm (blue), -5dBm (black) for 50 GHz Spacing (Left) & 37.5 GHz Spacing (Right)*
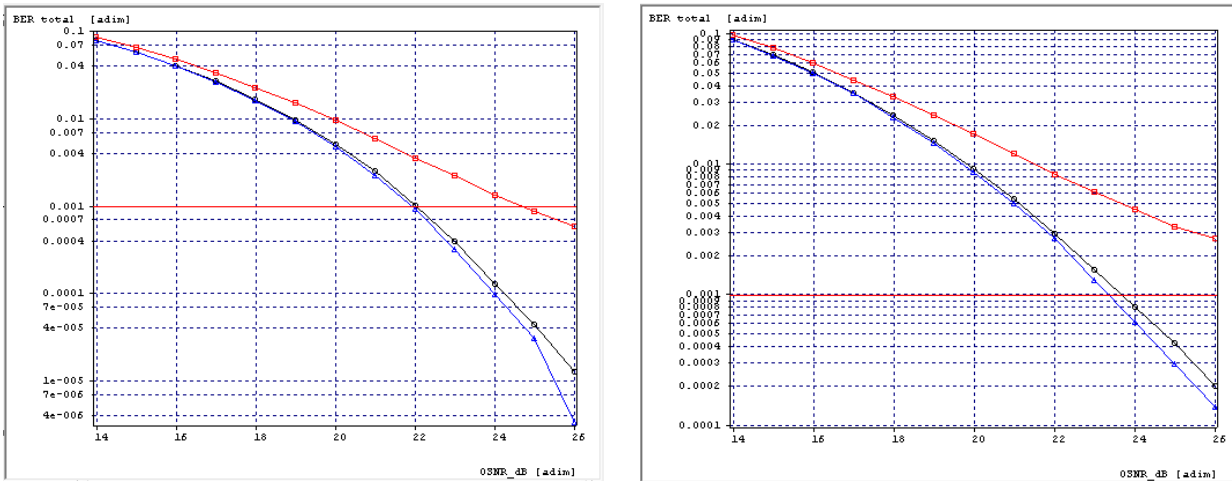
Table 5-7: *Results for Decreasing Channel Spacing from 50 GHz and 37.5 GHz for 2000 km PM-QPSK System*

Modulation Format	Net Bit Rate Per Channel (Gb/s)	Symbol Rate (Gbaud)	Number of Channels	Total Data Rate (Gb/s)	Grid (GHz)	Transmitted Power (dBm)	Distance (km)	Spectral Efficiency (bit/s/Hz)	OSNR pre-FEC BER = 10^{-3}
PM-QPSK	128	32	5	640	50	-5	2000	2.56	14.05
PM-QPSK	128	32	5	640	50	0	2000	2.56	14.10
PM-QPSK	128	32	5	640	50	5	2000	2.56	14.46
PM-QPSK	128	32	5	640	37.5	-5	2000	3.41	14.62
PM-QPSK	128	32	5	640	37.5	0	2000	3.41	14.69
PM-QPSK	128	32	5	640	37.5	5	2000	3.41	15.24

The results in table 5-7 for narrowing the channel spacing for the PM-QPSK system from 50 GHz to 37.5 GHz show that the required OSNR for a pre-FEC BER of 10^{-3} has increased from 14 dB to over 14.5 dB for launch powers of -5 and 0 dBm. The launch power of 5 dBm shows the biggest change from about 14.5 dB to over 15 dB. In order to provide a simplified visual aid for the above overall change in OSNR requirements in the PM-QPSK system due to decreasing channel spacing for the 2000 km systems, correlation diagrams are plotted overlaid on one another in figure 80 with the transmitted power held constant at -3 dBm. The orange line represents channel spacing at 50 GHz and the green line represents the 37.5 GHz spaced system.

Figure 5.69: PM-QPSK Narrowing Channel Spacing for 2000 km Transmission Distance, BER vs. OSNR with Output Power Level of -3 dBm 50 GHz (Orange) & 37.5 GHz (Green)

The correlation diagram in figure 5.69 provides a general visual of the OSNR penalties as a result of narrowing channel spacing from 50 GHz to 37.5 GHz or increasing spectral efficiency for a five channel 128 Gb/s 2000 km PM-QPSK system.

5.4.2.2   PM-16QAM WDM, Effects of Increased Transmission Distance

The resulting OSNR requirements for the PM-16QAM systems due to increasing the transmission distance from 1040 km to 2000 km for both channel plans are shown in the below correlation diagrams plotted overlaid on one another with the output power level held constant at -3 dBm. In figure 5.70, the change in BER vs. OSNR for the 50 GHz system is shown the left and 37.5 GHz system on the right.
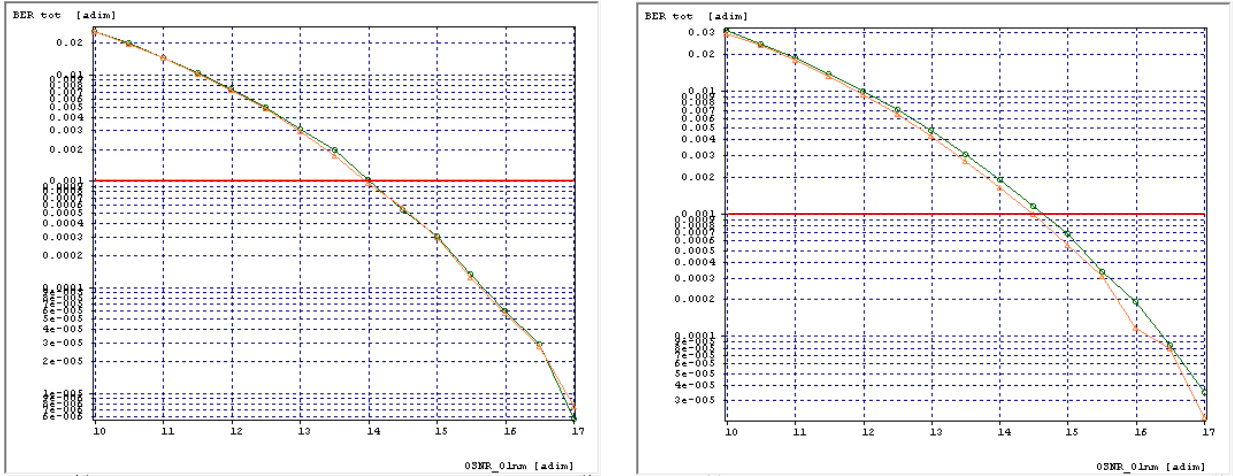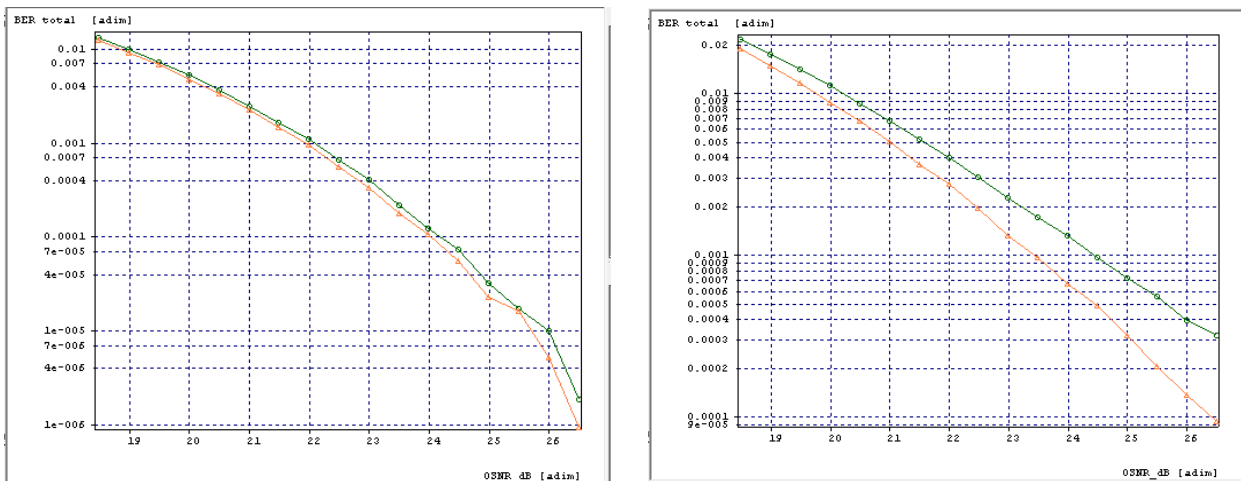

Fig. 5.70: PM-16QAM Transition to Longer Transmitted Distance, BER vs. OSNR with Output Power Level of -3 dBm 1000 km (Orange) & 2000 km (Green), 50 GHz Spacing (Left) & 37.5 GHz Spacing (Right)

60

Table 5-8: *Results for Increasing Transmission Distance of PM-16QAM Systems from 1040 km to 2000 km for 50 GHz and 37.5 GHz Channel Spacing*

Modulation Format	Net Bit Rate Per Channel (Gb/s)	Symbol Rate (Gbaud)	Number of Channels	Total Data Rate (Gb/s)	Grid (GHz)	Transmitted Power (dBm)	Distance (km)	Spectral Efficiency (bit/s/Hz)	OSNR pre-FEC BER = 10^{-3}
PM-16QAM	256	32	5	1280	50	-3	1040	5.12	21.97
PM-16QAM	256	32	5	1280	50	-3	2000	5.12	22.12
PM-16QAM	256	32	5	1280	37.5	-3	1040	6.83	23.47
PM-16QAM	256	32	5	1280	37.5	-3	2000	6.83	24.46

The results in table 5-8 for transitioning the PM-16QAM 50 GHz system from 1040 km to 2,000 km setup show that there is some effect on the overall required OSNR for achieving a pre-FEC BER of 10^{-3}, where the required OSNR has moved from almost 22 dB for the 1040 km system to just over 22 dB for the 2000 km system. This shows that the 50 GHz PM-16QAM system is stable when increasing the transmission distance from 1040 km to 2000 km.

The results show that the PM-16QAM 37.5 GHz system is only slightly more affected by increasing the fiber transmission distance from 1040 km to 2000 km, where the required OSNR has moved from almost 23.5 dB for the 1040 km system to almost 24.5 dB for the 2000 km system. This shows that the 37.5 GHz PM-16QAM system is less stable when increasing transmission distance from 1040 km to 2000 km.

In order to evaluate the effects of decreasing channel spacing for the 2000 km PM-16QAM systems, the BER vs. OSNR for the 2000 km systems with individual transmitted powers plotted at -5, 0 and 5 dBm are shown in figure 5.71 for the 50 GHz system on the left and 37.5 GHz on the right.
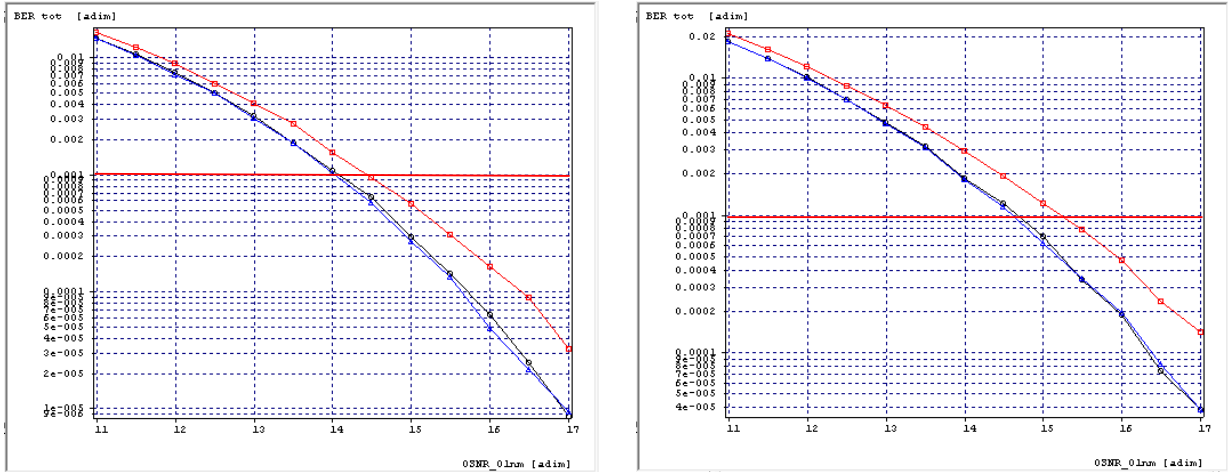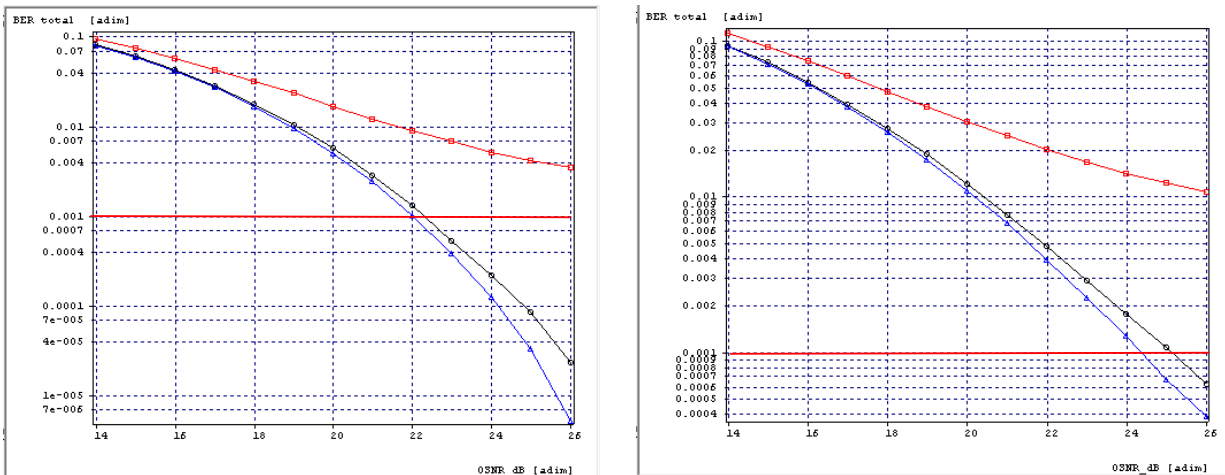

Fig. 5.71: *PM-16QAM 2000 km, BER vs. OSNR with Output Power Levels: 5 dBm (red), 0dBm (blue), -5dBm (black) for 50 GHz Spacing (Left) & 37.5 GHz Spacing (Right)*

Table 5-9: *Results for Decreasing Channel Spacing from 50 GHz and 37.5 GHz for 2000 km PM-16QAM System*

Modulation Format	Net Bit Rate Per Channel (Gb/s)	Symbol Rate (Gbaud)	Number of Channels	Total Data Rate (Gb/s)	Grid (GHz)	Transmitted Power (dBm)	Distance (km)	Spectral Efficiency (bit/s/Hz)	OSNR pre-FEC BER = 10^{-3}
PM-16QAM	256	32	5	1280	50	-5	2000	5.12	22.04
PM-16QAM	256	32	5	1280	50	0	2000	5.12	22.33
PM-16QAM	256	32	5	1280	50	5	2000	5.12	N/A
PM-16QAM	256	32	5	1280	37.5	-5	2000	6.83	24.39
PM-16QAM	256	32	5	1280	37.5	0	2000	6.83	25.16
PM-16QAM	256	32	5	1280	37.5	5	2000	6.83	N/A

The results in table 5-9 for narrowing the channel spacing for the PM-16QAM 2000 km system from 50 GHz to 37.5 GHz show that the required OSNR for a pre-FEC BER of 10^{-3} has increased from 22 dB to almost 24.5 dB for a launch power of -5 dBm. The required OSNR has also increased from just over 22 dB to about 25 dB for a launch power of 0 dB. The launch power of 5 dBm shows the biggest change when decreasing channel spacing from 50 GHz to 37.5 GHz for the 2000 km PM-16QAM system. Figure 5.72 outlines the overall change in OSNR requirements due to decreasing channel spacing for the 2000 km systems, correlation diagrams are plotted overlaid on one another with the output power level held constant at -3 dBm. The orange line represents the channel spacing at 50 GHz and the green line represents the 37.5 GHz spaced system.
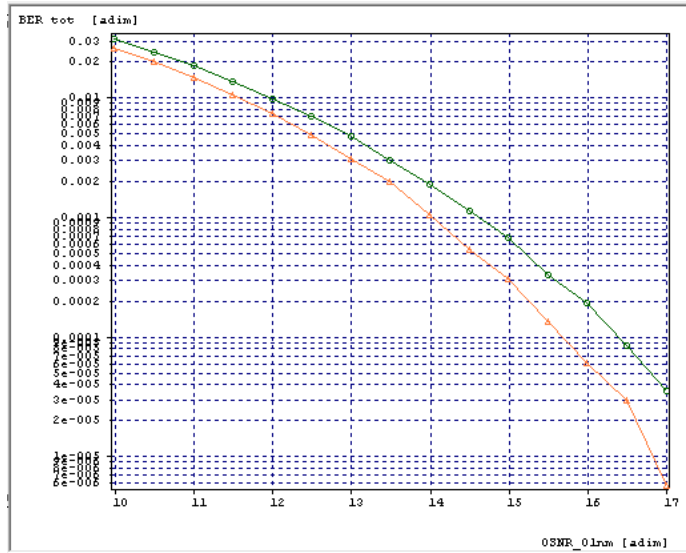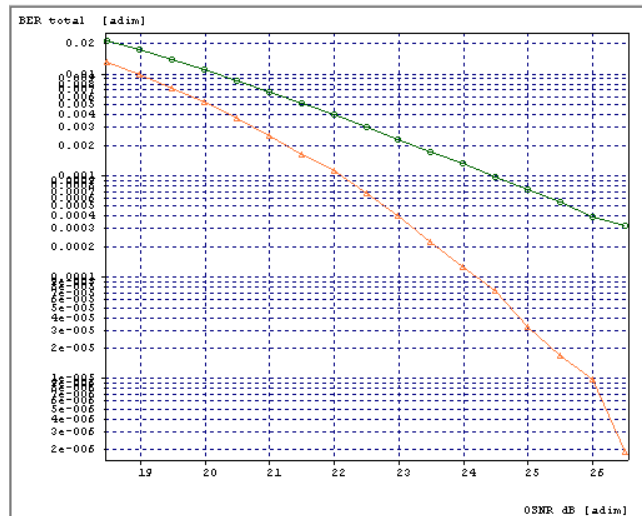

Fig. 5.72: *PM-16QAM Narrowing Channel Spacing for 2000 km Transmission Distance, BER vs. OSNR with Output Power Level of -3 dBm 50 GHz (Orange) & 37.5 GHz (Green)*

The correlation diagram, figure 5.72, provides a general visual of the OSNR penalties as a result of narrowing channel spacing from 50 GHz to 37.5 GHz or increasing spectral efficiency for a five channel 128 Gb/s 2000 km PM-16QAM system.

5.4.3 Results Overview, PM-16QAM & PM-QPSK WDM Transmission Distances Vs. Channel Spacing

In order to provide a conclusive overview of the results; correlation diagrams in figure 5.73 shows the transitions for both PM-QPSK and PM-16QAM at 1040 km, the change from 50 GHz to 37.5 GHz, and at 2000 km, the change from 50 GHz to 37.5 GHz.

5.4.3.1 Results Overview, PM-QPSK WDM Transmission Distances Vs. Channel Spacing

The below results include changes in BER vs. OSNR for PM-QPSK 1040 km, 50 GHz (Orange), 1040 km 37.5 GHz (Blue), 2000 km 50 GHz (Brown) and PM-QPSK 2000 km 37.5 GHz (Green).
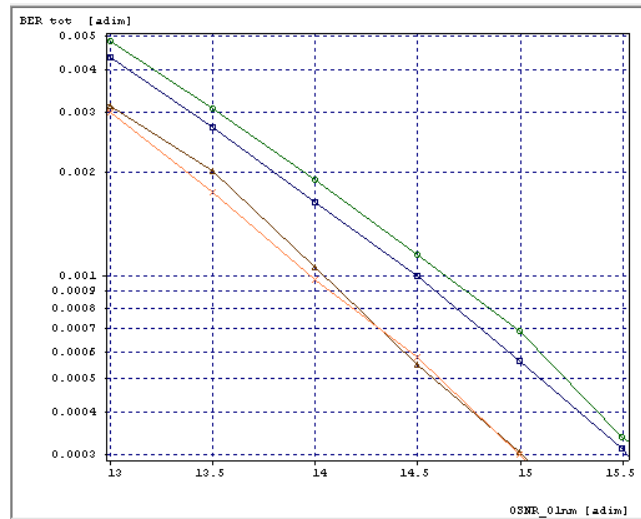
Fig. 5.73: *PM-QPSK BER vs. OSNR Transitions for 1000 km 50 GHz (Orange), 1000 km 37.5 GHz (Blue) & 2000 km 50 GHz (Black), 2000 km 37.5 GHz (Green) with Output Power Level of -3 dBm*

Table 5-10: *Results Overview for PM-QPSK Transmission Distances Vs. Channel Spacing*

Modulation Format	Net Bit Rate Per Channel (Gb/s)	Symbol Rate (Gbaud)	Number of Channels	Total Data Rate (Gb/s)	Grid (GHz)	Transmitted Power (dBm)	Distance (km)	Spectral Efficiency (bit/s/Hz)	OSNR pre-FEC BER = 10^{-3}
PM-QPSK	128	32	5	640	50	-3	1040	2.56	13.98
PM-QPSK	128	32	5	640	37.5	-3	1040	3.41	14.50
PM-QPSK	128	32	5	640	50	-3	2000	2.56	14.04
PM-QPSK	128	32	5	640	37.5	-3	2000	3.41	14.64

As the results show in table 5-10 for this five channel PM-QPSK system, a reduction in channel spacing from 50 GHz to 37.5 GHz at either 1000 km or 2000 km has greater effect on the BER vs. OSNR results in comparison to increasing the transmission length for either channel spacing. When the channel spacing is reduced for a 2000 km transmission distance, the required OSNR is affected just slightly more than reducing the channel spacing for the 1000 km link. These results show that PM-QPSK is very stable for long-haul transmission distances.

5.4.3.2 Results Overview, PM-16QAM WDM Transmission Distance Vs. Channel Spacing

The results in figure 5.74 include changes in BER vs. OSNR for PM-16QAM 1040 km, 50 GHz (Orange), 1040 km 37.5 GHz (Blue), 2000 km 50 GHz and PM-QPSK 2000 km 37.5 GHz (Green).
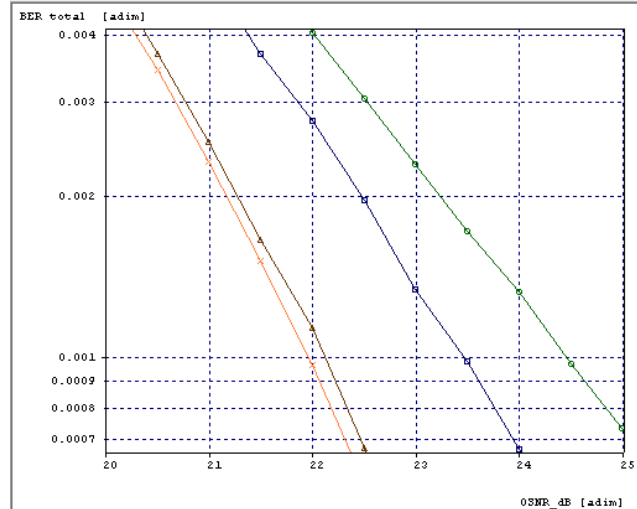
Figure 5.74: *PM-16QAM BER vs. OSNR Transitions for 1000 km 50 GHz (Orange), 1000 km 37.5 GHz (Blue) & 2000 km 50 GHz (Black), 2000 km 37.5 GHz (Green) with Output Power Level of -3 dBm*

Table 5-11: *Results Overview for PM-16QAM Transmission Distances Vs. Channel Spacing*

Modulation Format	Net Bit Rate Per Channel (Gb/s)	Symbol Rate (Gbaud)	Number of Channels	Total Data Rate (Gb/s)	Grid (GHz)	Transmitted Power (dBm)	Distance (km)	Spectral Efficiency (bit/s/Hz)	OSNR pre-FEC BER = 10^{-3}
PM-16QAM	256	32	5	1280	50	-3	1040	5.12	21.97
PM-16QAM	256	32	5	1280	37.5	-3	1040	6.83	23.47
PM-16QAM	256	32	5	1280	50	-3	2000	5.12	22.12
PM-16QAM	256	32	5	1280	37.5	-3	2000	6.83	24.46

As the results show in table 5-11 for this five channel PM-16QAM system, a reduction in channel spacing from 50 GHz to 37.5 GHz at either 1000 km or 2000 km has greater effect on the BER vs. OSNR results in comparison to increasing the transmission length for either channel spacing. When the channel spacing is reduced for a 2000 km transmission distance, the required OSNR is affected more than reducing the channel spacing for the 1000 km link. These results show that PM-16QAM is not as stable for long-haul transmission distances, requires a higher OSNR, but has double the spectral efficiency.

At larger fiber lengths, the PM-16QAM is much more sensitive to non-linear effects in comparison to the PM-QPSK system, especially at a higher transmitted power. Given this information, it can be inferred that at even greater fiber spans, the PM-16QAM system will be overwhelmed with non-linearities. The next set of simulations demonstrates the strong non-linear effects exhibited after longer distances in both systems.

5.4.4 PM-16QAM & PM-QPSK WDM: 3040 km & 4000 km, 50 GHz Channel Spacing

The purpose of the next simulation is to briefly demonstrate the potential of ultra-long-haul transmission for PM-QPSK and the physical limitations of using PM-16QAM for transmission at very long distances. The results in figure 5.75 show that the PM-16QAM system has reached the limits of its potential for long distance transmission at 3040 km. However, the results do show the potential of implementing ultra-long-haul systems using PM-QPSK with an optimized configuration. In figure 5.75, the correlation diagram, PM-QPSK at 3040 km is shown green, PM-QPSK at 4000 km is shown in brown, PM-16QAM at 3040 km is shown in blue and PM-16QAM at 4000 km is shown in orange.
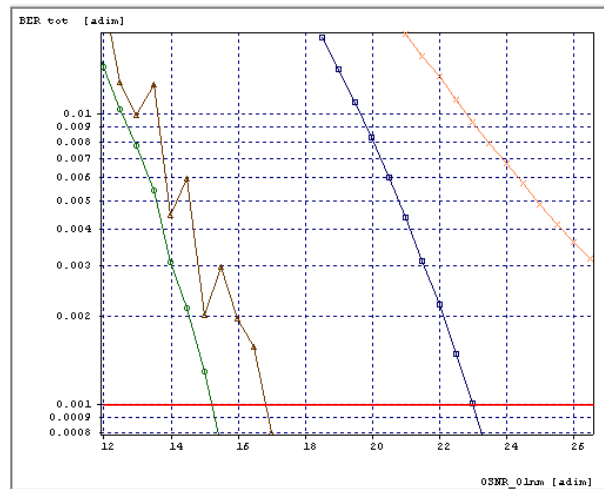
Fig. 5.75: BER vs. OSNR with Output Power Level of -3 dBm for PM-QPSK 3040 km (Green), PM-QPSK 4000 km (Brown) & PM-16QAM 3040 km (Blue), PM-16QAM 4000 km (Orange)

Table 5-12: Results for 3040 km & 4000 km Transmission Distances for PM-QPSK & PM-16QAM

Modulation Format	Net Bit Rate Per Channel (Gb/s)	Symbol Rate (Gbaud)	Number of Channels	Total Data Rate (Gb/s)	Grid (GHz)	Transmitted Power (dBm)	Distance (km)	Spectral Efficiency (bit/s/Hz)	OSNR pre-FEC BER = 10⁻³
PM-QPSK	128	32	5	640	50	-3	3040	2.56	15.23
PM-QPSK	128	32	5	640	50	-3	4000	2.56	16.84
PM-16QAM	256	32	5	1280	50	-3	3040	5.12	23.01
PM-16QAM	256	32	5	1280	50	-3	4000	5.12	N/A

The results from table 5-12 for the PM-16QAM system show that long-distance transmission is limited given its sensitivity to noise and high OSNR requirements. In this configuration, the PM-16QAM system was unable to reach the target BER at even 26.5 dB (orange curve in figure 5.75). Although, the spectral efficiency of the PM-16QAM was doubled as a result of the increase in the number of constellation points in comparison to PM-QPSK, the reduction in system reach was a result of the high OSNR requirements of higher order modulation formats, which are typically more sensitive to practical implementation issues or system impairments (e.g. cross-talk and phase noise) [32].

The results in table 5-12 demonstrate the potential for implementing PM-QPSK systems at ultra-long-haul distances given an optimal set of parameters in order to improve these results. For the 4000 km PM-QPSK system in figure 5.75 (shown in brown), strong nonlinearities are observed. Due to propagation through many fiber spans over thousands of kilometers, ASE builds up in the system. Therefore, when the phase tracking algorithm is applied at the receiver, the receiver can be affected by so-called cycle-slips, i.e., the effect of losing the absolute phase reference as a result of a correction done based on an incorrectly decided symbol [42]. According to [61], the single-ended 90-degree Hybrid component used here, may be susceptible to the possible insertion of an angle inaccuracy that alters the component behavior. For this reason, in the next set of simulations in section 5.5, an attempt is made to further optimize the PM-QPSK system by utilizing an external local oscillator in combination with a polarization rotator as an additional input into a 90-degree Hybrid component, as opposed to using the Hybrid component with a built-in local oscillator (LO). Given the possible limitations of the built-in local oscillator (LO) Hybrid component and nonlinearities observed in the figure 5.75; the reasoning for implementing an external local oscillator is that the system may benefit by both specifying the external local oscillator gain as well as possible improved phase-matching when simulating over ultra-long-haul distances.

5.5   Ultra-Long-Haul PM-QPSK

As ultra-long-haul links, both terrestrial and submarine, usually have distances way beyond 2000 km, the 400G super-channels will most likely to be based on lower order constellation such as QPSK or eventually 8QAM [1]. Again, I am leaving 8QAM out of my consideration due to its higher sensitivity to noise. The first set of simulations are completed at distances of 4500 km and the second set of simulations are taken at distances of 6600 km and the final set of simulations at 9000 km. As a real-world example of transmission at such distances, many submarine optical cable links traverse distances greater or even double the 4500 km distances. Trans-Atlantic cables connecting the United States to Europe reach over 6,600 km, while trans-pacific cables connecting the US to Asia reach over 11,000 km. As an example of a trans-Atlantic link, the "Dunant" link between Virginia Beach, VA and Saint-Hilaire-de-Riez, France, spans 6,600 km. The below figure of the Dunant link, which will be ready for service in 2020, is included (Fig. 5.76) to serve as a visual aid of this type of distance [65].
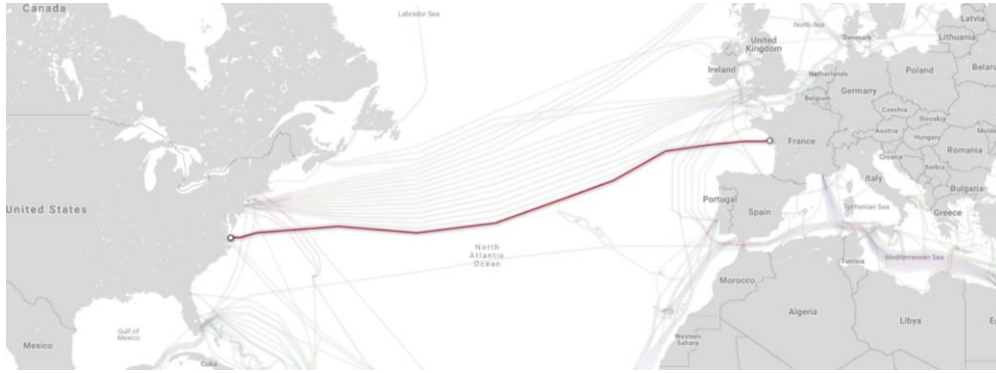
Fig. 5.76: Submarine Optical Cable 6600 km Link, Dunant [65]

5.5.1 Ultra-Long-Haul PM-QPSK 4500 km: 37.5 GHz & 50 GHz

The next simulations demonstrate ultra-long-haul coherent PM-QPSK Nyquist WDM systems. As mentioned in section 5.4.4, an external local oscillator is used in combination with a polarization rotator as an additional input (in addition to the input signal) into an alternative 90-degree Hybrid component, known as *sc4by8_loin*, from [61]. This is used as opposed to using the Hybrid component used in previous simulations with a built-in local oscillator (LO). Since the goal is to optimize the transmission of ultra-long-haul transmission, the parameter scans include the calculation of BER vs. output power levels from -2 to 7 dBm to pinpoint an optimum launch power for the system. An additional simulation is included with channel spacing at 50 GHz to explore the trade-offs associated with channel spacing for this setup. The layout is shown in figure 5.77.
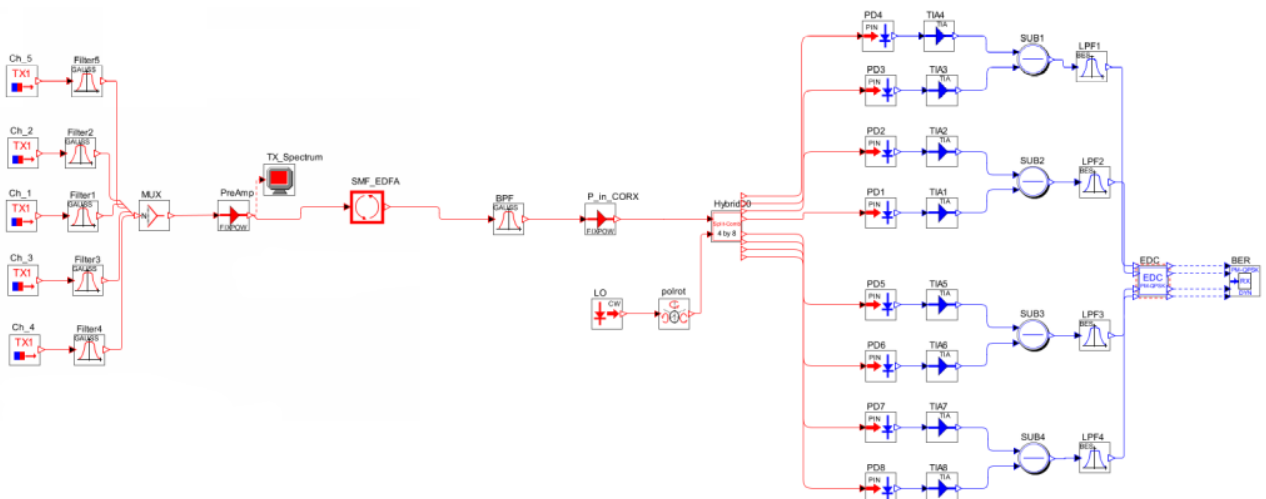
Fig. 5.77: Ultra-Long-Haul, 4500 km, PM-QPSK System

In the five channel WDM system shown in figure 5.77, the 4500 km transmission distance comprises of 30 spans of 150 km fiber spans followed by an amplifier in each span that compensates for the fiber loss at the expense of adding its own noise in the process. Channel spacing is 37.5 GHz between

the five channels with the baud rate of the four QPSK channels at 32 Gb/s. Dispersion is compensated in the electric domain after detection. The dynamically tracking receiver (section 4.3.1) uses a training sequence and implements digital signal processing for estimation of phase and counting of errors. The transmitted spectrum is shown in figure 5.78 on left has a channel spacing of 37.5 GHz between the five channels with the baud rate of the four QPSK channels at 32 Gb/s, which falls in line with quasi-Nyquist WDM systems [35]. The transmitted spectrum of the 50 GHz channel plan is shown on the right.
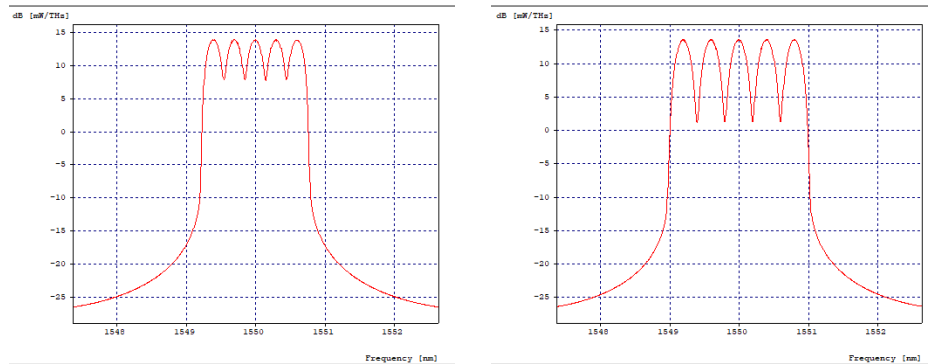
Fig. 5.78: Transmitted 5 Channel PM-QPSK Spectrum with 37.5 GHz Channel Spacing (Left) and 50 GHz Channel Spacing (Right)

With channel spacing of 37.5 GHz and a bit rate of 128 Gb/s, the spectral efficiency of this system is 3.41 Gb/s/Hz and with 50 GHz channel spacing the spectral efficiency is 2.56 Gb/s/Hz.

The correlation diagram (Fig. 5.79) provides insight into effects of launch power on the BER. The BER is calculated from a parameter scan correlated with values of launch power from -2 dBm to 7 dBm at 0.5 dBm increments.
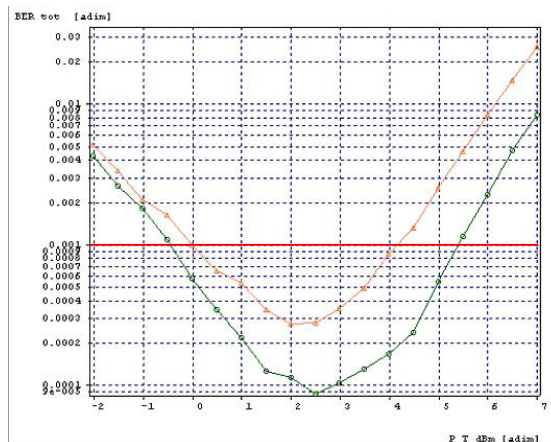
Fig. 5.79: BER Vs. Per Channel with Output Power Levels Ranging from -2 dBm to 7 dBm: 37.5 GHz Channel Spacing (Orange) & 50 GHz Channel Spacing (Green)

For the 37.5 GHz system in orange, the correlation diagram shows that a launch power of 2 dBm provides the lowest pre-FEC BER for the 37.5 GHz system. Additionally, the diagram provides insight

into the suitable launch powers that reach a satisfactory pre-FEC BER of 10^{-3}, which are transmitted powers from 0 dBm to 4 dBm.

For the 50 GHz channel plan, the ideal launch power is shown to be 2.5 dBm. At the expense of the lowered spectral efficiency, the BER is improved overall and the acceptable pre-FEC BER range for the 50 GHz channel plan is now widened with acceptable transmitted power values ranging from -0.5 dB to 5.5 dBm.

These results again show that by sacrificing spectral efficiency, an improvement in the BER can be achieved. Additionally, at the consequence of spectral efficiency, the results indicate a drop in non-linear effects as a wider range of transmitted powers fall within the acceptable pre-FEC BER range of 10^{-3}. Furthermore, it can be noted that the curve of the correlation diagram follows figure 2.7 from section 2.3, where lower values of transmitted power are affected by ASE and higher by nonlinear effects.

At the expense of spectral efficiency, reach can be extended and therefore, the BER achieved at a certain OSNR can be improved as well. This PM-QPSK system is proven to be capable of long-distance transmission and in the following simulations, I have increased fiber lengths in order to push its limits.

5.5.2 Ultra-Long-Haul PM-QPSK 6600 km: 37.5 GHz & 50 GHz

Individual fiber span length is kept the same at 150 km per span and the number of spans is increased to 44, providing a total distance of 6600 km. This also means that 44 EDFAs are required for the link as well. The following pre-FEC BER is calculated with all parameters kept the same as the previous simulations aside from adjusting the channel spacing with results provided for both 37.5 and 50 GHz. The following BER curves in figure 5.80 are again calculated for launch powers from -2 to 7 dBm in 0.5 dBm increments.
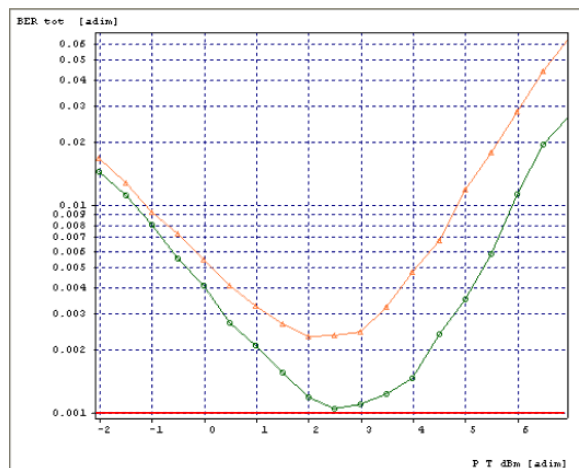
Fig. 5.80: BER Performance for 37.5 GHz Channel Spacing (yellow line) & 50 GHz Channel Spacing (green line) for 6600 km Link

69

The correlation diagram shows that an acceptable pre-FEC BER is achieved for the 50 GHz channel plan at 6,600 km. Also, these simulations prove that the stability of using PM-QPSK as a modulation format for ultra-long-haul links. The next section provides a comparison of the results achieved for the 4500 km and 6600 km links using the two channel plans.

5.5.3   Ultra-Long-Haul PM-QPSK Results Comparisons: 4500 km & 6600 km

The correlation diagram, figure 5.81, is included for comparison purposes for links of both distances and both 37.5 and 50 GHz channel plans. This provides a visual aid in how total fiber length and channel spacing induces non-linearities in the systems. Again, the correlation diagrams are representative of ASE vs. nonlinearities (from section 2.3), where optimal launch powers fall between ASE & nonlinear limits, with ASE affecting the lower valued launch powers and nonlinear limitations affecting the higher valued launch powers. The typical behavior of limiting performance by ASE and nonlinear impairments with respect to launch power is shown in the results in the correlation diagrams (Fig. 5.81), where the curves start to flatten at the longer transmission distance of 6600 km and at the shorter transmission distance of 4500 km, the curves are steeper where the effects of ASE and nonlinear effects are more differentiated.
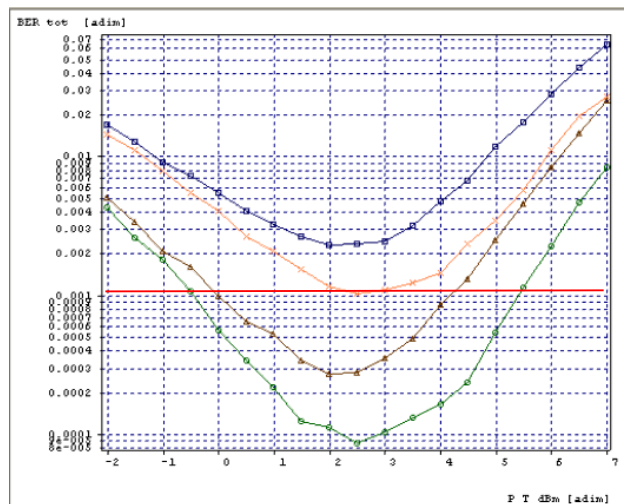
Fig. 5.81: BER Performance for 4500 km & 6600 km Lengths for 37.5 GHz & 50 GHz Channel Spacing. 4500 km, 37.5 GHz (Brown), 4500 km 50 GHz (Green), 6600 km, 37.5 GHz (Blue), 6600 km, 50 GHz (Orange)

Figure 5.81 provides more insight into the effects of channel spacing on non-linear effects between systems of different distances. When increasing the channel spacing from 37.5 GHz to 50 GHz for the 4500 km link, the improvement of BER is greater than the improvement of seen for the 6600 km link when increasing the channel spacing. This result suggests that since the buildup of ASE at lower transmitted powers and non-linear effects at higher transmitted powers is effectively limiting performance after longer distances of fiber, therefore the increase in channel spacing has a smaller effect on BER improvement.

Given this information, the purpose of the next set of simulations explores how different lengths of fiber span, e.g. lengths less than the 150 km spans used in the previous simulations, effect BER rate performance at various transmitted powers. Simulations will be performed at 37.5 GHz channel spacing with a total fiber length of 4500 km. The changes will be applied to the individual fiber span lengths and number of fiber spans, so that the total 4500 km length remains the same.

5.5.4   Influence of Fiber Span Lengths on Ultra-Long-Haul PM-QPSK

In this set of simulations, the 37.5 GHz spaced WDM PM-QPSK system is simulated using different fiber span lengths in order to demonstrate the influence of fiber span length on system performance. The fiber spans lengths used here are; 50 km, 75 km, 100 km, 125 km, 150 km and 180 km. The shorter the fiber spans, the more spans of single mode fiber and EDFA amplifiers that are required to cover the 4500 km distance. In the next correlation diagram (Fig. 5.82); the 50 km lengths (green curve) require 90 spans of single mode fiber and EDFA amplifiers, the 75 km (brown curve) with 60 spans, 100 km (blue curve) with 45 spans, 125 km (purple) with 36 spans, 150 km (teal) with 30 spans, and finally the 180 km length (180 km) requires 25 spans of fiber with EDFA amplifiers for each span.
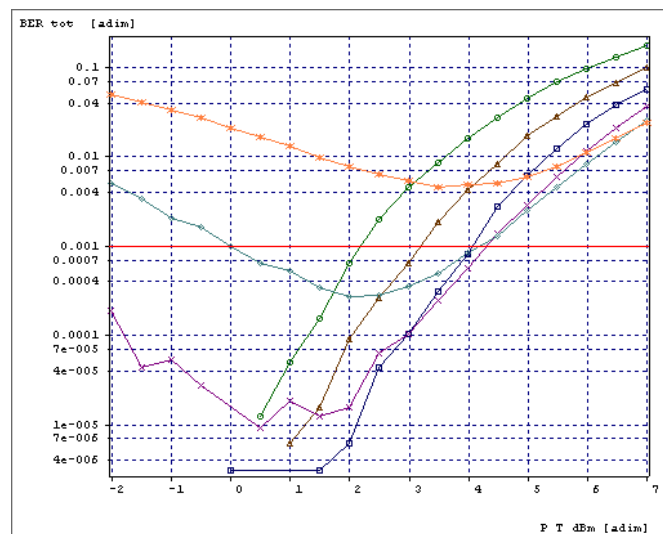
Fig. 5.82: Influence of Fiber Span Lengths on BER: 50 km Fiber Spans (Green), 75 km (Brown), 100 km (Blue), 125 km (Purple), 150 km (Teal), & 180 km (Orange)

The BER curves show varying results where the BER lowered, on the nonlinear effects side of the curves, from increasing fiber span length from 50 km (green) to 75 km (brown) and once again to 100 km (blue), then the BER is increased with fiber span length increases to 125 km (purple), 150 km and much higher with 180 km (orange) spans. The 125 km span length is a bit more stable than the 100 km span length at higher transmitted powers (at or above 3 dBm) and as a compromise between the results of

the two span lengths, I have chosen a span length 120 km to test for long distance transmission in the next simulations.

5.5.5   Optimized Fiber Span Length, WDM PM-QPSK 6600 km System

In order to test the benefits of using shorter fiber spans than the 150 km fiber spans used in the previous 6600 km links, the next simulation includes 120 km fibers spans with a total reach of 6600 km. This is tested at a channel spacing of 37.5 GHz and 50 GHz. Finally, these results are compared against the original correlation diagrams of the 6600 km link with 150 km spans (both 37.5 GHz and 50 GHz). But firstly, in figure 5.83, the 37.5 GHz spaced system is represented by the orange line and the 50 GHz based system is represented by the green curve.
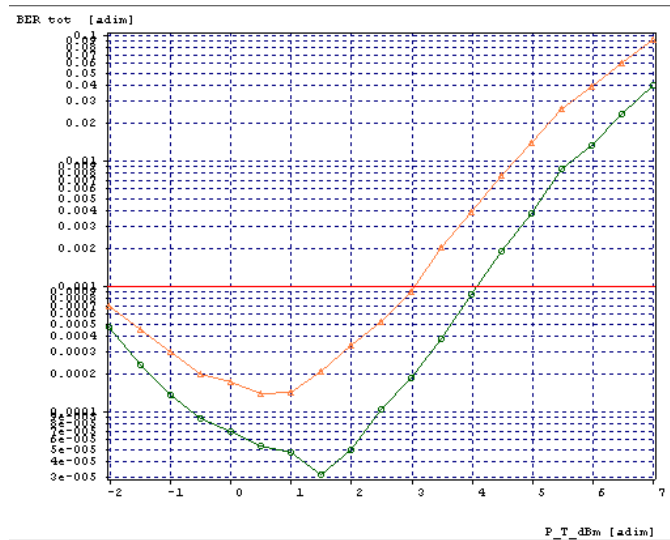
Fig. 5.83: BER Performance for 120 km Spans, 37.5 GHz Channel Spacing (yellow line) & 50 GHz Channel Spacing (green line) for 6600 km Link

The results from figure 5.83 demonstrate the benefits of shortening the fiber spans from 150 km to 120 km as there is a significant improvement in the BER for the 6600 km link. In order to gauge the change in BER from including 55 spans of 120 km of fiber and EDFA amplifiers in place of 44 spans of 150 km fiber, the results are included in one correlation diagram in figure 98. The 150 km per span 37.5 GHz system is shown in blue, the 150 km per span at 50 GHz is shown in orange, the 120 km per span 37.5 GHz system is shown in brown and finally, the 120 km per span 50 GHz system is shown in Green.
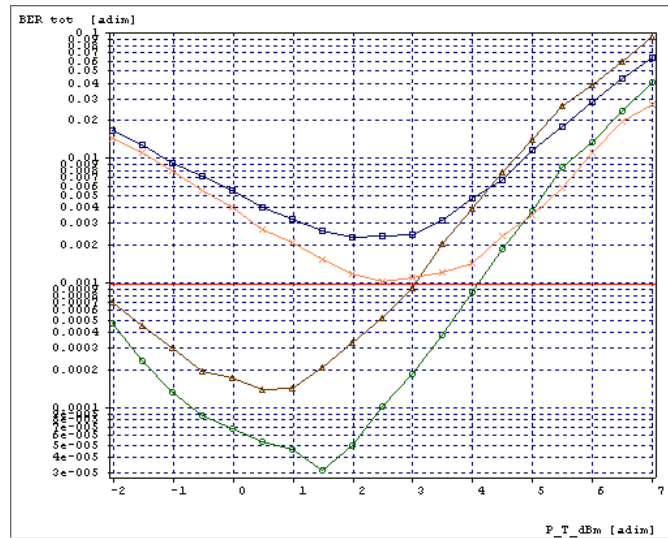
Fig. 5.84: *BER Performance Comparison Between 150 km & 120 km Fiber Spans for 37.5 GHz & 50 GHz Channel Spacing. 120 km 37.5 GHz (Brown), 120 km 50 GHz (Green) & 150 km 37.5 GHz (Blue), 150 km 50 GHz (Orange)*

In figure 5.84, for the 120 km spans (brown and green) curves, the optimal launch powers are lower in comparison to the 150 km spans (blue and orange). For the 120km spans with 37.5 GHz spacing, the optimal launch powers fall between -0.5 dBm and 1.5 dBm. For the 120 km spans with 50 GHz spacing the optimal launch powers fall between 0.5 dBm and 2 dBm. Whereas the 150 km span systems fall between higher launch powers between 1.5 and 3.5 dBm. Furthermore, higher launch powers produce higher nonlinear effects in the 120 km span systems in comparison to the 150 km span systems.

A potential tradeoff here is that the 120 km span lengths require the installation of more span locations and EDFA amplifiers, which could be difficult to implement, depending on the physical constraints on land or water. However, this further highlights the versatility and ultra-long-haul capabilities of PM-QPSK systems.

5.5.6   Optimized Fiber Span Length & Increased Transmission Distance, 9000 km

Given the fact that the 120 km span lengths offer a substantial improvement in the BER, the purpose of the next simulation is to test the limits of the WDM PM-QPSK system by increasing the total transmission distance to 9000 km. The following simulations utilize 75 spans of 120 km length single mode fiber with EDFAs. In figure 5.85 the correlation diagram, the 37.5 GHz spaced system is represented by the orange curve and the 50 GHz based system is represented by the green curve.
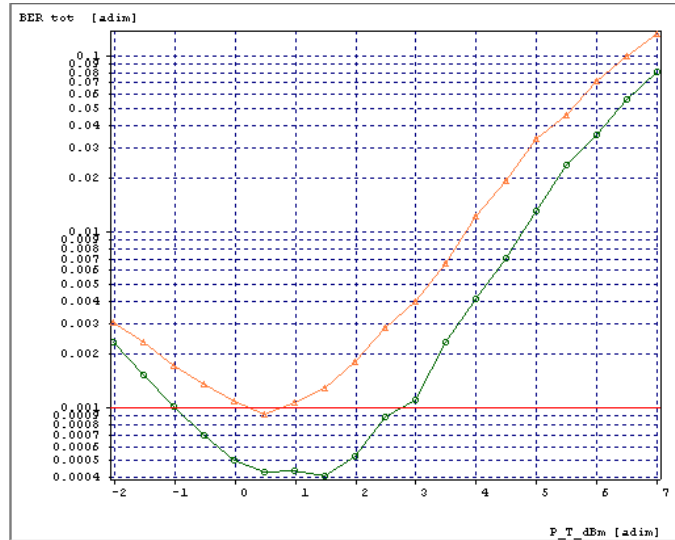
Fig. 5.85: *BER Performance for 9000 km Link with 120 km Spans, 37.5 GHz Channel Spacing (Orange) & 50 GHz Channel Spacing (Green)*

5.6   Influence of Fiber Span Length on WDM PM-16QAM

Given that the adjustment of fiber span length had a positive effect on increasing transmission length of the high bit rate PM-QPSK system, a similar method is implemented in order to test the influence of fiber span length on a long-haul transmission PM-16QAM system. The same schematic PM-16QAM with 3000 km total fiber length from the previous comparison section 5.4 is used. The original schematic employed 80 km fiber span lengths (38 spans) for a total reach of 3040 km. For a quick comparison, span lengths of 100 km, 120 km and 150 km are compared against the 3000 km link and plotted into a BER vs. OSNR diagram (Fig. 5.86).
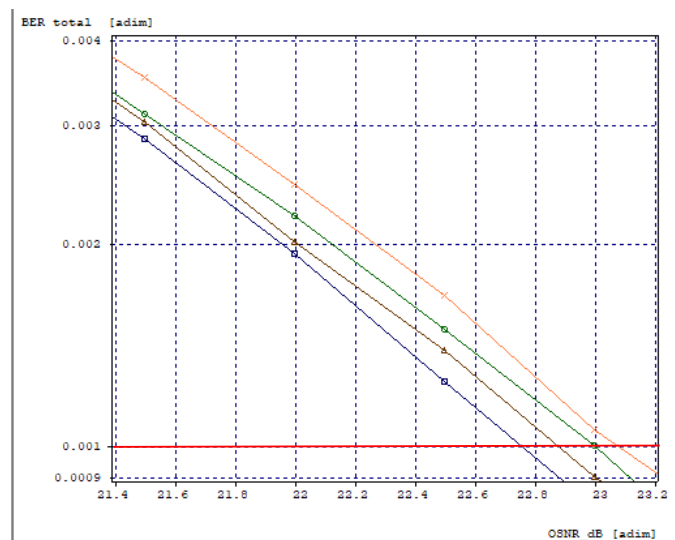
Fig. 5.86: *BER Performance for Span Lengths: 80 km (Green), 100 km (Brown), 120 km (Blue) & 150 km (Orange)*

74

Table 5-13: Results for 3000 km Transmission Distance with Different Spans Lengths for PM-16QAM

Modulation Format	Net Bit Rate Per Channel (Gb/s)	Symbol Rate (Gbaud)	Number of Channels	Total Data Rate (Gb/s)	Grid (GHz)	Transmitted Power (dBm)	Span Length (km)	Spectral Efficiency (bit/s/Hz)	OSNR pre-FEC BER = 10^{-3}
PM-16QAM	256	32	5	1280	50	-3	80	5.12	23.00
PM-16QAM	256	32	5	1280	50	-3	100	5.12	22.88
PM-16QAM	256	32	5	1280	50	-3	120	5.12	22.76
PM-16QAM	256	32	5	1280	50	-3	150	5.12	23.08

The results in table 5-13 show that in comparison to the PM-QPSK system, the PM-16QAM system does not respond as dramatically to optimizing the fiber span length. However, there is some improvement in the required OSNR that achieves the required BER when increasing the span length from 80 km to 100 km, and slightly more improvement when increasing the span length to 120 km per span. The required OSNR increases with the 150 km span length. Therefore, the optimized fiber span length for this PM-16QAM system is also 120 km. Also, it is worth noting that here the resulting required OSNR of 22.76 dB for this 3000 km PM-16QAM system (with 120 km span lengths) is now closer to the OSNR results for the 2000 km 80 km span length PM-16QAM system, where the required OSNR was 22.12 dB (section 5.4.2.2 in table 5-8). The next simulation explores the possibility of improving the system performance further by testing various transmitted powers.

5.6.1 Influence of Transmitted Power: WDM PM-16QAM with Optimized Span Length

As shown from the previous simulations, PM-16QAM is more sensitive to higher transmitted powers, therefore, the next simulations test transmitted powers of -5 dBm, -4 dBm, -3 dBm (used previously), -2 dBm, -1 dBm, 0 dBm and 1 dBm with results plotted in figure 5.87.

Fig. 5.87: BER Performance: Transmitted Powers for 120 km Spans, -5 dBm (Gray), -4 dBm (Green), -3 dBm (Red), -2 dBm (Black), -1 dBm (Orange), 0 dBm (Blue) & 1 dBm (Pink)

Table 5-14: Results for PM-16QAM 3000 km Transmission Distance with 120km Spans Lengths at Transmitted Powers (-5 dBm to 1 dBm)

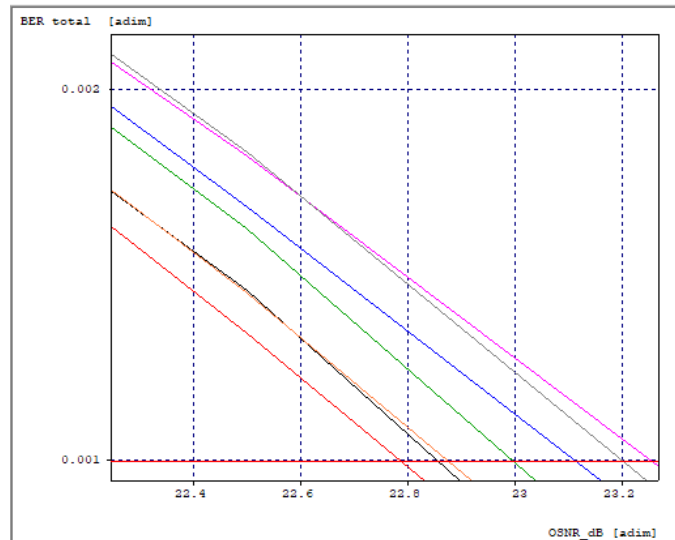| Modulation Format	Net Bit Rate Per Channel (Gb/s)	Symbol Rate (Gbaud)	Number of Channels	Total Data Rate (Gb/s)	Grid (GHz)	Transmitted Power (dBm)	Span Length (km)	Spectral Efficiency (bit/s/Hz)	OSNR pre-FEC BER = 10^{-3}
PM-16QAM	256	32	5	1280	50	-5.00	120	5.12	23.20
PM-16QAM	256	32	5	1280	50	-4.00	120	5.12	23.00
PM-16QAM	256	32	5	1280	50	-3.00	120	5.12	22.76
PM-16QAM	256	32	5	1280	50	-2.00	120	5.12	22.85
PM-16QAM	256	32	5	1280	50	-1.00	120	5.12	22.87
PM-16QAM	256	32	5	1280	50	0.00	120	5.12	23.11
PM-16QAM	256	32	5	1280	50	1.00	120	5.12	23.25

The parameter scan with results shown in table 5-14 show that a transmitted power of -3 dBm is the optimum launch power for this PM-16QAM system with 120 km fiber spans with a total reach of 3000 km. Although, improvement was not achieved from the prior results, this does indeed provide insight into the behavior regarding the physical limitations of a PM-16QAM system and its feasibility of long-haul transmission and the effects of various transmitted powers.

6   Conclusions

In this thesis, the methods of scaling the capacity of optical systems were outlined and then implemented. The initial simulations included comparison of advanced modulation formats which provided examples of the consequences involved in implementing modulation formats with a higher number of constellation points. The higher order modulation formats achieved higher data rates in comparison to PM-QPSK yet required higher OSNR in order to achieve the required BER due to the noise susceptibility at the receiver increasing with the order of the modulation format. These limitations were then further demonstrated by implementing an 80 km fiber span in the PM-64QAM system, where the required BER was not achievable, even at an OSNR of 30 dB.

The next sections, 5.2.1 and 5.2.2, explored topics such as 200G/400G and WDM Nyquist Super-Channels for next-generation optical transmission. The WDM Nyquist Super-Channel demonstrated the great potential of PM-16QAM for satisfying increasing demand for larger capacity systems. Although, an implementation with fiber spans and EDFA amplification was not realized in these sections due to the high bit rate, tight channel spacing and dense PM-16QAM modulation format, the nine channels achieved a bit rate of roughly 2 Tb with a high spectral efficiency of 7.2 bit/s/Hz.

Section 5.3 demonstrated the use of PM-QPSK as the current State of the Art best-in-class solution for commercial long-haul transmission. The system utilized a nine-channel WDM coherent system with DSP at the receiver, achieving approximately 1 Tb long-haul transmission. It was then pointed out that the system could be improved by using more advanced DSP used at the receiver. The DSP used in this system was memoryless, and although it receiver the polarization and phase rotations using the Viterbi &

Viterbi algorithm, the use of dynamic receivers discussed in section 4.3.1, could offer improvement as the LMS algorithm enabled compensation of pattern dependent phenomena such as residual chromatic dispersion and polarization mode dispersion.

The next section 5.4, implemented the use of the dynamic receivers discussed in section 4.3.1, and provided in-depth comparisons of the WDM PM-QPSK and PM-16QAM systems. The physical limitations were thoroughly explored and the trade-offs between spectral efficiency and reach was highlighted in the results provided. PM-16QAM provided double the spectral efficiency but was limited in terms of achievable reach due to the high OSNR requirements as a result of the noise induced at the receiver. It was shown that PM-QPSK was much more resilient to the effects of reducing channel spacing, increased transmitted power and increased transmission distance in comparison to the PM-16QAM system. Both systems were more sensitive to increased transmitted power when the channel spacing was narrowed from 50 GHz to 37.5 GHz, however, the PM-16QAM proved to be much more sensitive to higher transmitted powers at 37.5 GHz channel spacing due to the increased nonlinear effects induced when channel spacing is tight. When studying the effects of increasing transmission distance for the PM-QPSK system, it was shown in section 5.4.3 that a reduction in channel spacing had more detrimental effects on BER vs. OSNR (receiver sensitivity) in comparison to increasing the transmission length at either channel spacing (when that increase was from 1000 km to 2000 km). Similar results were seen in the PM-16QAM system, where reduced channel spacing had more detrimental effects on noised induced at the receiver in comparison to increased transmission length at either channel spacing. However, where the PM-QPSK did not incur greater penalties at a reduction in channel spacing when increasing transmission length, the PM-16QAM system did, thus proving the high resiliency of PM-QPSK at longer transmission distances and the versatility it shows when reducing channel spacing at those distances.

Ultra-long-haul transmission using PM-QPSK was simulated in section 5.5.1 to better understand the physical limitations of PM-QPSK as well as better understand suitable transmitted powers and fiber span lengths. Noise loading was omitted in this system (for OSNR calculation) as the focus was no longer on receiver sensitivity, but the effects of the transmitted power on the BER. Parameter scans were set up to plot BER vs. Transmitted Powers from -2 to 7 dBm in 0.5 dBm increments so that the graphs reflected the effects described in section 2.3.2, where typically an optimal launch power exists, where at lower launch powers, the system is limited by ASE noise and higher launch powers, the system is limited by nonlinear effects. The lowest point in the resulting graphs, represented the optimal launch power, where at lower, or higher launch powers, signal degeneration would be dominated by either ASE or nonlinear effects (respectively). Adjusting channel spacing showed that tighter channel spacing (37.5 GHz in comparison to 50 GHz) caused the optimal transmitted power to shift to lower transmitted powers. In the case for the 4500 km system, the optimal transmitted power was 2 dBm with 37.5 GHz spacing and 2.5 dBm with 50

GHz channel spacing. This proves that nonlinear effects in the system are induced earlier on the ASE vs. nonlinear effects curve when channel spacing is tighter. This can be seen in figure 5.79 from section 5.5.1. The results of increasing transmission distance demonstrated that decreased channel spacing at larger distances (6600 km in this case) had more detrimental effects than at shorter distances, as expected. In section 5.5.4 the influence of fiber span lengths was explored and it was found that reducing the fiber spans spacing with EDFA amplifiers from 150 km to 120 km, helped in achieving in longer transmission distances, where it was demonstrated that the PM-QPSK system is capable of reaching 9000 km with both 37.5 GHz and 50 GHz spacing.

In section 5.6, the WDM PM-16QAM 3000 km system used in section 5.5.4, was optimized by testing various span lengths. The BER vs. OSNR results showed that using 120 km offered some improvement compared to the 80 km span lengths used in previous sections for this system. Further optimization was attempted by creating parameter scans for different transmitted powers, however further optimization could not be achieved. This did however prove that PM-16QAM is capable of long-haul transmission at 200G per channel.

In consideration of problem statement and related comments in section 1, this thesis has covered the methods achieving high bit rates systems, greater than 100G, while considering degenerative effects. The physical limitations of these systems were explored, and various trade-offs discussed after providing detailed results. Potential further study could be testing the simulated results experimentally as the simulations provided in this thesis give direction regarding the parameters to consider. Another possible follow up for study, since the focus of this thesis was general in achieving higher bit rates, could be the exploration of and mitigation of specific nonlinear effects related to high capacity optical systems. Another idea that comes to mind is the study of trans-Atlantic optical transmission and its optimization. In section 5.5.4, it was seen that lower fiber span lengths e.g. 50 km, 75 km and 100 km, results from the parameter scans gave a zero BER for lower transmitted powers. This would require verification by studying experimentally, and/or by confirming with OptSim the validity of the results and their implications. Furthermore, after completing this thesis, it seems the exploration of ultra-long-haul spectrally efficient transmission by using PM-16QAM with advanced DSP in order to mitigate nonlinear impairments would be a topic for discussion.

REFERENCES

[1]   Technology Options for 400G Implementation OIF-Tech-Options-400G-01.0, The Optical Internetworking Forum. July 2015.

[2]   Telecommunication standardization sector of ITU, "Optical fibres, cables and systems," 2009. [Online]. Available: http://www.itu.int/dms pub/itu-t/opb/hdb/T-HDB-OUT.10-2009-1-PDF-E.pdf

[3]   D. Richardson, Frontiers in Optical Communications Part 1: "Some History and Fundamentals, Optoelectronics Research Centre Southampton University United Kingdom" [Online]. Available:

https://www.sif.it/static/SIF/resources/public/files/va2014/Richardson_talk.pdf

[4]   G. Agrawal, Fiber-Optic Communication Systems. Wiley Series in Microwave and Optical Engineering, Wiley, 4th ed., 2012.

[5]   M. Islam, "Raman amplifiers for telecommunications," IEEE Journal of Selected Topics in Quantum Electronics, vol. 8, no. 3, pp. 548–559, 2002.

[6]   L. Spiekman, J. Wiesenfeld, A. Gnauck, L. Garrett, G. Van Den Hoven, T. Van Dongen, M. Sander-Jochem, and J. Binsma, "Transmission of 8 DWDM channels at 20 Gb/s over 160 km of standard fiber using a cascade of semiconductor optical amplifiers," IEEE Photonics Technology Letters, vol. 12, no. 6, pp. 717–719, 2000.

[7]   Z. Tong, C. Lundström, P. A. Andrekson, C. J. McKinstrie, M. Karlsson, D. J. Blessing, E. Tipsuwannakul, B.J. Puttnam, H. Toda, and L. Grüner-Nielsen, "Towards ultrasensitive optical links enabled by low-noise phase-sensitive amplifiers," Nature Photonics, vol.5, no.7, pp.430–436, 2011.

[8]   P. Becker, N. Olsson, and J. Simpson, Erbium-Doped Fiber Amplifiers, 1st ed. Elsevier Academic Press, 1999.

[9]   Y. Thareja, G. Singh, "Effect of SRS-XPM-FWM-ASE Nonlinearity in Optical Communication System," International Journal of Advanced Research in Electrical, Electronics and Instrumentation Engineering Vol. 2, Issue 7, July 2013.

[10]   J. K. Patel, "Optical Communication Systems Overview of Technologies and Challenges," RSOFT Training Materials, Synopsys, Inc. 2018.

[11]   D. Gloge, "Dispersion in weakly guiding fibers," Appl. Opt., vol. 10, no. 11, pp. 2442–2445, Nov. 1971.

[12]   Corning, "Corning R LEAF R optical fiber," Dec. 2012. [Online]. Available: https://www.corning.com/media/worldwide/coc/documents/Fiber/LEAF%20optical%20fiber.pdf

[13]   P. Bayvel, C. Behrens, David S. Millar, "Digital Signal Processing (DSP) and Its Application in Optical Communication Systems" in Optical Fiber Telecommunications VIB, Academic Press, 2013.

[14]   M. Alfiad, D. van den Borne, A. Napoli, A. Koonen, and H. de Waardt, "A DPSK receiver with enhanced CD tolerance through optimized demodulation and MLSE," IEEE Photon. Technol. Lett., vol. 20, no. 10, pp. 818–820, May 2008.

[15]   OFS, A Furuka Company, "Allwave R ZWP fiber (zero water peak)," Apr. 2013. [Online]. Available: http://www.ofsoptics.com/resources/AllWave-117-web.pdf

[16]   D. Breuer, H.-J. Tessmann, A. Gladisch, H.-M. Foisel, G. Neumann, H. Reiner, and H. Cremer, "Measurements of PMD in the installed fiber plant of Deutsche Telekom," in Digest of the IEEE/LEOS Summer Topical Meetings, Vancouver, Canada, , pp. MB2.1/5–MB2.1/6. July 2003.

[17]   X. Liu, X. Wei, A. H. Gnauck, C. Xu, and L. K. Wickham, "Suppression of intrachannel four-wave-mixing induced ghost pulses in high-speed transmissions by phase inversion between adjacent marker blocks," Opt. Lett., vol. 27, no. 13, pp.1177–1179, Jul. 2002.

[18]   J. Latal, J. Vitasek, P. Koudelka, P. Siska, R. Poboril, Lukas Hajek, A. Vanderka, V. Vasinek., "Simulation of modulation formats for optical access network based on WDM-PON", 16th International Conference on Transparent Optical Networks. 2014.

[19]   P. Winzer and R. Essiambre, "Advanced optical modulation formats," Proc. of the IEEE, vol. 94, no. 5, pp. 952–985, May 2006.

[20]   E. Ip and JM. Kahn., "Compensation of Dispersion and Nonlinear Impairments Using Digital Backpropagation," Lightwave Technologies, 2008.

[21]   M. Secondini and E. Forestieri, "On XPM mitigation in WDM Fiber-optic Systems," IEEE, Photon Technologies, 2014.

[22]   D. van den Borne, V. Veljanovski, E. De Man, U. Gaubatz, C. Zuccaro, C. Paquet, Y. Painchaud, S. Jansen, E. Gottwald, G.-D. Khoe, and H. de Waardt, "Cost-effective 10.7-Gbit/s long-haul transmission using fiber bragg gratings for in-line dispersion

compensation," in Proc. Optical Fiber Communication Conference (OFC), Anaheim, California, paper OThS5., Mar. 25–29 2007.

[23] L. Gruner-Nielsen, M. Wandel, P. Kristensen, C. Jorgensen, L. Jorgensen, B. Edvold, B. Palsdottir, and D. Jakobsen, "Dispersion-compensating fibers," J. Lightwave Technologies, vol. 23, no. 11, pp. 3566–3579, Nov. 2005.

[24] P. J. Winzer, R. Ryf, S. Randel, "Spatial Multiplexing Using Multiple-Input Multiple-Output Signal Processing" in Optical Fiber Telecommunications VIB, Academic Press, 2013.

[25] S. Inao, T. Sato, S. Senstsui, T. Kuroha, Y. Nishimura, "Multicore optical fiber", In Proc. Optical Fiber Communication Conf., Washington, DC, USA, paper WB1, 1979.

[26] S. Berdague, P. Facq, "Mode division multiplexing in optical fibers", Applied Optics, vol. 21, no. 11, pp. 1950–1955, 1982.

[27] H. Takara, A. Sano, T. Kobayashi, H. Kubota, H. Kawakami, A. Matsuura, Y. Miyamoto, Y. Abe, H. Ono, K. Shikama, Y. Goto, K. Tsujikawa, Y. Sasaki, I. Ishida, K. Takenaga, S. Matsuo, K. Saitoh, M. Koshiba, T. Morioka, "1.01-Pb/s (12 SDM/222 WDM/456 Gb/s) crosstalk-managed transmission with 91.4-b/s/Hz aggregate spectral efficiency", in Proc. ECOC, Amsterdam, Netherlands, paper Th.3.C.1, Sep. 2012.

[28] W. Idler, F. Buchali, "Higher-Order Modulation Formats – Concepts and Enabling Devices", Fibre Optic Communication. Springer Series in Optical Sciences, vol 161. 2017.

[29] International Telecommunications Union, "G.694.1 spectral grids for WDM applications: DWDM frequency grid", Series G: Transmission Systems and Media, Digital Systems and Networks, 2012.

[30] B. Batsuren, H. Hwan Kim, C. Yong Eom, J. Joo Choi, and J. Seung Lee1 "Optical VSB Filtering of 12.5-GHz Spaced 64×12.4 Gb/s WDM Channels Using a Pair of Fabry-Perot Filters", Journal of the Optical Society of Korea Vol. 17, No. 1, pp. 63-67, February 2013.

[31] R. J. Essiambre and R. W. Tkach, "Capacity Trends and Limits of Optical Communication Networks", Proceedings of the IEEE, vol. 100, no. 5, May 2012.

[32] G. B. Bosco, D. Pilori, P. P. Poggiolini, A. Carena Carena, F. P. Guiomar, "Scalable Modulation Technology and the Tradeoff of Reach, Spectral Efficiency and Complexity", SPIE Photonics, January 2017.

[33] J. K. Patel, "Modeling Polarization-Multiplexed Coherent Fiber-Optic Communication Systems in OptSim," Synopsys, Inc., April 2016.

[34] P. J. Winzer, "High-Spectral-Efficiency Optical Modulation Formats", Journal of Lightwave Technology, vol. 30, no. 24, pp. 3824-3835, Dec. 2012.

[35] A. D. Ellis, F.C. Garcia Gunning, "Spectral density enhancement using coherent WDM", IEEE Photonics Technology Letter, vol. 17, no. 2, pp. 504-506, Feb. 2005.

[36] S. Chandrasekhar, X. Liu, Fellow, "OFDM Based Superchannel Transmission Technology", Journal of Lightwave Technology, vol. 30, no. 24, pp. 3816-3823, December 2012.

[37] E. Lach, W. Idler, "Modulation formats for 100G and beyond," Optical Fiber Technology, Elsevier Inc., August 2011.

[38] M. Salsi, A. Ghazisaeidi, P. Tran, R. Muller, L. Schmalen, J. Renaudier, H. Mardoyan, P. Brindel, G. Charlet, and S. Bigo, "31 Tb/s transmission over 7,200 km using 46 Gbaud PDM-8QAM with optimized error correcting code rate," in Proc. OptoElectronics and Communications Conference (OECC), Kyoto, Japan, July 2013.

[39] P. Leoni, V. Sleiffer, S. Calabro`o, and B. Lankl, "Constellation expansion and iterative demapping and decoding for 100G systems," in Proc. European Conference on Optical Communication (ECOC), London, United Kingdom, Sep. 22–26 2013.

[40] H. Zhang, J.-X. Cai, H. G. Batshon, M. Mazurczyk, O. Sinkin, D. Foursa, A. Pilipetskii, G. Mohs, and N. Bergano, "200 Gb/s and dual wavelength 400Gb/s transmission over transpacific distance at 6 b/s/Hz spectral efficiency," in Proc. Optical Fiber Communication Conference (OFC), Anaheim, California, Mar.17–21 2013.

[41] F. Buchali, K. Schuh, L. Schmalen, W. Idler, E. Lach, and A. Leven, "1-Tbit/s dual-carrier DP 64QAM transmission at 64Gbaud with 40% overhead soft-FEC over 320km SSMF," in Proc. Optical Fiber Communication Conference (OFC), Anaheim, California, Mar. 17–21 2013.

[42] J. K. Patel, " Coherent Communication Systems ", Synopsys, Inc. April 2016.

[43] OSA. Ip, et al., "Coherent detection in optical fiber systems," Optics Express, vol. 16, no. 2, January 2008.

[44] A. W. Davis, M. J. Pettitt, J. P. King, and S. Wright, "Phase diversity techniques for coherent optical receivers," J. Lightwave Technologies, vol. 5, no. 4, pp. 561–572, April 1987.

[45] T. J. Schmidt, D. R.Stauer, and K. Gass, "Implementation Agreement for Intradyne Coherent Receivers," Optical Internetworking Forum, Tech. Rep., April 2010.

[46] M. Seimetz and C.-M. Weinert, Options, feasibility, and availability of 2x4 90-degree hybrids for coherent optical systems," J. Lightwave Technologies, vol. 24, no. 3, pp.1317-1322, 2006.

[47] A. Carena, V. Curri, P. Poggiolini, F. Forghieri, "Optical vs. Electronic Dispersion Compensation in WDM coherent PM-QPSK systems at 111 Gb/s," IEEE., OFC/NFOEC, 2008.

[48] C. Laperle, et al. "WDM Performance and PMD Tolerance of a Coherent 40-Gbit/s Dual Polarized QPSK Transceiver," IEEE., JLT, pp. 168-175, Jan 2008.

[49] OSA. Savory, S. J., Gaviolli, G., Kellye, R. I., Bayvel, P., "Transmission of 42.8 Gb/s Polarization Multiplexed NRZQPSK over 6400km of Standard Fiber with no Optical Dispersion Compensation," Optical Fiber Communication Conference, March 2007.

[50] Godard, D. N., "Self-recovering equalization and carrier tracking in two-dimensional data communication systems," IEEE Transactions on Communications, Volume: 28 , Issue: 11, Nov 1980.

[51] Connexions, D. Jones, "The Constant-Modulus Algorithm and Property-Restoral Principle", [Online]. Available: https://archive.cnx.org/contents/bd9a5e09-f970-425f-9575-4927a1f5345a@1/the-constant-modulus-algorithm-and-the-property-restoral-principle

[52] T. F. Detwiler, et al., "Asynchronously sampled blind source separation for coherent optical links," Proceedings Of SPIE, Vol. 7960, p. 79600D, 2011.

[53] D. van den Borne, et al. "Carrier Phase Estimation for Coherent Equalization of 43-Gb/s POLMUX NRZ DQPSK Transmission with 10.7-Gb/s NRZ Neighbors," ECOC 2007.

[54] S. Nowlan, J., G. E. Hinton, "A Soft Decision-Directed Algorithm for Blind Equalization," IEEE Trans. Comm., pp. 275-279. February 1993.

[55]   ASE cable system, NEC, [online]. Available: http://www.nec.com, 2013.

[56]   G. Bruno, "Evolutions of a pan-European Network over TrueWave-RS fiber enabled by flexible grid and coherent detection", OFC/NFOEC, paper JW2A.5, Mar. 2012.

[57]   Bell Labs, "Metro Network Traffic Growth: An Architecture Impact Study", White Paper, [online]. Available: http://www.tmcnet.com/tmc/whitepapers/documents/ whitepapers/2013/9378-bell-labs-metro-network-traffic-growth-an-architecture.pdf, 2013.

[58]   J. K. Patel, "Training Course – OptSim and ModeSYS", RSOFT Training Materials, Synopsys, Inc. 2015.

[59]   J. K. Patel, "Considerations for Performance Estimation," RSOFT Support, Synopsys, Inc. February 2018.

[60]   S. M. Jahangir Alam, M. Rabiul Alam, G. Hu, Md. Zakirul Mehrab, "Bit Error Rate Optimization in Fiber Optic Communications", International Journal of Machine Learning and Computing, Vol. 1, No. 5, December 2011.

[61]   RSoft Design Group OptSim Models Reference: Sample Mode, pp. 466 – 577.

[62]   J. K. Patel, "Summary of EDFA Models in Samplemode of OptSim", RSOFT Support, Synopsys, Inc. February 2018.

[63]   J. K. Patel, "How to build a transmitter", RSOFT Support, Synopsys, Inc. February 2018.

[64]   G. Bosco, "Spectral Shaping in Ultra-Dense WDM Systems: Optical vs. Electrical Approaches", Politecnico di Torino, OFC, paper OM3H.1, 2012.

[65]   Submarine cable map, [online]. Available:
https://www.submarinecablemap.com/#/submarine-cable/dunant